

NOTICE

This document is disseminated under the sponsorship of the Department of Transportation in the interest of information exchange. The United States Government assumes no liability for its contents or use thereof. This report does not constitute a standard, specification, or regulation.

The United States Government does not endorse products or manufacturers. Trade or manufacturers' names appear herein solely because they are considered essential to the object of this document.

1. Report No. FAA-EE-92-01		2. Government Accession No.		3. Recipient's Catalog No.	
4. Title and Subtitle Analysis of Aircraft Noise Levels in the Vicinity of Start-of-Takeoff Roll at Baltimore-Washington International Airport				5. Report Date May 1992	
				6. Performing Organization Code	
7. Author(s) Richard D. Horonjeff*				8. Performing Organization Report No. DOT-VNTSC-FAA-92-5	
9. Performing Organization Name and Address Foster-Miller, inc. ** 350 Second Avenue Waltham, MA 02154-1196				10. Work Unit No. (TRAIS) FA265/A2004	
				11. Contract or Grant No. DTRS-57-89-00009	
12. Sponsoring Agency Name and Address U.S. Department of Transportation Federal Aviation Administration Office of Environment and Energy 800 Independence Avenue, S.W. Washington, DC 20591				13. Type of Report and Period Covered Final-Report November 1991 - May 1992	
				14. Sponsoring Agency Code AEE - 120	
15. Supplementary Notes *Hams, Miller, Miller, & Hanson, Inc. 429 Marrett Road Lexington, MA 02173 **Under Contract to: U.S. Department of Transportation Research and Special Programs Administration Volpe National Transportation System Center Cambridge, MA 02142					
<p>The sound level prediction accuracy of the Federal Aviation Administration's Integrated Noise Model (INM) is receiving closer scrutiny today than at its inception due to a shifting emphasis in the model's application. In addition to the traditional land use planning application, the INM is now used as resource arbiters for local and federally funded noise mitigation programs.</p> <p>The increased model scrutiny has led to a reinspection of modeling assumptions in the vicinity of start-of-takeoff roll and the subsequent need for a well documented empirical database. This study focused on the gathering of such a database. The completed database consists of measured sound exposure levels (SELs) and maximum A-weighted sound levels at five sites in the hemicycle behind the aircraft at brake release and at distances of 2,000 to 4,000 ft from the brake release point. Independent variables include measurement site/runway geometry, aircraft type, engine type, aircraft gross weight, wind speed and direction, temperature, relative humidity, barometric pressure, aircraft ground roll distance versus time, and time to liftoff. This information is all contained in standard dBase III database files.</p> <p>Findings shown in this report include the effects on SEL of wind speed and direction, and the interaction effects of wind speed direction and measurement site location. Also discussed are comparisons of measured SELs and the predicted values of INM Version 3.10.</p>					
17. Key Words Integrated Noise Model, Sound Exposure Level, Airport Noise Model, Start-of-Takeoff Roll				18. Distribution Statement Document is available to the public through the National Technical Information Service Springfield, VA 22161	
19. Security Classif. (of this report) Unclassified		20. Security Classif. (of this page) Unclassified		21. No. of Pages 98	
				22. Price	

SI* (MODERN METRIC) CONVERSION FACTORS

APPROXIMATE CONVERSIONS TO SI UNITS

APPROXIMATE CONVERSIONS FROM SI UNITS

Symbol	When You Know	Multiply By	To Find	Symbol	Symbol	When You Know	Multiply By	To Find	Symbol
LENGTH					LENGTH				
in	Inches	25.4	millimeters	mm	mm	millimeters	0.039	Inches	in
ft	feet	0.305	meters	m	m	meters	3.28	feet	ft
yd	yards	0.914	meters	m	m	meters	1.09	yards	yd
mi	miles	1.61	kilometers	km	km	kilometers	0.621	miles	mi
AREA					AREA				
in ²	square Inches	645.2	millimeters squared	mm ²	mm ²	millimeters squared	0.0016	square inches	in ²
ft ²	square feet	0.093	meters squared	m ²	m ²	meters squared	10.764	square feet	ft ²
yd ²	square yards	0.836	meters squared	m ²	m ²	meters squared	1.195	square yards	ac
ac	acres	0.405	hectares	ha	ha	hectares	2.47	acres	mi ²
mi ²	square miles	2.59	kilometers squared	km ²	km ²	kilometers squared	0.386	square miles	
VOLUME					VOLUME				
fl oz	fluid ounces	29.57	milliliters	ml	ml	milliliters	0.034	fluid ounces	fl oz
gal	gallons	3.785	liters	l	l	liters	0.264	gallons	gal
ft ³	cubic feet	0.028	meters cubed	m ³	m ³	meters cubed	35.71	cubic feet	ft ³
yd ³	cubic yards	0.765	meters cubed	m ³	m ³	meters cubed	1.307	cubic yards	yd ³
MASS					MASS				
oz	ounces	28.35	grams	g	g	grams	0.035	ounces	oz
lb	pounds	0.454	kilograms	kg	kg	kilograms	2.202	pounds	lb
T	short tons (2000 lb)	0.907	megagrams	Mg	Mg	megagrams	1.103	short tons (2000 lb)	T
TEMPERATURE (exact)					TEMPERATURE (exact)				
°F	Fahrenheit temperature	5(F-32)/9 or (F-32)/1.8	Celcius temperature	°C	°C	Celcius temperature	1.8C + 32	Fahrenheit temperature	°F
ILLUMINATION					ILLUMINATION				
fc	foot-candles	10.76	lux	l	lx	lux	0.0929	foot-candles	fc
fl	foot-Lamberts	3.426	candela/m ²	cd/m ²	cd/m ²	candela/m ²	0.2919	foot-Lamberts	fl
FORCE and PRESSURE or STRESS					FORCE and PRESSURE or STRESS				
lbf	poundforce	4.45	newtons	N	N	newtons	0.225	poundforce	lbf
psi	poundforce per square Inch	6.89	kilopascals	kPa	kPa	kilopascals	0.145	poundforce per square inch	psi

* SI is the symbol for the International System of Units

(Revised January 1992)

ACKNOWLEDGMENTS

The contractor team gratefully acknowledges the assistance of several people and organizations who were instrumental in the successful completion of this project. First, the contractor is indebted to the Aviation Noise Program Office of the Maryland Aviation Administration for providing much of the coordination effort in using Baltimore-Washington International Airport (**BWI**) as the site of the data acquisition program. The contractor team is also indebted to this Office for providing key personnel who assisted in the data collection effort. Largely through their efforts the contractor was successful in obtaining the gate weights of the vast majority of departing aircraft the contractor measured during the course of **the** project.

The contractor would also like to thank the station managers and personnel of **USAir**, American Airlines, Continental Airlines, Delta Airlines, **Trans** World Airlines, United Airlines, and Air **Cancun** for their willingness to provide these aircraft weights.

The contractor also wishes to acknowledge the assistance of the Federal Aviation Administration in allowing it access to the **BWI** control tower for nine days of data collection. The excellent vantage point afforded by the control tower was instrumental to **the** cost-effective method of aircraft tracking employed in this study as well as to maintaining surveillance of other aircraft activity. Thanks also go to the FAA Office of Environment and Energy who provided the installed engine type information for each of **the** over **200** different aircraft observed during the nine days of measurements.

The contractor is also indebted to the National Weather Service for their assistance in providing hourly surface weather observations.

With regards to providing sites for the acoustic measurements the contractor is indebted to four homeowners as well as Butler Aviation Inc. for generously allowing us access to their property.

Last, but not least, the contractor wishes to thank **VNTSC** for their continued input throughout the project as well as their assistance in performing a number of **INM** test runs to provide model predictions of aircraft sound levels at each of our noise measurement sites.

ACKNOWLEDGMENTS

The contractor team gratefully acknowledges the assistance of several people and organizations who were instrumental in the successful completion of this project. First, the contractor is indebted to the Aviation Noise Program **Office** of the Maryland Aviation Administration for providing much of the coordination effort in using Baltimore-Washington International Airport (**BWI**) as the site of the data acquisition program. The contractor team is also indebted to this Office for providing key personnel who assisted in the data collection effort. Largely through their efforts the contractor was successful in obtaining the gate weights of the vast majority of departing aircraft the contractor measured during the course of **the** project.

The contractor would also like to thank the station managers and personnel of **USAir**, American Airlines, Continental Airlines, Delta Airlines, **Trans** World Airlines, United Airlines, and Air **Cancun** for their willingness to provide these aircraft weights.

The contractor also wishes to acknowledge the assistance of the Federal Aviation Administration in allowing it access to the **BWI** control tower for nine days of data collection. The excellent vantage point afforded by the control tower was instrumental to the cost-effective method of aircraft tracking employed in this study as well as to maintaining surveillance of other aircraft activity. Thanks also go to the FAA Office of Environment and Energy who provided the installed engine type information for each of **the** over **200** different aircraft observed during the nine days of measurements.

The contractor is also indebted to the National Weather Service for their assistance in providing hourly surface weather observations.

With regards to providing sites for the acoustic measurements the contractor is indebted to four homeowners as well as Butler Aviation Inc. for generously allowing us access to their property.

Last, but not least, the contractor wishes to thank **VNTSC** for their continued input throughout the project as well as their assistance in performing a number of **INM** test runs to provide model predictions of aircraft sound levels at each of our noise measurement sites.

Table of Contents

APPENDIX A. RUNWAY / MEASUREMENT SITE GEOMETRY	63
APPENDIX B. WEATHER DATA	69
APPENDIX C. DATABASE STRUCTURE	81
APPENDIX D. SEL COMPUTATION SOFTWARE OPERATION	87

List of Tables

TABLE 1. INDEPENDENT MEASUREMENT VARIABLES	2
TABLE 2. DEPENDENT MEASUREMENT VARIABLES	2
TABLE 3. AZIMUTH AND DISTANCE TO ACOUSTIC MEASUREMENT SITES . . .	7
TABLE 4. SUMMARY OF ACOUSTIC DATA COLLECTION.	24
TABLE 5. OBSERVED AIRCRAFT/ENGINE TYPES AND GROSS WEIGHTS	32
TABLE 6. COMPARISON OF MEASURED AND INM 3.10 PREDICTED SELS	56

List of Illustrations

FIGURE 1. AIRPORT AND ACOUSTIC MEASUREMENT SITE LAYOUT	6
FIGURE 2. TERRAIN PROFILE - BRAKE RELEASE TO MEASUREMENT SITE 1 . .	8
FIGURE 3. TERRAIN PROFILE - BRAKE RELEASE TO MEASUREMENT SITE 2 . .	8
FIGURE 4. TERRAIN PROFILE - BRAKE RELEASE TO MEASUREMENT SITE 3 . .	9
FIGURE 5. TERRAIN PROFILE - BRAKE RELEASE TO MEASUREMENT SITE 4 . .	9
FIGURE 6. TERRAIN PROFILE - BRAKE RELEASE TO MEASUREMENT SITE 5 . .	10
FIGURE 7. BLOCK DIAGRAM OF ACOUSTIC DATA ACQUISITION SYSTEM	11
FIGURE 8. NOISE MONITOR TIMING METHODOLOGY	13
FIGURE 9. AIRCRAFT OBSERVER LOG	14
FIGURE 10. VISUAL CUES USED FOR AIRCRAFT POSITION TRACKING	15
FIGURE 11. JET TRANSPORT LANDING LOG	17
FIGURE 12. GENERAL AVIATION RUNWAY ACTIVITY LOG	18
FIGURE 13. BLOCK DIAGRAM OF WIND SENSOR DATA ACQUISITION SYSTEM .	20
FIGURE 14. FIELD OF VIEW FOR VIDEOTAPE DATA	21
FIGURE 15. OVERVIEW OF DATABASE STRUCTURE	26
FIGURE 16. BLOCK DIAGRAM OF SOUND LEVEL METRIC COMPUTATION . . .	
PROCESS	28
FIGURE 17. SOUND LEVEL INTERACTIVE GRAPHIC INTERFACE	29
FIGURE 18. REPRESENTATIVE PLOT OF AIRCRAFT POSITION AND TIMING	
DATA	34
FIGURE 19. SUMMARY OF WIND AND TEMPERATURE MEASUREMENT	
CONDITIONS	35
FIGURE 20. SEL VERSUS WIND SPEED FOR B-727:100/200 AT 'SITE 1'	37
FIGURE 21. SEL VERSUS WIND SPEED FOR B-727:100/200 AT SITE 2	37
FIGURE 22. SEL VERSUS WIND SPEED FOR B-727:100/200 AT SITE 3	38
FIGURE 23. SEL VERSUS WIND SPEED FOR B-727:100/200 AT SITE 4	38
FIGURE 24. SEL VERSUS WIND SPEED FOR B-727:100/200 AT SITE 5	39
FIGURE 25. SEL VERSUS WIND SPEED FOR B-737:200 AT SITE 1	40
FIGURE 26. SEL VERSUS WIND SPEED FOR B-737:200 AT SITE 2	40
FIGURE 27. SEL VERSUS WIND SPEED FOR B-737:200 AT SITE 3	41
FIGURE 28. SEL VERSUS WIND SPEED FOR B-737:200 AT SITE 4	41
FIGURE 29. SEL VERSUS WIND SPEED FOR B-737:200 AT SITE 5	42
FIGURE 30. SEL VERSUS WIND SPEED FOR B-737:300/400 AT SITE 1	43
FIGURE 31. SEL VERSUS WIND SPEED FOR B-737:300/400 AT SITE 2	43
FIGURE 32. SEL VERSUS WIND SPEED FOR B-737:300/400 AT SITE 3	44
FIGURE 33. SEL VERSUS WIND SPEED FOR B-737:300/400 AT SITE 4	44
FIGURE 34. SEL VERSUS WIND SPEED FOR B-737:300/400 AT SITE 5	45
FIGURE 35. SEL VERSUS WIND SPEED FOR DC-9 (ALL MODELS) AT SITE 1 . . .	46
FIGURE 36. SEL VERSUS WIND SPEED FOR DC-9 (ALL MODELS) AT SITE 2 . . .	46
FIGURE 37. SEL VERSUS WIND SPEED FOR DC-9 (ALL MODELS) AT SITE 3 . . .	47
FIGURE 38. SEL VERSUS WIND SPEED FOR DC-9 (ALL MODELS) AT SITE 4 . . .	47
FIGURE 39. SEL VERSUS WIND SPEED FOR DC-9 (ALL MODELS) AT SITE 5 . . .	48
FIGURE 40. SEL VERSUS WIND SPEED FOR MD-80 (ALL MODELS) AT SITE 1 . .	49
FIGURE 41. SEL VERSUS WIND SPEED FOR MD-80 (ALL MODELS) AT SITE 2 . .	49
FIGURE 42. SEL VERSUS WIND SPEED FOR MD-80 (ALL MODELS) AT SITE 3 . .	50
FIGURE 43. SEL VERSUS WIND SPEED FOR MD-80 (ALL MODELS) AT SITE 4 . .	50
FIGURE 44. SEL VERSUS WIND SPEED FOR MD-80 (ALL MODELS) AT SITE 5 . .	51
FIGURE 45. A-LEVEL TIME HISTORIES UNDER DOWNWIND CONDITIONS	53
FIGURE 46. A-LEVEL TIME HISTORIES UNDER UPWIND CONDITIONS	54
FIGURE 47. SEL CONTOURS FOR TWO STARTING SPEEDS (727D17)	58
FIGURE 48. SEL CONTOURS FOR TWO STARTING SPEEDS (737300)	59

1. INTRODUCTION

This study of start-of-takeoff roll noise was performed under contract to the **Volpe** National Transportation Systems Center (**VNTSC**) by Foster-Miller, Inc. (**FMI**) and Harris Miller Miller & Hanson Inc. (**HMMH**) in support of continuing efforts to improve and refine the computational algorithms of the Federal Aviation Administration's (FAA) Integrated Noise Model (**INM**). At the time of inception almost twenty years ago, the primary objective was the creation of a land use planning tool by which the impact of present and future airfield operational scenarios could be assessed. While this need still continues today, the **INM** is now seeing a new and more demanding application: to **define** noise impact zone boundaries which draw the line between qualifying and non-qualifying residents for local and federally funded homeowner assistance programs. These programs most commonly take the form of residential sound proofing projects and purchase assurance programs.

The **INM** has come under increasing scrutiny by the public and government agencies alike. Often fueled by large quantities of long term continuous airport noise monitor data, the demand for **modelling** accuracy (or at least an understanding of **measurement/modelling** discrepancies) is greater today than at the model's inception.

While the **INM** does well in predicting the noise levels of aircraft in flight, the added complexities of noise generation and sound propagation during aircraft ground roll have resulted in an understandably greater uncertainty in the model's predictive ability around the start-of-takeoff roll and along the runway sideline. The purpose of this investigation was to acquire a database of empirical information which could serve to document the extent of various cause/effect relationships, as well as provide insight for future model improvements or additional research needs.

1.1 Purpose and Goals

The purpose of this study was to provide the data needed by **VNTSC** and FAA to (1) assess **single-event** aircraft noise levels in the vicinity of start-of-takeoff roll and to suggest any parameter adjustments to the **INM** deemed necessary to quickly bring the model into the closest possible agreement with the data, and (2) establish direction for longer term research and potential model changes which might be accomplished through changes to the computational algorithms themselves. In support of this purpose four specific project goals were identified:

- (1) Provide measured Sound Exposure Level (**SEL**) information at selected locations for direct comparison with Integrated Noise Model predictions (Version **3.10**),
- (2) Create a documented, empirical database to support future analyses of the noise generation and sound propagation process,
- (3) Conduct preliminary data analyses to provide guidance for future model revisions and identify if and where future research may be needed, and
- (4) Perform feasibility investigations for simple model changes.

1.2 General Approach

In order to achieve the above goals, the following approach was followed. The first step of the approach involved the selection of measurement variables and an airport at which to conduct the measurements. Next, the data acquisition program was designed and conducted. After the data were returned from the field they were reduced to develop the empirical database. This database served as the basis for all analyses performed on the data. In a stand-alone effort, a single parameter value was modified within the **INM** to determine whether it could serve to fine-tune the predicted noise levels in the area around start-of-takeoff roll, but not elsewhere.

1.3 Identification of Variables

In consultation with VNTSC and FAA, ten independent and three dependent variables were identified for measurement in this program. *The ten independent variables are shown in Table 1.*

TABLE 1. INDEPENDENT MEASUREMENT VARIABLES

Source:	Aircraft Type Engine Type Aircraft Gross Weight Start of Roll Scenario (Static or Rolling) Ground Roll Distance versus Time
Propagation Path:	Average Wind Vector (Speed & Direction) Temperature Relative Humidity Barometric Pressure
Receiver:	Range and Azimuth to Measurement Site

The aircraft and engine types contained in FAA **records** for an observed registration number (eg. **B727/200, JT8D-9**) is **the** source of aircraft/engine data for this study. The gross weight is the gate weight of the aircraft and does not account for any fuel **burndown** prior to takeoff. The start-of-roll scenario is a binary variable identifying whether the aircraft began its roll from a standing start *on* the *runway* or whether it rolled onto the runway and did not stop prior to initiating its takeoff roll.

Ground Roll Distance versus Time relates the aircraft position along the runway centerline to time-of-day. This vector variable serves three purposes: **(1)** to enable evaluation of aircraft acceleration performance, **(2)** to enable time-synchronized relationships between the A-weighted sound level time history and aircraft position on the runway, and **(3)** determine the distance to liftoff from the runway threshold.

The average wind vector is a time-average speed and direction observed at a height of **10** meters above ground level when start of takeoff occurs. Temperature, relative humidity, and barometric pressure are slowly varying parameters over time and can be adequately interpolated **from** hourly readings.

Range and azimuth to the measurement site are relative to the brake release point and runway heading, respectively. In order to ensure experimental leverage in this variable, azimuths of **80** to **165** degrees, and ranges from **2000** to **4000** feet were selected.

The three dependent variables are shown in Table 2.

TABLE 2. DEPENDENT MEASUREMENT VARIABLES

A-Weighted Sound Level Time History Maximum A-weighted Sound Level Sound Exposure Level

The A-weighted sound level time history is the series of “slow” sound level meter A-weighted sound levels acquired every **0.5** seconds from **60** seconds prior to brake release to **150** seconds after brake release. The maximum sound level is the largest of the “slow” sound level meter samples during time history associated with the event. The sound exposure level is the time integration of the “slow” sound level meter time history of **0.5** second samples.

1.4 Report Organization

Section 2 of this report provides a description of the data acquisition phase of the project. It includes a complete description of how each variable was measured or determined. Section 3 describes the data reduction phase. This phase takes all of the raw field data and reduces it to a spreadsheet format suitable for sorting, plotting and inferring variable relationships. Section 4 discusses the various analyses performed on the data. It also provides interpretations of the findings of these analyses.

Section 5 discusses a simple method for fine tuning **INM-predicted SEL** values in the vicinity of start-of-takeoff roll. The concept is discussed as well as the results of limited, trial computations.

Section 6 provides a number of recommendations regarding the completed work.

Appendix A provides tables showing the geometric relationship between the runway and the measurement sites. Appendix B shows hourly surface weather observations by the National Weather Service. Appendices C and D describe additional work products of the investigation submitted under separate cover. These include videotapes of the entire data acquisition phase of the project, database files generated during the data reduction phase of the work, and the software developed to calculate **SELs** and maximum A-weighted sound levels from the A-weighted **time-history** data.

The A-weighted sound level time history is the series of “slow” sound level meter A-weighted sound levels acquired every **0.5** seconds from **60** seconds prior to brake release to **150** seconds after brake release. The maximum sound level is the largest of the “slow” sound level meter samples during time history associated with the event. The sound exposure level is the time integration of the “slow” sound level meter time history of **0.5** second samples.

1.4 Report Organization

Section 2 of this report provides a description of the data acquisition phase of the project. It includes a complete description of how each variable was measured or determined. Section 3 describes the data reduction phase. This phase takes all of the raw field data and reduces it to a spreadsheet format suitable for sorting, plotting and inferring variable relationships. Section 4 discusses the various analyses performed on the data. It also provides interpretations of the findings of these analyses.

Section 5 discusses a simple method for fine tuning **INM-predicted SEL** values in the vicinity of start-of-takeoff roll. The concept is discussed as well as the results of limited, trial computations.

Section 6 provides a number of recommendations regarding the completed work.

Appendix A provides tables showing the geometric relationship between the runway and the measurement sites. Appendix B shows hourly surface weather observations by the National Weather Service. Appendices C and D describe additional work products of the investigation submitted under separate cover. These include videotapes of the entire data acquisition phase of the project, database files generated during the data reduction phase of the work, and the software developed to calculate **SELs** and maximum A-weighted sound levels from the A-weighted **time-history** data.

2. DATA ACQUISITION

This section of the report provides a complete description of the data acquisition phase of the project. It discusses the means by which each variable was acquired and how time synchronization was achieved for variables needing such treatment.

The entire data acquisition phase of the work was conducted at Baltimore-Washington International Airport (**BWI**). Baltimore-Washington is an air carrier airport located approximately **10** miles south of the city of Baltimore, Maryland. Data were collected at **BWI** during two field visits: **22-25** October **1991** and **15-19** December **1991**. The data acquisition effort was performed by **HMMH**, with considerable support provided by the Aviation Noise Program Office of the Maryland Aviation Administration. Note: data collection during the October visit was performed under contract to Maryland Aviation Administration. These data are included here to increase statistical integrity.

BWI currently serves as a hub for **USAir**, but is also served by a number of other domestic and international airlines. The **hubbing** operation results in **traffic** concentrations several times per day. The concentrations consist of **30** to **45** minutes of heavy arrival activity, followed by a brief pause of **30** minutes, and then a **30** to **45** minute concentration of departures. During the departure phase of the cycle it is not uncommon for a queue of several aircraft to be waiting on the **taxiways** for both the commuter as well as jet transport runways (**33R** and **28**, respectively), and for departures to occur every one to two minutes.

Data acquisition was completely passive in the sense that no external controls were exercised over aircraft or pilots. In order to measure all of the variables shown in Tables 1 and 2 it was necessary to collect information from a number of geographically dispersed sources, many of which required careful time synchronization. Time synchronization was achieved by referencing each data acquisition device's clock to a single digital wrist watch. This master clock was initially set to within one second of the National Institute of Standards and Technology (**NIST**, formerly National Bureau of Standards) Coordinated Universal Time announcement (radio station **WWV**). The details of the time synchronization process are explained in the subsections below.

All ground geometry relationships in this study were established using the Maryland State Plane Coordinate System. These relationships included the location of acoustic measurement sites and runways. The coordinate system was also used as a directional reference for wind velocity (the state coordinate system is aligned within one degree of true north at **BWI**).

2.1 Airport and Measurement Site Geometry

Figure 1 shows the runway complex at **BWI** as well as the locations of the acoustic measurement sites. Depending on prevailing wind conditions, **BWI** operates in one of two modes: east flow or west flow. The preferential mode is west flow and all measurements for **this** study were conducted under this condition.

In west flow, all jet transport aircraft depart on runway **28** (the east-west runway). These departures are indicated by the heavy black arrows in the figure. The five acoustic measurement sites are indicated by the numbered, solid diamonds. Sites **1**, **3** and **5** were chosen to cover a range of azimuth angles relative to the aircraft location and heading at the nominal brake release point. Sites **2.1**, **2.2**, **3** and **4** were meant to cover a range of distances along a nominally constant radial from the start of takeoff roll on runway **28**. Table 3 summarizes these azimuth and distance relationships to the sites. Appendix A provides tables with additional detail. These tables show range and azimuth from the aircraft to each measurement site as a function of ground roll distance from the nominal brake release point. Note: Sites **2.1** and **2.2** were located within four houses of one another. Site **2.1** was used during the October measurements and site **2.2** was used during the December measurements. No further distinction is made between sites **2.1** and **2.2** in this report.

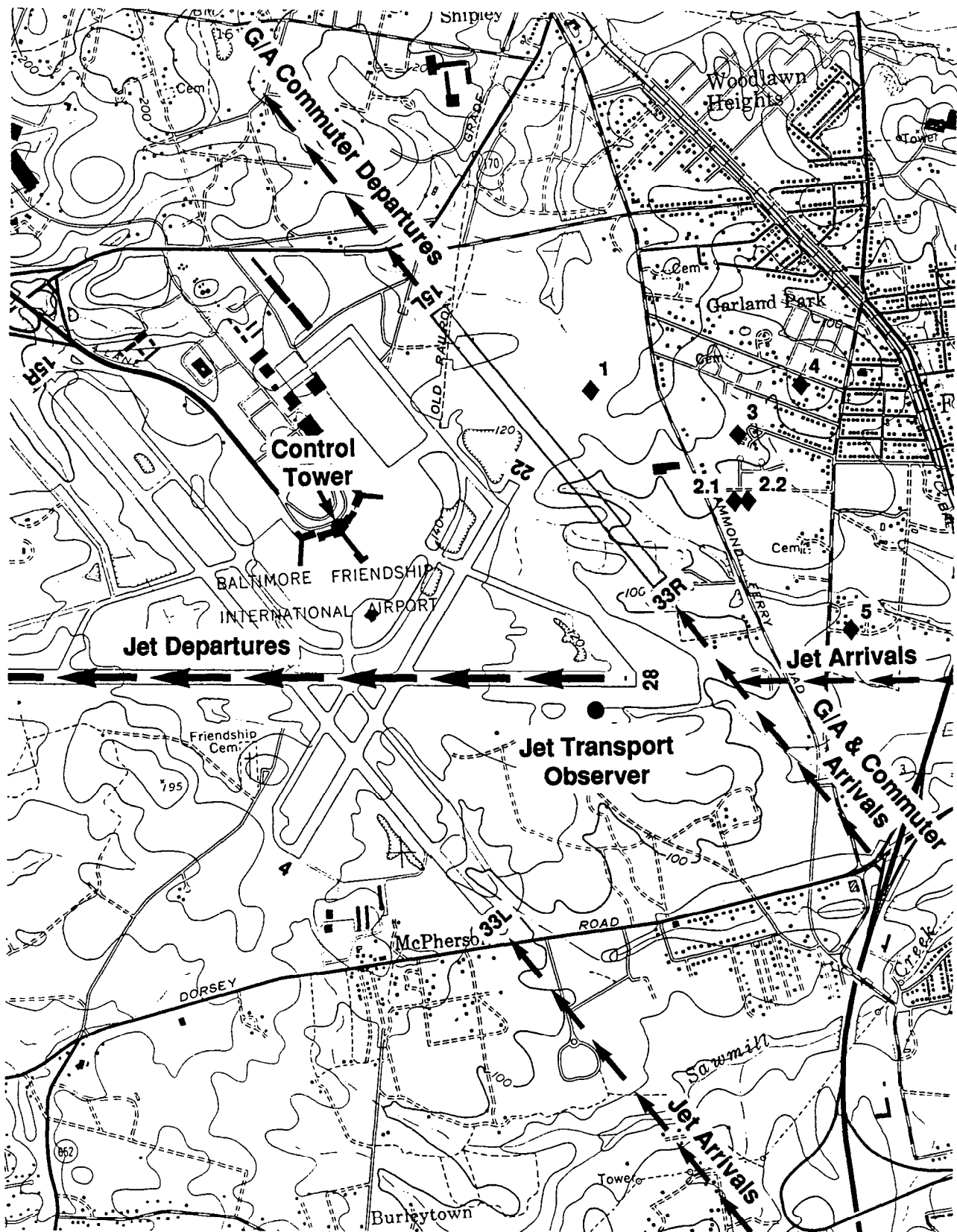


FIGURE 1. AIRPORT AND ACOUSTIC MEASUREMENT SITE LAYOUT

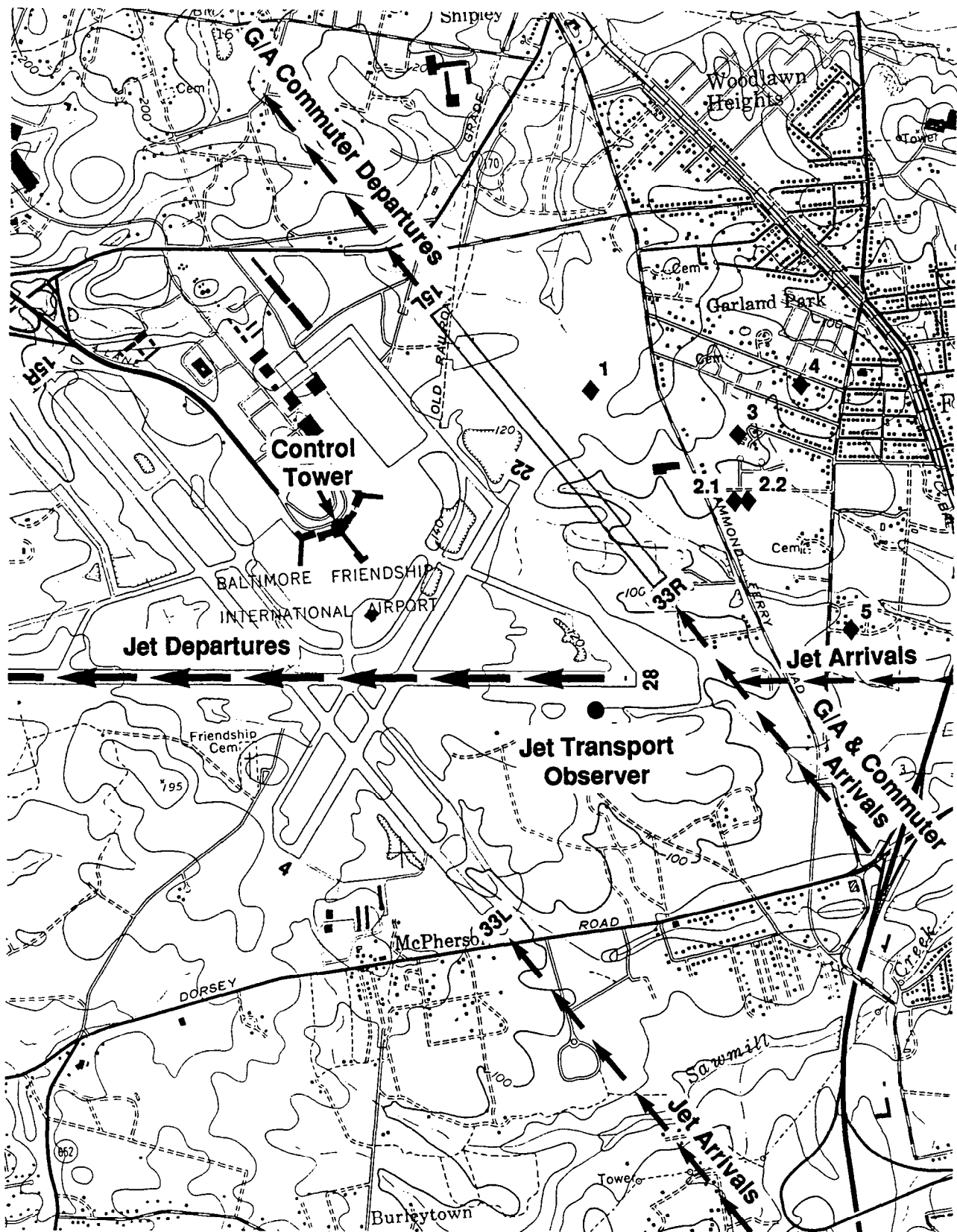


FIGURE 1. AIRPORT AND ACOUSTIC MEASUREMENT SITE LAYOUT

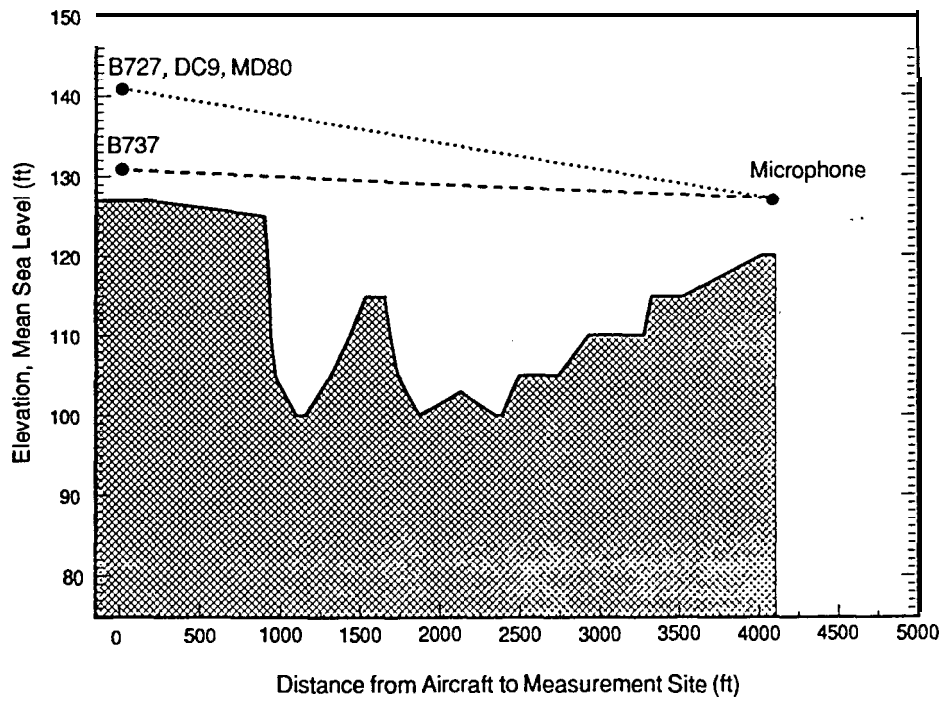


FIGURE 2. TERRAIN PROFILE - BRAKE RELEASE TO MEASUREMENT SITE 1

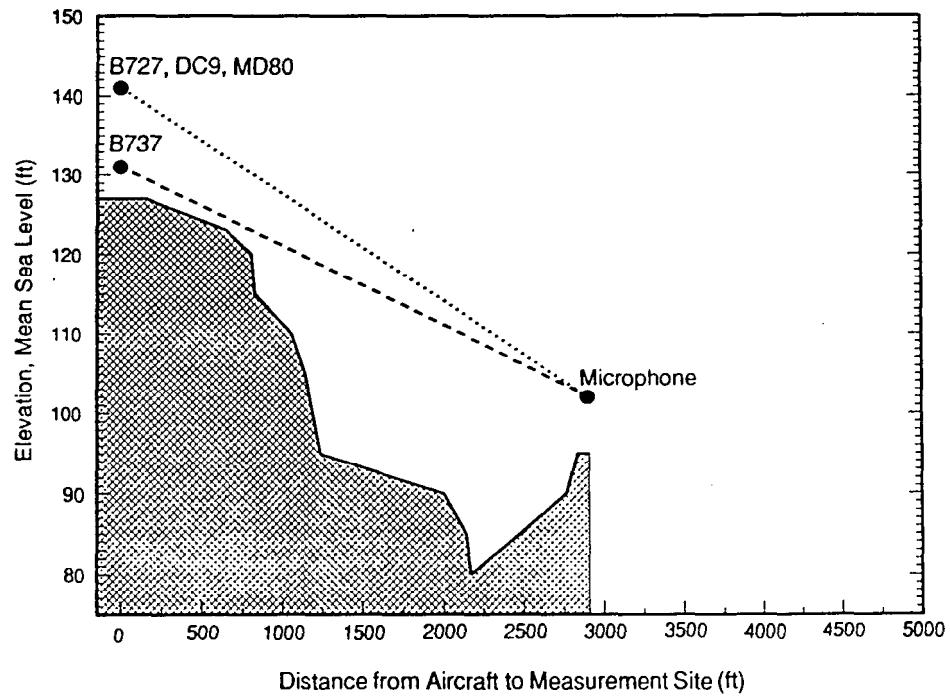


FIGURE 3. TERRAIN PROFILE - BRAKE RELEASE TO MEASUREMENT SITE 2

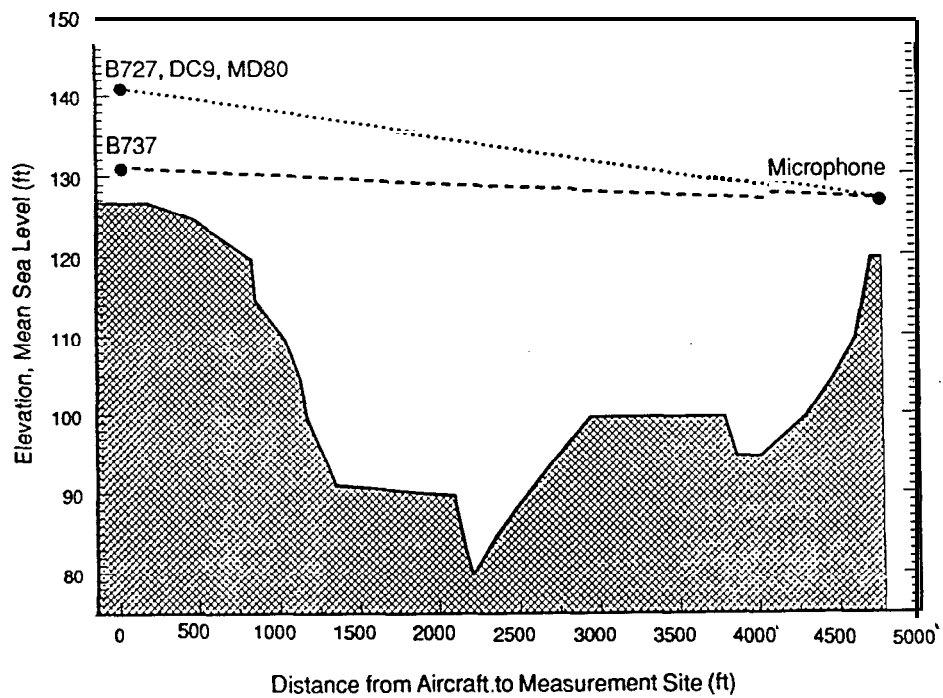


FIGURE 4. TERRAIN PROFILE - BRAKE RELEASE TO MEASUREMENT SITE 3

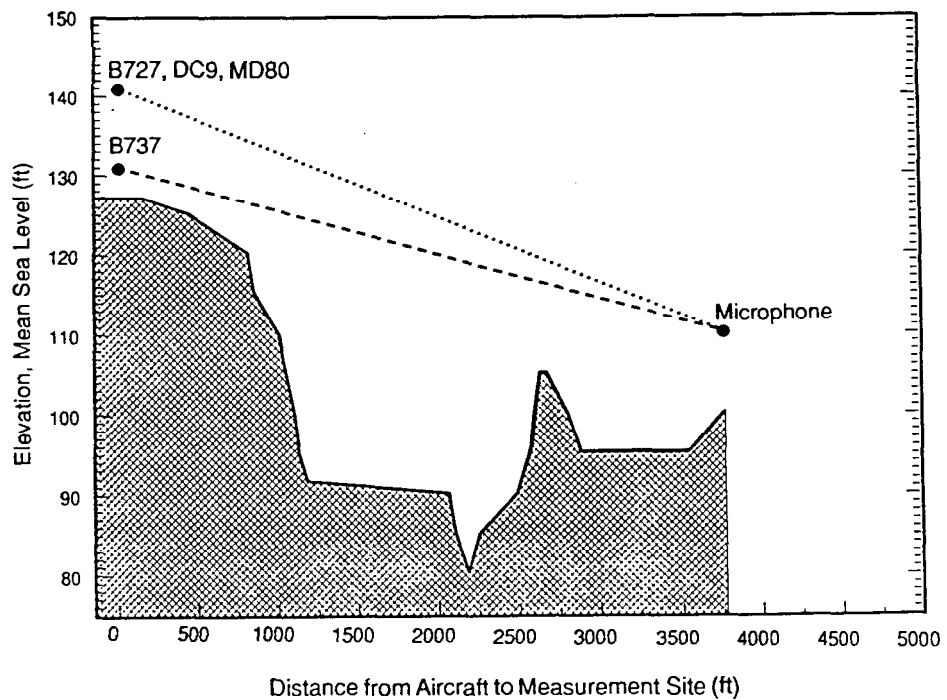


FIGURE 5. TERRAIN PROFILE - BRAKE RELEASE TO MEASUREMENT SITE 4

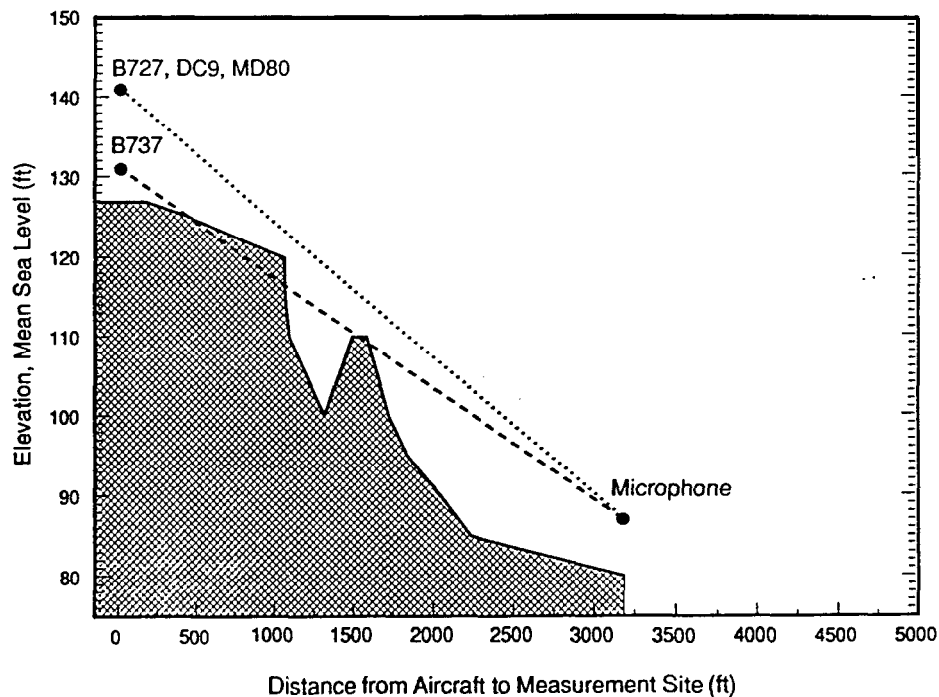


FIGURE 6. TERRAIN PROFILE - BRAKE RELEASE TO MEASUREMENT SITE 5

2.3 Individual Data Sources

This subsection describes how each of the various data types (acoustic, atmospheric, aircraft tracking, etc.) were collected.

2.3.1 Acoustic Data

All acoustic data in this study were collected using unattended sound level monitors. These monitors continuously recorded the A-weighted sound pressure level every 1/2 second.

Equipment. Unattended measurements were conducted at each site using a **Bruel & Kjaer Model 4155** 1/2-inch electret microphone, Larson-Davis Model **827-0V** or **900B** microphone preamplifiers, and Larson-Davis Model **820** or **870** Precision Sound Level Meters. A 3-inch, open cellular foam windscreen was used during all measurements. Calibrations were performed with a **GenRad Model 1987** acoustic calibrator, traceable to **NIST**.

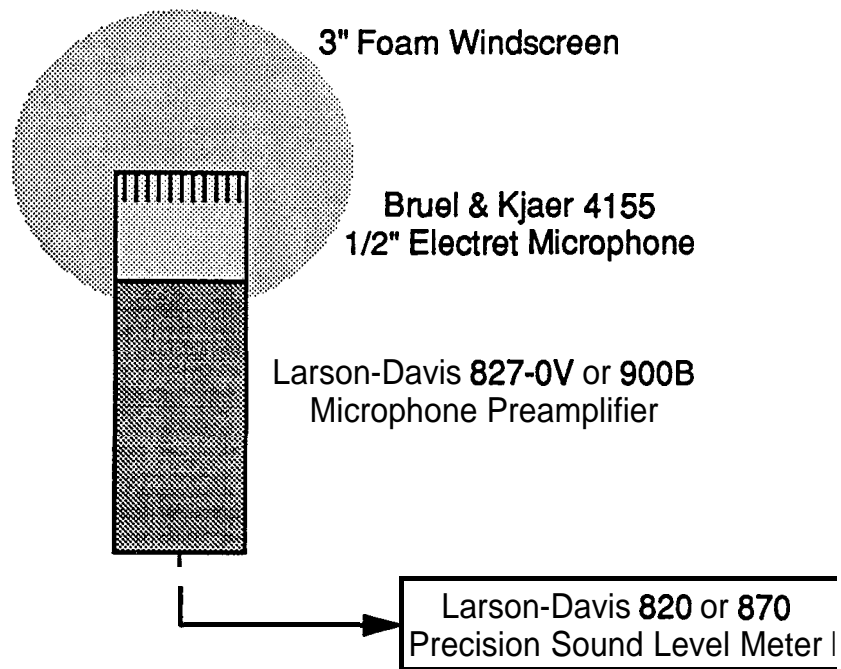


FIGURE 7. BLOCK DIAGRAM OF ACOUSTIC DATA ACQUISITION SYSTEM

Measurement Protocol. The acoustic measurement protocol consisted of a rigorous daily routine of instrument calibration, instrument deployment, data acquisition, instrument retrieval, and post calibration. The steps involved in this routine are described below. The description generically refers to the Larson-Davis **820** and **870** precision sound level meters as “the noise monitor” or just “the monitor.” While, there are distinct differences between the two models., **there** are also numerous similarities. In fact, all instrument functions (calibration, data **acquisition**, and data retrieval) needed for this study were functionally identical in the two models. Hence, no further distinction is made between them in this report.

The first element of the daily protocol, **instrument** calibration, was performed prior to field deployment. With all five monitors located side-by-side, the monitors were turned on and all operating parameters set. These parameters included:

Sound Level Meter Dynamics:	RMS SLOW
Frequency Weighting:	A
Data Acquisition Mode:	CONTINUOUS, 0.5 SECOND SAMPLES
Sound Level Resolution:	0.1 dB.

Next, the clock in each monitor was manually set to the nearest second using the master clock as a reference. Then each unit was amplitude calibrated with its own microphone and preamplifier using a **GenRad Model 1987** acoustics calibrator.

The last step of the calibration procedure was the timing calibration. Although the noise monitor clock display (to the nearest second) and the **0.5** second data sampler are driven from the same

internal clock, there is no guarantee that alternate **0.5** second samples start and stop precisely at the seconds change in the, clock display. In fact, when data acquisition is started by depressing the monitor's Run/Stop key, the starting time of the time history is recorded internally only to the nearest second. Neither is there any guarantee that the monitor clock speed is the same as the master clock (although they were very close and within less than 3 seconds at the end of the day). Therefore, to achieve the desired **100** millisecond timing accuracy between the master clock and the **1/2** second samples an independent timing calibration was performed each day.

This timing calibration was achieved by starting the data acquisition on all monitors while **they** were all side-by-side (once started, data acquisition was not interrupted until the units were retrieved from the field and post calibrated.) The output of a single microphone and preamplifier was then connected in parallel to all five monitors. The calibrator was turned on and placed on the microphone to produce a **simultaneous**, constant voltage input signal to all monitors. All monitors were then inspected to ensure that the **0.5** second sound level readings had stabilized. At a precisely noted time on the master clock (worst case reading error of plus or minus **200** milliseconds) the calibrator was turned off. The **1/2** second sound level readings then began a slow decay over time (approximate decay rate of **5 dB/second**) as a result of the **RC** averaging circuit in the monitor.

A plot of the successive sound level readings is shown in Figure **8**. Since each sound level sample is numbered consecutively within the monitor, time calibration can be achieved by equating the sample number where the decay began with the time the input signal was turned off. The abscissa in Figure 8 plots the sample number and the ordinate plots the sound level. The point in the sampling sequence when the signal was turned off can be determined from the intersection of two lines: (1) the horizontal line connecting the points of constant signal level before the onset of decay, and (2) a regression line through the points during the **RC** decay process. The fractional sample number so determined corresponds to the master clock time-of-day reading when the signal was turned off. This process was repeated four times.

With the timing calibration complete, the monitors were left running (so as not to interrupt the precisely timed sampling sequence), taken to their respective measurement sites, and deployed for the day's data collection. The microphones were mounted on tripods and adjusted to be 6 feet above ground level. This height was selected as a compromise between the 4 foot FAR Part **36**¹ reference requirement and a sufficient height so that normal voice level conversation near the tripod (should it occur) would not adversely affect the unattended measurements. After the monitors had been set up they were again acoustically calibrated by placing the **1000** Hz calibrator on the microphone and recording the observed sound level in a calibration log. The monitor keyboards were then locked, and the monitors themselves physically locked inside a weathertight case to prevent tampering.

Midday acoustic calibrations were performed as time permitted to ensure the stability of the microphones over the normal diurnal patterns of temperature and humidity.

At the end of each day the monitors were post calibrated in the field with the **0.5** second sampling still in progress. The units were then retrieved (still sampling) and brought together where four more timing calibrations were performed as described above. Taken together, the eight timing datapoints (sample number versus time-of-day) enabled a regression line to be fit for relating sample number to time-of-day. These fits were performed daily for each monitor. As a point of interest, the data point residuals about the regression line rarely exceeded **100** milliseconds, implying that the **100** millisecond accuracy goal had been met.

¹ Code of Federal Regulations, Title **14**, Subchapter **1**, "Airports", Part **36**, "Noise Standards: Aircraft Type and Airworthiness Certification", Appendix A, Section **A36.3**, June 1974 (revised May 1988).

internal clock, there is no guarantee that alternate **0.5** second samples start and stop precisely at the seconds change in the, clock display. In fact, when data acquisition is started by depressing the monitor's Run/Stop key, the starting time of the time history is recorded internally only to the nearest second. Neither is there any guarantee that the monitor clock speed is the same as the master clock (although they were very close and within less than 3 seconds at the end of the day). Therefore, to achieve the desired **100** millisecond timing accuracy between the master clock and the **1/2** second samples an independent timing calibration was performed each day.

This timing calibration was achieved by starting the data acquisition on all monitors while they were all side-by-side (once started, data acquisition was not interrupted until the units were retrieved from the field and post calibrated.) The output of a single microphone and preamplifier was then connected in parallel to all five monitors. The calibrator was turned on and placed on the microphone to produce a **simutaneous**, constant voltage input signal to all monitors. All monitors were then inspected to ensure that the **0.5** second sound level readings had stabilized. At a precisely noted time on the master clock (worst case reading error of plus or minus **200** milliseconds) the calibrator was turned off. The **1/2** second sound level readings then began a slow decay over time (approximate decay rate of **5 dB/second**) as a result of the **RC** averaging circuit in the monitor.

A plot of the successive sound level readings is shown in Figure 8. Since each sound level sample is numbered consecutively within the monitor, time calibration can be achieved by equating the sample number where the decay began with the time the input signal was turned off. The abscissa in Figure 8 plots the sample number and the ordinate plots the sound level. The point in the sampling sequence when the signal was turned off can be determined from the intersection of two lines: (1) the horizontal line connecting the points of constant signal level before the onset of decay, and (2) a regression line through the points during the **RC** decay process. The fractional sample number so determined corresponds to the master clock time-of-day reading when the signal was turned off. This process was repeated four times.

With the timing calibration complete, the monitors were left running (so as not to interrupt the precisely timed sampling sequence), taken to their respective measurement sites, and deployed for the day's data collection. The microphones were mounted on tripods and adjusted to be 6 feet above ground level. This height was selected as a compromise between the 4 foot FAR Part **36**¹ reference requirement and a sufficient height so that normal voice level conversation near the tripod (should it occur) would not adversely affect the unattended measurements. After the monitors had been set up they were again acoustically calibrated by placing the **1000** Hz calibrator on the microphone and recording the observed sound level in a calibration log. The monitor keyboards were then locked, and the monitors themselves physically locked inside a weathertight case to prevent tampering.

Midday acoustic calibrations were performed as time permitted to ensure the stability of the microphones over the normal diurnal patterns of temperature and humidity.

At the end of each day the monitors were post calibrated in the field with the **0.5** second sampling still in progress. The units were then retrieved (still sampling) and brought together where four more timing calibrations were performed as described above. Taken together, the eight timing datapoints (sample number versus time-of-day) enabled a regression line to be fit for relating sample number to time-of-day. These **fits** were performed daily for each monitor. As a point of interest, the data point residuals about the regression line rarely exceeded **100** milliseconds, implying that the **100** millisecond accuracy goal had been met.

¹ Code of Federal Regulations, Title **14**, Subchapter **1**, "Airports", Part **36**, "Noise Standards: Aircraft Type and Airworthiness Certification", Appendix A, Section **A36.3**, June 1974 (revised May 1988).

2.3.3 Aircraft Position Tracking

Aircraft position tracking was performed by a human observer located in the control tower. The observer logged each aircraft's brake release time and the time the aircraft passed eight easily identifiable landmarks. As the aircraft passed each landmark, the observer pressed one of the nine **number keys** on a laptop computer. Software running in the computer stored the contents of the computer system clock (to the nearest **0.01** second) in a database **file** each time a numeric key was struck. The **"1"** key was used to signal brake release. The **"2"** through **"9"** keys were used to log the times when the aircraft passed the visual cues shown in Figure 10. The **"0"** key was used to **log the liftoff time**. If the observer felt a mistake had been made at any point during a takeoff, the entire run was deleted (except for the brake release time) by pressing the "delete" key.

The computer clock was time-synchronized to a master clock at both the beginning and end of each measurement session by first configuring the DOS prompt to display the computer system clock to the nearest **0.01** second. To perform a calibration, the "Enter" key was pressed in sync with the second change on the master clock **16** to **20** times in succession. The average difference between the system clock time and the master clock time was used as an adjustment factor to correct all of the tracking data to master clock time. As an experiment to determine the accuracy of this time calibration method, ten such calibrations were performed back-to-back within a very brief period. The results of the experiment showed a total range of only **0.13** seconds in calculated adjustment factors across the ten trials.

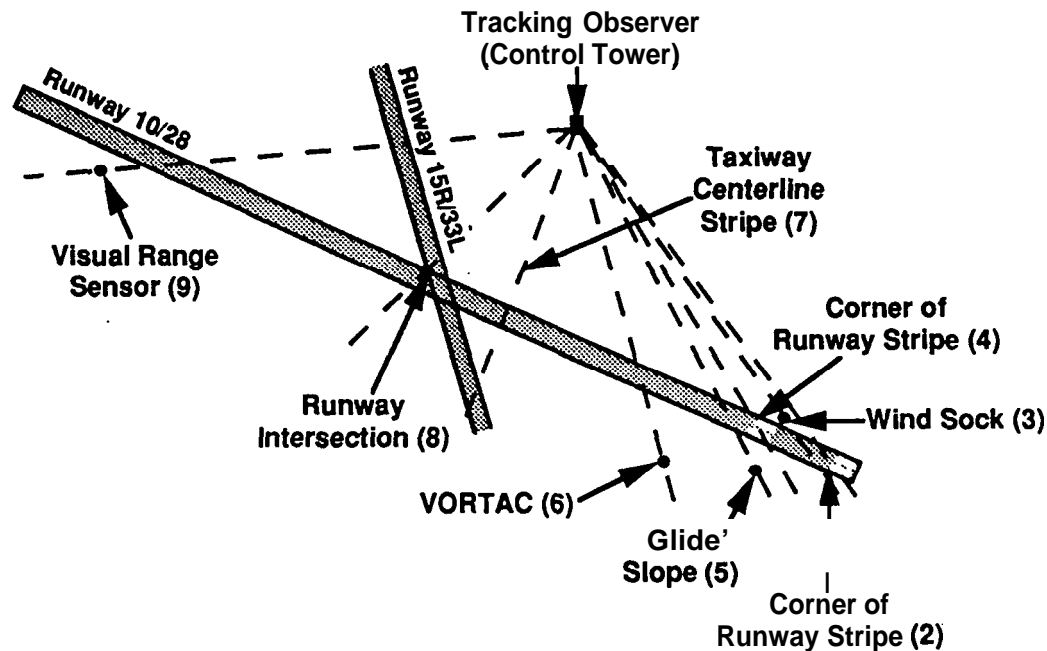


FIGURE 10. VISUAL CURS USED FOR AIRCRAFT POSITION TRACKING

2.3.3 Aircraft Position Tracking

Aircraft position tracking was performed by a human observer located in the control tower. The observer logged each aircraft's brake release time and the time the aircraft passed eight easily identifiable landmarks. As the aircraft passed each landmark, the observer pressed one of the nine **number keys** on a laptop computer. Software running in the computer stored the contents of the computer system clock (to the nearest **0.01** second) in a database **file** each time a numeric key was struck. The **"1"** key was used to signal brake release. The **"2"** through **"9"** keys were used to log the times when the aircraft passed the visual cues shown in Figure 10. The **"0"** key was used to **log the liftoff time**. If the observer felt a mistake had been made at any point during a takeoff, the entire run was deleted (except for the brake release time) by pressing the "delete" key.

The computer clock was time-synchronized to a master clock at both the beginning and end of each measurement session by first configuring the DOS prompt to display the computer system clock to the nearest **0.01** second. To perform a calibration, the "Enter" key was pressed in sync with the second change on the master clock **16** to **20** times in succession. The average difference between the system clock time and the master clock time was used as an adjustment factor to correct all of the tracking data to master clock time. As an experiment to determine the accuracy of this time calibration method, ten such calibrations were performed back-to-back within a very brief period. The results of the experiment showed a total range of only **0.13** seconds in calculated adjustment factors across the ten trials.

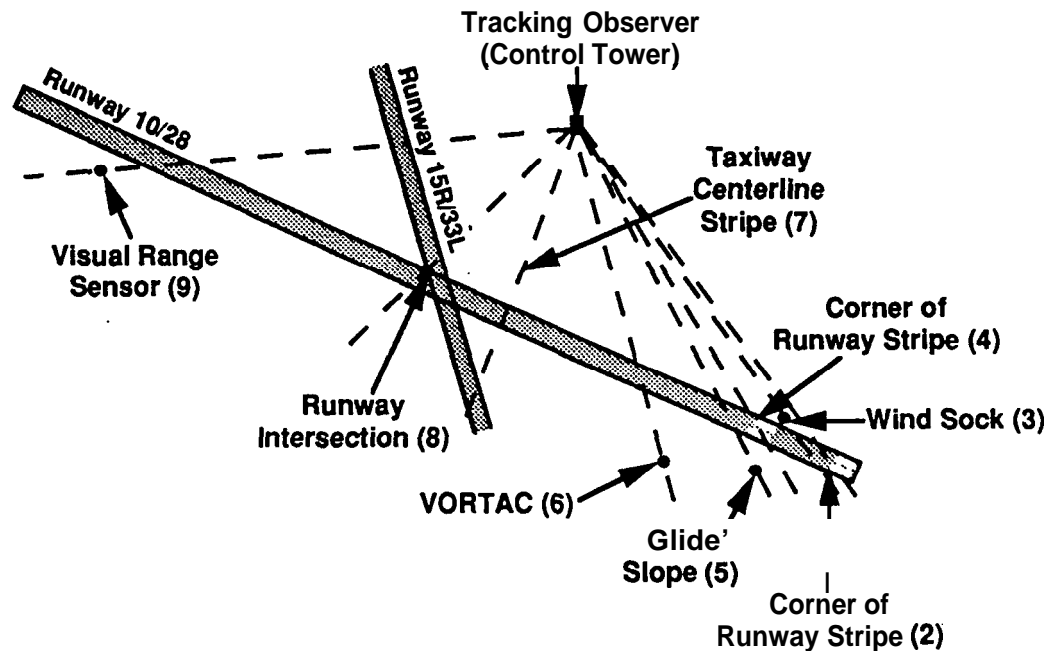


FIGURE 10. VISUAL CURS USED FOR AIRCRAFT POSITION TRACKING

JET TRANSPORT LANDING LOG

HMMH Project #: 291830

[illegible]

17

2.3.5 General Atmospheric Conditions

The United States Weather Service maintains weather sensors located atop the **BWI** control tower. Hourly tabulations of sensor readings were made available by the Weather Service on Form **MF1-10A**, "Surface Weather Observations". The variables of interest on these forms included the time-of-day (to the nearest minute), the visibility in miles, the temperature and dew point in degrees Fahrenheit, the wind speed and direction in miles per hour and tens of degrees, respectively, and the barometric pressure in inches of mercury. With the exception of wind speed and direction, these variables change slowly over time and precise time synchronization is not critical.

2.3.6 Wind Speed and Direction

The wind speed and direction associated with each aircraft noise event was obtained by an independent wind sensor located atop a **10** meter pole. The sensor was located approximately **25** feet from monitor site **1**.

The sensor was an **R.M. Young** model **5305** Wind Monitor. The sensor has a wind threshold starting speed of **0.9** miles per hour, and the vane orients within 5 degrees in winds of only **1.6** miles per hour. The two outputs from the sensor were connected to an **R.M. Young** signal conditioner, and the outputs of the signal conditioner were connected to two channels of a Remote Measurement Systems, Inc. Model **ADC-1** Analog-to-Digital converter. This battery powered converter provides an **RS-232** output which was connected to a battery powered laptop computer. The computer sampled the voltages from the sensor every 2 seconds and stored the readings directly on floppy disk. Figure **13** provides a schematic diagram of the wind monitor set-up.

Speed calibration was performed at the factory (**1** volt = **100** miles per hour). With an A-D converter resolution of **0.0001** volts, the resolution of the speed measurement was **0.01** miles per hour (probably more accurate than the instrument itself). Azimuth calibration was performed in the field using a photographic technique. A wooden stick was attached to the **10** meter pole and its direction was established to the nearest degree using a good quality magnetic compass. At periodic intervals, photographs were taken looking straight up from the bottom of the **10** meter pole. The photographs showed the reference stick as well as the direction sensor vane. The instant the photograph was taken the sensor voltage was also recorded. From the photographs, the magnetic heading of the vane could be determined, and these headings were plotted against the voltage measurements to provide a relationship between voltage and direction (the magnetic headings were ultimately converted to Maryland State Plane Coordinate System grid north by taking compass readings between objects whose state plane coordinates were known).

2.4 Videotape of Taxi Operations and Start of Roll

During the December measurements a continuous videotape was made of aircraft taxiing from gate positions to the runway threshold. The video camera was mounted on the handrail of the control tower catwalk which surrounded the tower. The camera was aimed in a general southwesterly direction. The field of view is shown in Figure **14**. The camera was a Sony Model **TR-06 8mm** Camcorder. This camera was selected because it provided a cost-effective means for encoding date and time on the videotape itself. This model allows date or time (but not both simultaneously) to be displayed in the lower righthand corner of the frame.

At the beginning of each **2-hour** tape the date is displayed. For the remainder of the tape the **time-of-day** is displayed (to the nearest second). The camcorder clock was set to within one second of the master clock at the beginning of each measurement day. This clock proved to be extremely stable and was maintained within one second of the master clock at all times. The 8 mm tapes were copied to **VHS** format and supplied to **VNTSC**.

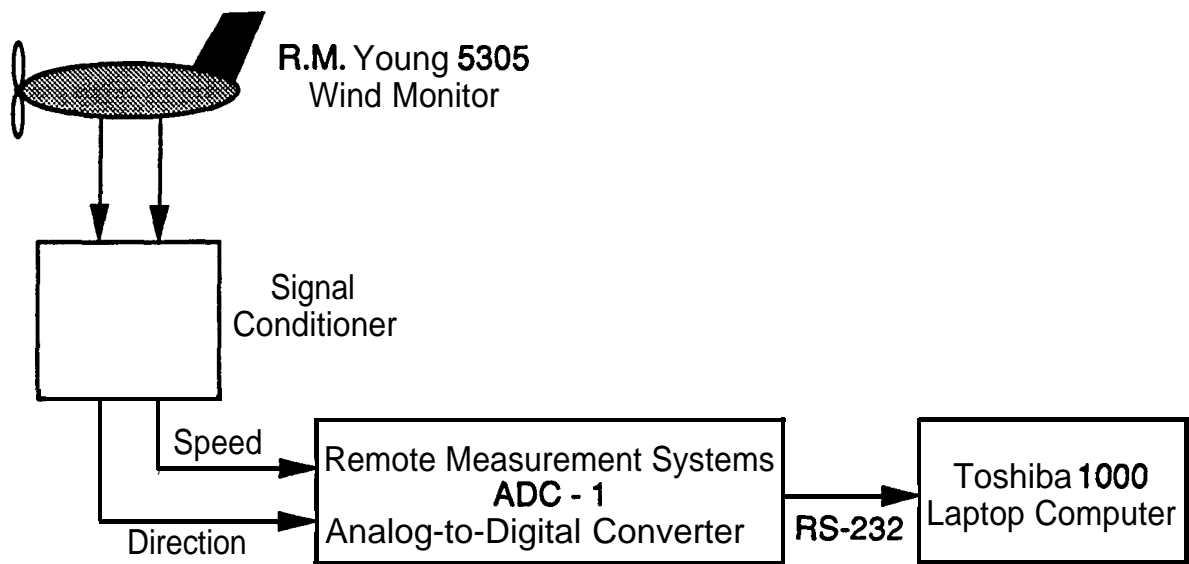


FIGURE 13. BLOCK DIAGRAM OF WIND SENSOR DATA ACQUISITION SYSTEM

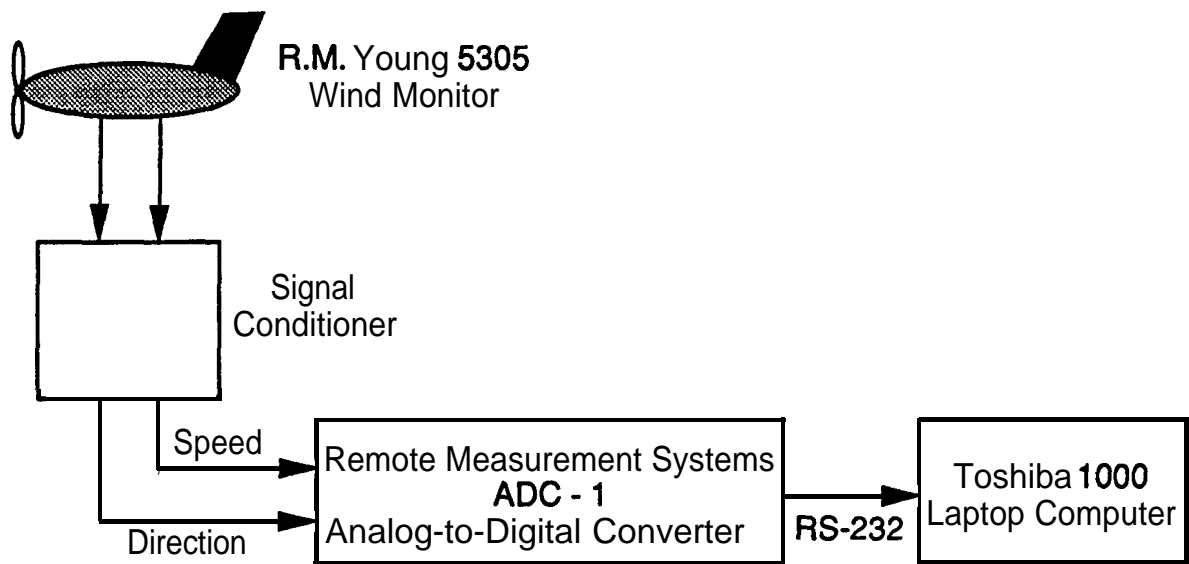


FIGURE 13. BLOCK DIAGRAM OF WIND SENSOR DATA ACQUISITION SYSTEM

3. DATA REDUCTION

Data reduction followed a four phase process. In the first phase each independent data source was committed to machine readable form (if it was not acquired that way) and calibration information was compiled to perform any needed time and sound pressure level adjustments. In the second phase, the data were brought together into a database format, with one record for each jet aircraft departure. During the third phase, **SELs** for each departure were computed from the measured sound level time history. For project management purposes the data from each measurement day were kept in separate files during these first three phases. In the fourth phase, the data from all days were brought together into a single database. The four subsections below (3.1 through 3.4) discuss these four phases.

3.1 Initial Processing of Individual Data Sources

Upon return from the field all data (acoustic, observer logs, atmospheric readings, etc.) were committed to ASCII text files. The details for each data source are described in the following paragraphs.

3.1.1 Acoustic Data

Acoustic data extracted from the noise monitors were written to individual disk files as continuous streams of A-weighted sound levels for each site-day of measurement. Using the timing calibration information discussed in Section 2.3.1, each file was processed to determine the true start time of each time history (to the nearest 0.1 second) and the true inter-sample period (nominally 0.5 seconds, but calculated to 6 decimal places based on beginning- and end-of-day timing calibration with measurement accuracy better than 0.2 in 40,000 seconds, or 1 part in 200,000).

Due to a misunderstanding of how the Larson-Davis 870 noise monitor reacts to a calibration request while data sampling is in progress, time synchronization was lost during some October measurement days at a few sites. Table 4 summarizes the acoustic data acquisition status at each site by showing those days when data were acquired, and whether the time synchronization of the acoustic data to the tracking data is reliable. A lack of time synchronization, however, does not affect the acoustic data quality or the ability to associate the correct aircraft movement with a noise event.

Sound level amplitude calibration was performed using a single adjustment factor for each instrument-day of data. This strategy was chosen because the observed differences between all of the on-site calibrations for any given instrument-day were 0.4 decibel or less, and no justifiable basis could be found for a time-of-day dependent adjustment factor which would enhance the measurement accuracy. Both the clock and sound level calibration factors were placed in a single ASCII text file for each site-day of measurements.

3.1.2 Aircraft Data

Each day's Jet Transport Observer Log (Figure 9) was committed to an ASCII text file by hand typing the information into a commercially available spreadsheet. These data were retained both as spreadsheet files as well as ASCII text files.

The daily spreadsheets were combined into a single spreadsheet in order to obtain a unique list of all aircraft (by registration number) which had been observed over the nine measurement days. This list was sent to the FAA Office of Environment and Energy via VNTSC to confirm the observed aircraft type as well as obtain the installed engine type and model. Upon return from FAA this master list was double-checked for completeness and consistency and became the basis for tagging the measured takeoffs with aircraft and engine types.

3. DATA REDUCTION

Data reduction followed a four phase process. In the first phase each independent data source was committed to machine readable form (if it was not acquired that way) and calibration information was compiled to perform any needed time and sound pressure level adjustments. In the second phase, the data were brought together into a database format, with one record for each jet aircraft departure. During the third phase, **SELs** for each departure were computed from the measured sound level time history. For project management purposes the data from each measurement day were kept in separate files during these first three phases. In the fourth phase, the data from all days were brought together into a single database. The four subsections below (3.1 through 3.4) discuss these four phases.

3.1 Initial Processing of Individual Data Sources

Upon return from the field all data (acoustic, observer logs, atmospheric readings, etc.) were committed to ASCII text files. The details for each data source are described in the following paragraphs.

3.1.1 Acoustic Data

Acoustic data extracted from the noise monitors were written to individual disk files as continuous streams of A-weighted sound levels for each site-day of measurement. Using the timing calibration information discussed in Section 2.3.1, each file was processed to determine the true start time of each time history (to the nearest 0.1 second) and the true inter-sample period (nominally 0.5 seconds, but calculated to 6 decimal places based on beginning- and end-of-day timing calibration with measurement accuracy better than 0.2 in 40,000 seconds, or 1 part in 200,000).

Due to a misunderstanding of how the Larson-Davis 870 noise monitor reacts to a calibration request while data sampling is in progress, time synchronization was lost during some October measurement days at a few sites. Table 4 summarizes the acoustic data acquisition status at each site by showing those days when data were acquired, and whether the time synchronization of the acoustic data to the tracking data is reliable. A lack of time synchronization, however, does not affect the acoustic data quality or the ability to associate the correct aircraft movement with a noise event.

Sound level amplitude calibration was performed using a single adjustment factor for each instrument-day of data. This strategy was chosen because the observed differences between all of the on-site calibrations for any given instrument-day were 0.4 decibel or less, and no justifiable basis could be found for a time-of-day dependent adjustment factor which would enhance the measurement accuracy. Both the clock and sound level calibration factors were placed in a single ASCII text file for each site-day of measurements.

3.1.2 Aircraft Data

Each day's Jet Transport Observer Log (Figure 9) was committed to an ASCII text file by hand typing the information into a commercially available spreadsheet. These data were retained both as spreadsheet files as well as ASCII text files.

The daily spreadsheets were combined into a single spreadsheet in order to obtain a unique list of all aircraft (by registration number) which had been observed over the nine measurement days. This list was sent to the FAA Office of Environment and Energy via VNTSC to confirm the observed aircraft type as well as obtain the installed engine type and model. Upon return from FAA this master list was double-checked for completeness and consistency and became the basis for tagging the measured takeoffs with aircraft and engine types.

independent variables for each aircraft departure as well as the calculated dependent variables such as maximum A-level and **SEL**. Five time history databases (one for each measurement site) contain the **0.5** second A-weighted sound levels. The rows of the database structure are individual jet transport takeoffs. The columns are the measured variables. In order to manage the data reduction process most **efficiently**, separate databases were maintained for each measurement day. A detailed description of these databases is provided in Appendix C.

3.2.1 Master Database

Stepping through the Jet Transport Observer Log one entry at a time, the algorithm used to generate the master database worked as follows. First, all of the data appearing in this log were loaded into the database. Second, the aircraft registration number was used to look up the FAA verified aircraft and engine type and place these variables in the database. Third, the aircraft tracking file was searched to find a brake release time which matched within plus or minus **10** seconds of the Jet Transport Observer Log brake release time. If a successful match was found, the tracking times were added to the database, otherwise the tracking time entries in the database were left blank.

All the remaining data were brought into the database using time-of-day as the lookup parameter. Since brake release time was independently logged by two observers (jet transport observer and the aircraft tracking observer) an overall review of the data was made to determine which of the two was generally the more accurate for determining the actual start of roll. The results of this review strongly suggested the tracking time to be the more accurate: Therefore, if a tracking time match was found, the brake release time from this source was used, otherwise, the Jet Transport Observer Log time was used.

Using the brake release time, the National Weather Service data variables were brought into the spreadsheet. The values were determined by finding the hourly observations which immediately preceded and succeeded the brake release time and then performing a linear interpolation using time as the interpolating variable.

The brake release time was also used to enter the time history of wind speed and direction to compute a **2-minute** average wind vector (beginning at brake release and continuing for 2 minutes thereafter). The averaging process resolved each speed and direction reading (acquired every 2 seconds) into X and Y components, averaged the X and Y components separately, and then converted the X and Y components back to a speed and direction.

The brake release time was also used to search for potential sources of acoustic interference: the Jet Transport Observer Log itself (for other takeoffs which immediately preceded or followed the one in question), the Jet Transport Landing Log, and the G/A Runway Observer Log. Any log entries which occurred **60** seconds prior to brake release and up to **150** seconds after brake release were brought into the database.

Cells were also built into the database to contain the maximum A-weighted sound levels and **SELs** from each of the five measurement sites. These values were subsequently calculated by a separate computer program and inserted into the cells.

3.2.2 Acoustic Databases

The brake release time was also used to build the five acoustic databases by searching the continuous time history files of each measurement site. From each file, **420 1/2-second** sound levels (**210** seconds) were extracted and placed in the appropriate acoustic database. The extracted portion of the time history started **60** seconds before brake release and continued until **150** seconds after brake release. The exact **time-of-day** of the first sample in the series was placed at the **beginning** of the record, followed by the instrument sampling rate in samples per hour (nominally **7200**).

3.3 Computation of Noise Metrics and Insertion in Master Database

The anticipated low signal-to-noise ratios that precluded automated acquisition of **SELs** and maximum A-weighted sound levels in the field also precluded complete automation during laboratory data reduction. An initial inspection of the A-level time histories revealed the need for human interaction in the computation of these two noise metrics. In particular, the following computational requirements were established:

- Subtract the estimated background noise from the measurements,
- Select the temporal integration period based on the following criteria:
 - a) **bracket** the acoustic energy from only the takeoff in question,
 - b) **brackets** all of the energy from the takeoff in question (especially time histories which exhibit more than one localized maximum sound level and separated by as much as **20** or **30** seconds),
 - c) **significant** acoustic energy from any interference source.

Figure 16 shows a block diagram of the computer assisted process used to compute the **SEL** and maximum A-weighted sound level values. Using the master database and the five sound level time history databases as input, a special purpose computer program displayed the time histories and other pertinent information of each event to the user. The user identified the temporal portions of each of the five time histories appropriate for computation of the metrics. The metric values were then calculated and added to the master database.

Figure 17 shows the interactive screen interface presented to the user for each takeoff. The screen is divided into six panels. From top to bottom, the top five panels show the A-weighted sound level time histories from measurement sites 1 through **5**, respectively. The bottom panel presents information on potential acoustic interference. The horizontal axis displays time, in seconds, from **60** seconds before brake release to **150** seconds after. The **graticule** tic marks are spaced horizontally at **30** seconds per division. The vertical axis of the five sound level panels is the “slow”, A-weighted sound level. In the vertical, the **graticule** tic marks are spaced at **10** decibels per division. Each panel displays the top **30** decibels of the time history. The maximum A-weighted sound level is displayed at the top left of each panel.

At the right of each panel are three **SEL** values labeled **SEL10**, **SEL15**, and **SEL20**. These values are the integrated A-weighted energy over the top **10**, **15** and **20** decibels, respectively, of the time history. The **SEL** computed over the top **20** decibels of the signal typically captures all but the last **0.1** decibel of energy in typical aircraft noise signatures. As such, it is the metric of choice in this study. In many cases, however, there is insufficient dynamic range between the background sound level and the maximum A-level of the event to integrate **20** decibels down from the maximum without including a considerable amount of background noise. A solution to this problem involves integrating over only **10** or **15** decibels (whatever the signature will allow) and then adding a small, empirically derived adjustment to estimate the complete energy found in the top **20** decibel integration. This process is discussed more fully in Section 4.

The computer program itself did not attempt to determine whether any or all of the three integrals were valid. This **judgement** was left to the user who provided the Y or N votes shown to the right of the **SELs**. In order to subtract any background noise effect, the operator also estimated the background noise level during each event. This estimate is displayed on the screen directly below each **SEL20**. In order to maximize the speed and accuracy with which this estimate could be made, the operator used the **graticules** in the display to estimate how many decibels down from the maximum the background noise lay. The very beginnings and ends of the time history provided the basis for background level estimation. The computer program then performed the numerical calculations to convert this easily read value to actual sound level, and then to energy subtract this value from the individual sound levels.

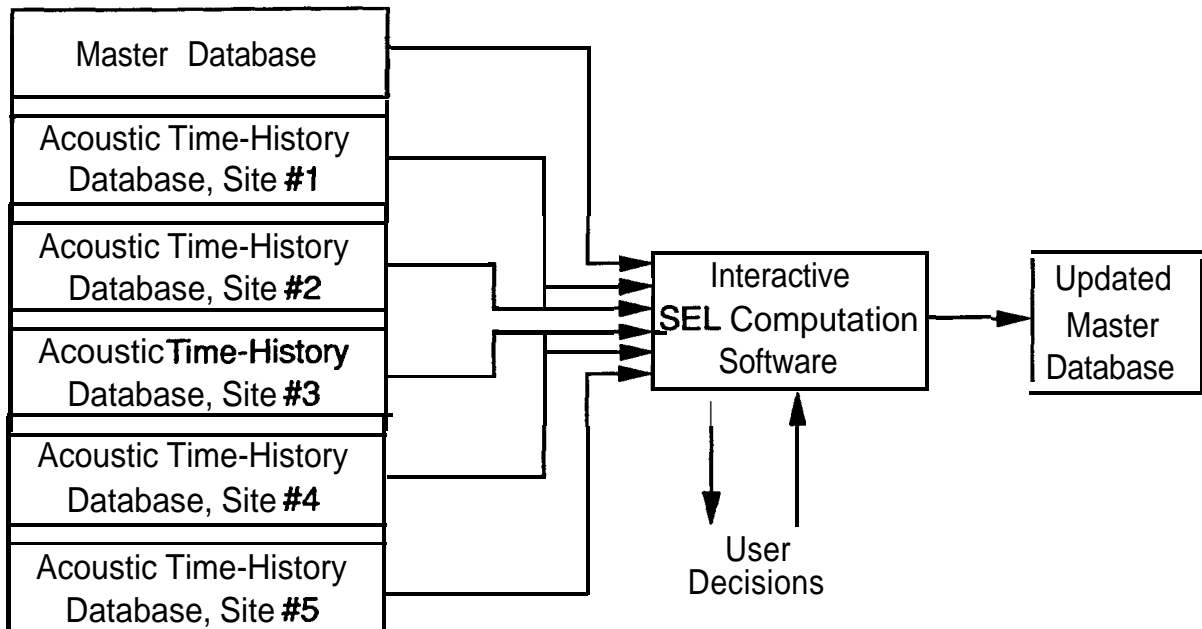


FIGURE 16. BLOCK DIAGRAM OF SOUND LEVEL METRIC COMPUTATION PROCESS

Moveable cursors (independently adjustable for each site) were used by the operator to window a portion of the time history. The window limited the temporal bound of the **SEL** as well as maximum A-level calculation. In setting the cursors, the operator not only used the noise level time history itself as a guide, but also referred to the interference information shown in the bottom panel of the screen.

Colored circles on the four lines of the interference panel indicate the times when interference events occurred. The second line in this panel, labeled "**JTO**" displays the time of all jet transport takeoffs, including the one in question which occurs at **T=0** seconds. For example, if two takeoffs occurred only **40** seconds apart, there is a good chance that they have acoustically interfered with each other and neither is usable. On the other hand, it may be possible that the top **10** decibels of the signal have not been corrupted even though the top **15** and **20** decibels have. In this case, **SELs** would be calculated, with a "**Y**" vote given to **SEL10**, and "**N**" votes given to **SEL15** and **SEL20**.

The first line in the acoustic interference panel, labeled "**LND**" displays the touchdown times of landings on all runways. Color coding was used to identify the runway (red for runway **28**, yellow for runway **33L**, and white for runway **33R**). The third line, labeled "**PTO**" shows all propeller aircraft takeoffs. Start-of-roll for any propeller aircraft operating on Runway **33R** is indicated here. This information is of special importance for interpreting the sound levels recorded at sites 1 and 2. The last line of the panel, labeled "**OPR**", shows the times when there was any kind of activity on the general aviation **taxiway**, all the way up to and including turning onto the runway.

All of the information shown on the screen is stored in the master database. For each measurement site this includes the maximum A-level, the three **SELs**, the three Y/N votes, the

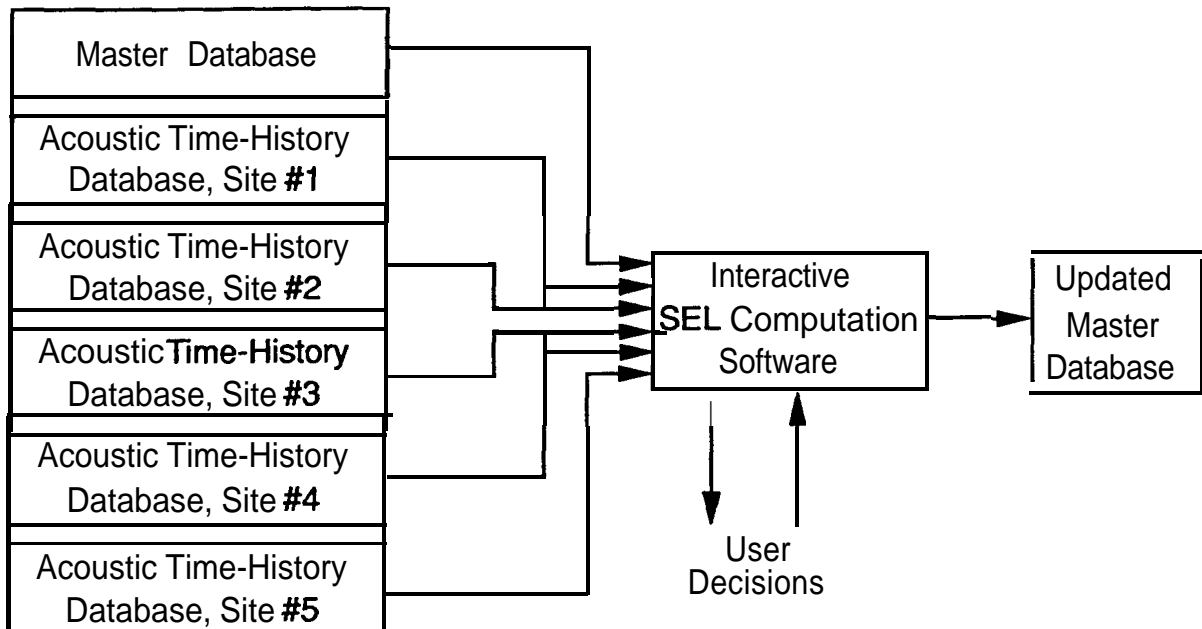


FIGURE 16. BLOCK DIAGRAM OF SOUND LEVEL METRIC COMPUTATION PROCESS

Moveable cursors (independently adjustable for each site) were used by the operator to window a portion of the time history. The window limited the temporal bound of the **SEL** as well as maximum A-level calculation. In setting the cursors, the operator not only used the noise level time history itself as a guide, but also referred to the interference information shown in the bottom panel of the screen.

Colored circles on the four lines of the interference panel indicate the times when interference events occurred. The second line in this panel, labeled "**JTO**" displays the time of all jet transport takeoffs, including the one in question which occurs at **T=0** seconds. For example, if two takeoffs occurred only **40** seconds apart, there is a good chance that they have acoustically interfered with each other and neither is usable. On the other hand, it may be possible that the top **10** decibels of the signal have not been corrupted even though the top **15** and **20** decibels have. In this case, **SELs** would be calculated, with a "**Y**" vote given to **SEL10**, and "**N**" votes given to **SEL15** and **SEL20**.

The first line in the acoustic interference panel, labeled "**LND**" displays the touchdown times of landings on all runways. Color coding was used to identify the runway (red for runway **28**, yellow for runway **33L**, and white for runway **33R**). The third line, labeled "**PTO**" shows all propeller aircraft takeoffs. Start-of-roll for any propeller aircraft operating on Runway **33R** is indicated here. This information is of special importance for interpreting the sound levels recorded at sites 1 and 2. The last line of the panel, labeled "**OPR**", shows the times when there was any kind of activity on the general aviation **taxiway**, all the way up to and including turning onto the runway.

All of the information shown on the screen is stored in the master database. For each measurement site this includes the maximum A-level, the three **SELs**, the three Y/N votes, the

3.4 Merging of Daily Master Databases

In order to perform the analyses described in Section 4, the nine daily databases were combined into one large spreadsheet. The size of the spreadsheet was made more manageable by eliminating events where no **SELs** were calculated, and by eliminating a number of columns where data was of little interest (eg. graphic cursor positions).

At this point, average differences of **SEL20** minus **SEL15**, and **SEL20** minus **SEL10** were calculated using all data (independent of aircraft type weather condition, etc.) where "Y" votes could be found on both members of the pair. The empirically derived differences are:

Comparison	Empirical Difference	Theoretical Difference
SEL20 - SEL10	0.70 dB	0.40 dB
SEL20 - SEL15	0.16 dB	0.11 dB

As a point of comparison, theoretical differences were also calculated. The theoretical differences are based on a triangular time history of constant rise and decay rates (although the rise rate need not be the same as the decay rate). The theoretical and empirical differences agree well, and it is not surprising that the empirical values exceed slightly the theoretical ones since the actual signal decay often contained a second peak which added more energy than embodied in the theoretical consideration.

As a further matter of convenience, the data were split into five separate spreadsheets, one for each measurement site. At this level, data could be quickly sorted and analyzed to show trends and prepare summary graphics.

4. DATA ANALYSIS AND RESULTS

This section of the report provides an overview of types of analyses performed and presents the results.

4.1 Summary of Independent Variables

This subsection describes the of ranges of observed independent variables.

4.1.1 Aircraft Related Parameters

Thirty-eight different jet transport aircraft/engine type combinations were observed during the field measurements. Table 5 identifies these combinations and provides summary statistics on each. The first and second columns in the table list the aircraft and engine type, respectively. The third column lists the total number of movements observed during the measurements. The fourth column shows the number of movements where an **SEL** could be calculated at at least one of the five measurement sites. The fifth column shows the average gross weight for the aircraft/engine combination across all observed aircraft. The last column lists the average gross weight for the data subset where an **SEL** could be calculated at at least one of the five measurement sites.

The data presented in Table 5 suggest five aircraft categories with sufficient numbers of datapoints for performing the noise level analyses of this study. They are:

B727-100/200
B737-200
B737-300/400
DC9-14/15/31/32/33/51
MD81/82/88

The **B727-100/200** aircraft showed a nearly even distribution of engine types between the **JT8D-7**, **-9**, **-15**, and **-17** engines. Of the **B737-200** aircraft, one-quarter were equipped with the **JT8D-9** engine, and three-quarters were equipped with the **-15** engine. For the **B737-300/400** aircraft, one-quarter of the aircraft (from which **SELs** could be calculated) were observed with the **CFM56-3B-1** engine and the remaining three-quarters were equipped with the **-2** engine. The vast majority of **DC9** aircraft were equipped with the **JT8D-7** engine (**75%**), with lesser numbers equipped with the **-9** engine (**20%**) and **-17** engine (**5%**). **MD80** aircraft were almost equally split between the **82** and **88** series, with the **81** series constituting only about **5%** of the sample.

The **B737-300/400** aircraft suffered the highest data mortality rate of any of the five groups in the sense that **SELs** could only be calculated for about **20** percent of the aircraft movements. Two situations arose which lead to the data loss, but the underlying cause was the substantially lower sound levels emitted by this aircraft than any of the others. First, the lower sound level resulted in very low signal-to-noise ratios at the measurement sites (often less than **10** decibels between the maximum A-weighted sound level and the nominal **50 dB[A]** background level). This limited the number of events from which **SELs** with acceptable levels of uncertainty could be calculated. Second, back-to-back departures (separated by **90** seconds or less), where either the preceding or following noise event resulted from a higher noise level aircraft, resulted in contamination of the **B737-300/400** event.

4. DATA ANALYSIS AND RESULTS

This section of the report provides an overview of types of analyses performed and presents the results.

4.1 Summary of Independent Variables

This subsection describes the of ranges of observed independent variables.

4.1.1 Aircraft Related Parameters

Thirty-eight different jet transport aircraft/engine type combinations were observed during the field measurements. Table 5 identifies these combinations and provides summary statistics on each. The first and second columns in the table list the aircraft and engine type, respectively. The third column lists the total number of movements observed during the measurements. The fourth column shows the number of movements where an **SEL** could be calculated at at least one of the five measurement sites. The fifth column shows the average gross weight for the aircraft/engine combination across all observed aircraft. The last column lists the average gross weight for the data subset where an **SEL** could be calculated at at least one of the five measurement sites.

The data presented in Table 5 suggest five aircraft categories with sufficient numbers of datapoints for performing the noise level analyses of this study. They are:

B727-100/200
B737-200
B737-300/400
DC9-14/15/31/32/33/51
MD81/82/88

The **B727-100/200** aircraft showed a nearly even distribution of engine types between the **JT8D-7**, **-9**, **-15**, and **-17** engines. Of the **B737-200** aircraft, one-quarter were equipped with the **JT8D-9** engine, and three-quarters were equipped with the **-15** engine. For the **B737-300/400** aircraft, one-quarter of the aircraft (from which **SELs** could be calculated) were observed with the **CFM56-3B-1** engine and the remaining three-quarters were equipped with the **-2** engine. The vast majority of **DC9** aircraft were equipped with the **JT8D-7** engine (**75%**), with lesser numbers equipped with the **-9** engine (**20%**) and **-17** engine (**5%**). **MD80** aircraft were almost equally split between the **82** and **88** series, with the **81** series constituting only about **5%** of the sample.

The **B737-300/400** aircraft suffered the highest data mortality rate of any of the five groups in the sense that **SELs** could only be calculated for about **20** percent of the aircraft movements. Two situations arose which lead to the data loss, but the underlying cause was the substantially lower sound levels emitted by this aircraft than any of the others. First, the lower sound level resulted in very low signal-to-noise ratios at the measurement sites (often less than **10** decibels between the maximum A-weighted sound level and the nominal **50 dB[A]** background level). This limited the number of events from which **SELs** with acceptable levels of uncertainty could be calculated. Second, back-to-back departures (separated by **90** seconds or less), where either the preceding or following noise event resulted from a higher noise level aircraft, resulted in contamination of the **B737-300/400** event.

FIGURE 5 (CON'T). OBSERVED AIRCRAFT/ENGINE TYPES AND GROSS WEIGHTS

Aircraft Type	Engine Type	Number of Aircraft		Average Weight (Lbs)	
		Total Observed	w/SEL	Total Observed	w/SEL
DC9	(N/A)	5	5	93,705	93,705
DC9-14	JT8D-7	1	1	79,811	79,811
DC9-15MC	JT8D-7	1	0	---	---
DC9-15RC	JT8D-7	2	2	---	---
DC9-31	JT8D-7	48	42	91,197	91,637
DC9-31	JT8D-9	6	5	88,096	88,096
DC9-31	JT8D-9A	7	6	88,665	88,311
DC9-32	JT8D-7B	1	1	98,774	98,774
DC9-32	JT8D-9	1	1	104,042	104,042
DC9-33F	JT8D-9A	1	1	94,184	94,184
DC9-51	JT8D-17	5	3	102,362	103,312
F100	TAY-650-15	22	7	87,957	89,476
F100	(N/A)	2	0	84,272	---
F28-1000	RB183-555-1	14	6	58,746	57,862
F28-4000	RB183-555-1	5	2	60,933	56,531
MD81	JT8D-209	5	2	118,880	110,779
MD82	JT8D-217	18	15	121,781	121,503
MD88	JT8D-219	25	16	125,299	125,310
MD80	(N/A)	5	3	119,129	118,417
MD80	(N/A)	1	1	143,700	143,700

(N/A) = Not Ascertained

4.1.2 Aircraft Position Tracking

The tracking data were spot checked for consistency using a commercially available spreadsheet to plot distance from brake release to each visual cue (see Figure 10) as a function of the time the aircraft passed the cue. A sample plot is shown in Figure 18. On the vertical axis, the plot shows distance from the beginning of the runway to the visual cue (nominal brake release point was 200 to 300 feet from the end). The horizontal axis shows time (in seconds) from start of roll. The diamond shaped datapoints plot the observed data. The solid line through the data points is a third-order regression line fit to all the data points except for the brake release time (which was sometimes difficult to determine with the same temporal precision as the other points). The square datapoint identifies the liftoff point by plotting the observed liftoff time and the regression line estimate of aircraft position. The numbers above the diamond datapoints indicate the number of feet by which the datapoints deviate vertically from the regression line.

The text block in the upper **lefthand** corner of the graph shows the brake release time-of-day and two values calculated from the third-order regression line: **(1)** the distance from the beginning of the runway when the inferred velocity was zero, and **(2)** the time when the inferred velocity was zero.

These data were not analyzed in this study but were made a part of the database for potential future analyses. The excellent fit of the third order curve suggests that detailed analyses of velocity and acceleration could be conducted with a high degree of confidence.

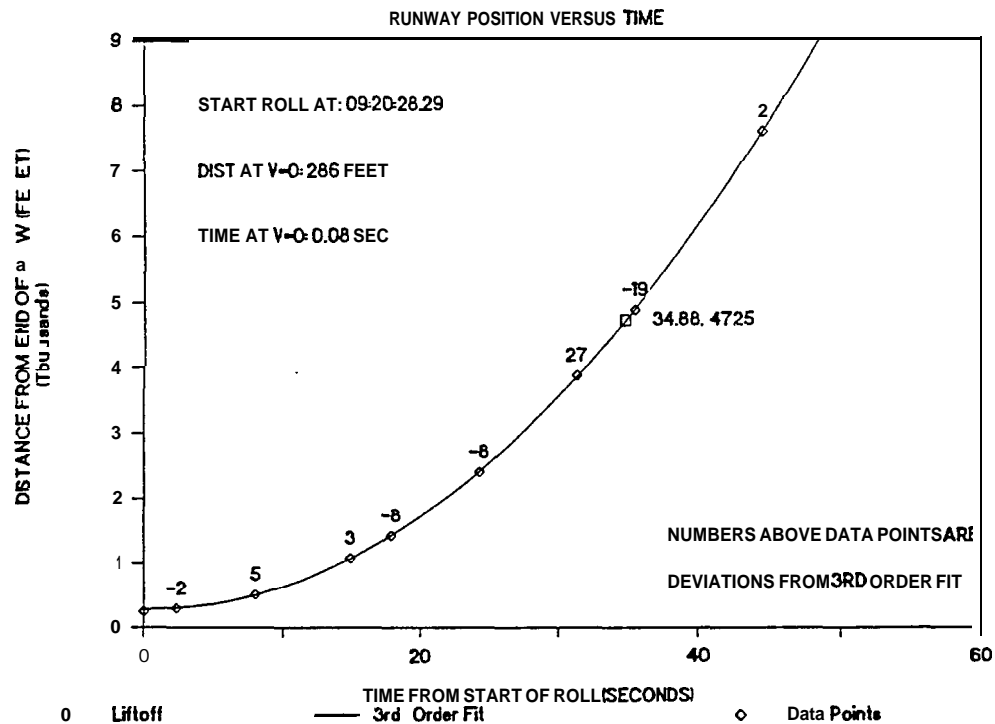


FIGURE 18. REPRESENTATIVE PLOT OF AIRCRAFT POSITION AND TIMING DATA

4.1.3 Weather Conditions

Weather encountered during the course of the measurements covered a broad range of conditions. Barometric pressures ranged from **30.03 to 30.29 inches** of mercury during the October measurements and from **29.75 to 30.67 inches** during the December trip.

Temperatures were mild during the October measurements and ranged **from 50 to 72 degrees Fahrenheit**. Most of the measurements, however, were made in the **60's and low 70's**. In contrast, the December measurements saw considerably lower temperatures, with a range of **22 to 45 degrees**. Most of the December measurements were made from the **high 20's up through 40 degrees**.

The text block in the upper **lefthand** corner of the graph shows the brake release time-of-day and two values calculated from the third-order regression line: **(1)** the distance from the beginning of the runway when the inferred velocity was zero, and **(2)** the time when the inferred velocity was zero.

These data were not analyzed in this study but were made a part of the database for potential future analyses. The excellent fit of the third order curve suggests that detailed analyses of velocity and acceleration could be conducted with a high degree of confidence.

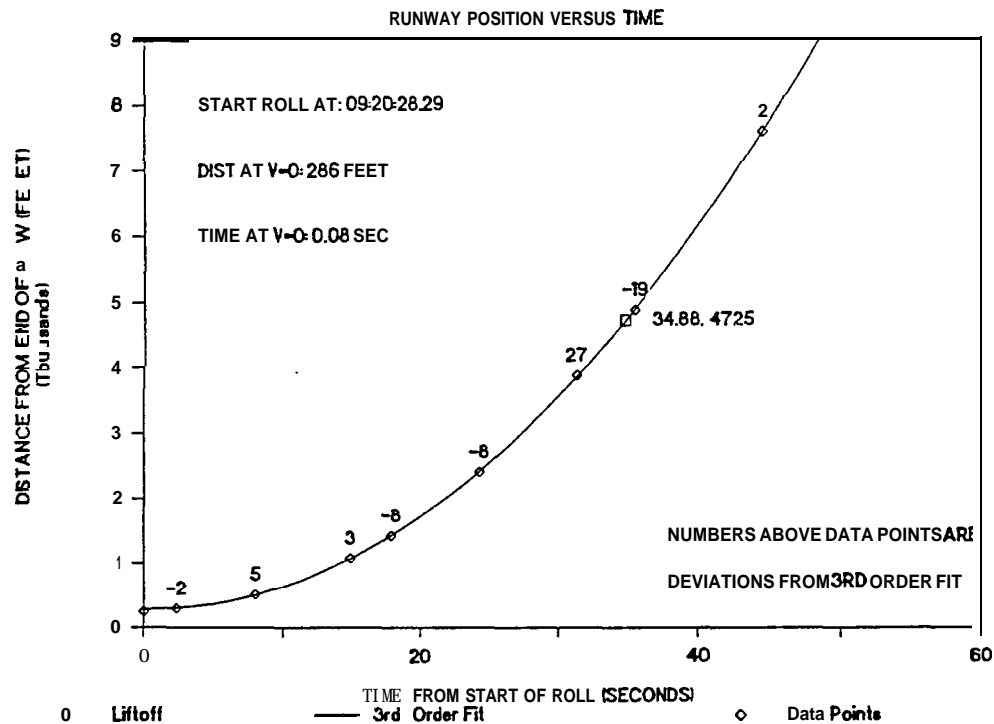


FIGURE 18. REPRESENTATIVE PLOT OF AIRCRAFT POSITION AND TIMING DATA

4.1.3 Weather Conditions

Weather encountered during the course of the measurements covered a broad range of conditions. Barometric pressures ranged from **30.03** to **30.29 inches** of mercury during the October measurements and from **29.75** to **30.67** inches during the December trip.

Temperatures were mild during the October measurements and ranged from **50** to **72** degrees Fahrenheit. Most of the measurements, however, were made in the **60's** and low **70's**. In contrast, the December measurements saw considerably lower temperatures, with a range of **22** to **45** degrees. Most of the December measurements were made from the high **20's** up through **40** degrees.

4.2 Relationships Between Noise Level and Independent Variables

While a rigorous statistical analysis of all of the dependent and independent variables is beyond the scope of this study, a hierarchical analysis of variables historically known to show major effects was undertaken as a part of this work. Those analyses *not* undertaken, but showing some promise of providing useful information, are recommended for future study.

The three independent variables expected to explain the majority of the variance in **SEL** were:

- (1) Measurement Site,
- (2) Aircraft Type, and
- (3) Wind Speed & Direction.

Of major interest was how the **SELs** measured under downwind sound propagation conditions compared with the predictions of **INM Version 3.10**. In order to perform these analyses, all of the data from the nine measurement days was brought into a single spreadsheet where many of the unneeded columns (such as curser positions, interference variables, etc.) were discarded in order to handle the useful data in the most efficient and expeditious manner. The data were then sorted by aircraft type to determine those aircraft types with sufficient amounts of data to undertake the desired analyses. Five aircraft analysis categories were chosen:

B-727:100/200
B-737:200
B-737:300/400
DC-9 (All Models, 10-50)
MD-80 (All Models, 81, 82, 88)

The data were then further sorted by measurement site, and split into **25** smaller spreadsheets (**5** sites by **5** aircraft categories).

4.2.1 Sound Level as a Function of Wind Velocity

Using the runway and measurement site state plane coordinates, the **2-minute** average wind vector associated with each sound level measurement was projected onto a line connecting the reference position on the runway where the maximum A-weighted sound level under downwind conditions was presumed to occur and the measurement site. This **400** foot reference position was chosen because the maximum sound level under downwind conditions at all sites (except site **1**) occurred within a **few** seconds of brake release. Figures **20** through **44** show measured **SEL** (top **20 dB** integrations, *or* estimates thereof) as a function of wind component speed in miles per hour. Positive components indicate downwind sound propagation conditions (the wind component was blowing from *source to receiver*), and negative components indicate upwind sound propagation conditions (wind component blowing from *receiver to source*). In general, the figures report expected trends: downwind conditions yield higher **SELs** than upwind conditions, and downwind propagation **SELs** show no pronounced dependency on speed.

Average *downwind* **SELs** were calculated in each graph by energy averaging the **SELs** with wind speeds of + 1 mile per hour or greater (**+6** miles per hour for site **5**³). The horizontal lines through the data points show these values. The solid portion of the lines indicate the windspeed range over which datapoints were used to compute the energy average **SELs**. The dashed portions of the lines provide a frame of reference for comparing upwind component datapoints with the downwind average values.

³ Discussed at greater length later in this subsection.

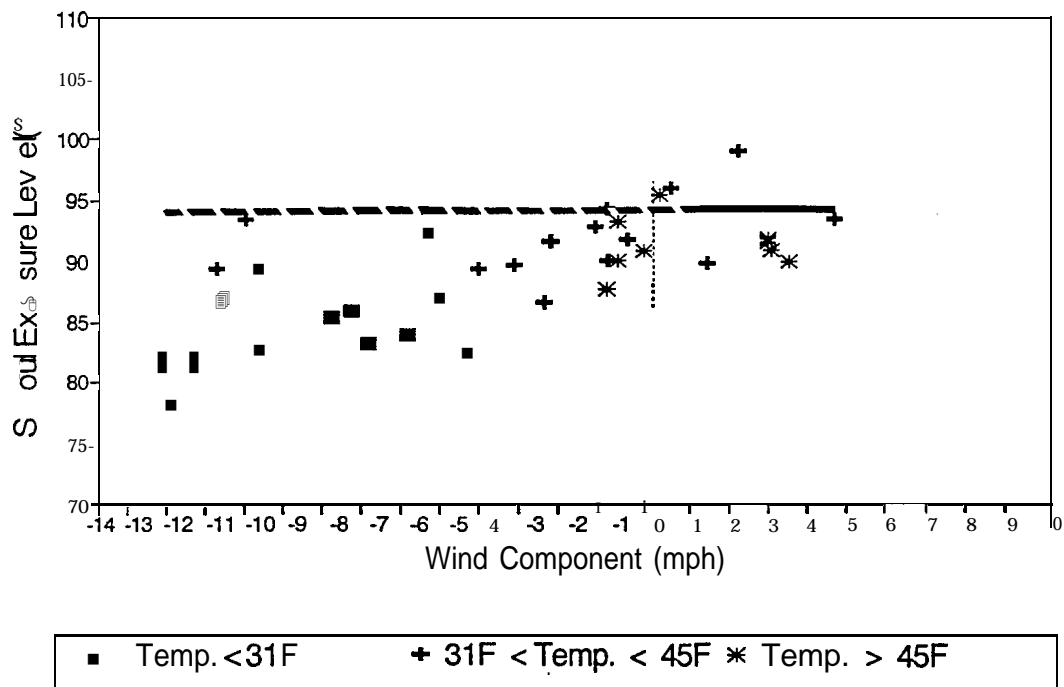


FIGURE 20. SEL VERSUS WIND SPEED FOR B-727:100/200 AT SITE 1

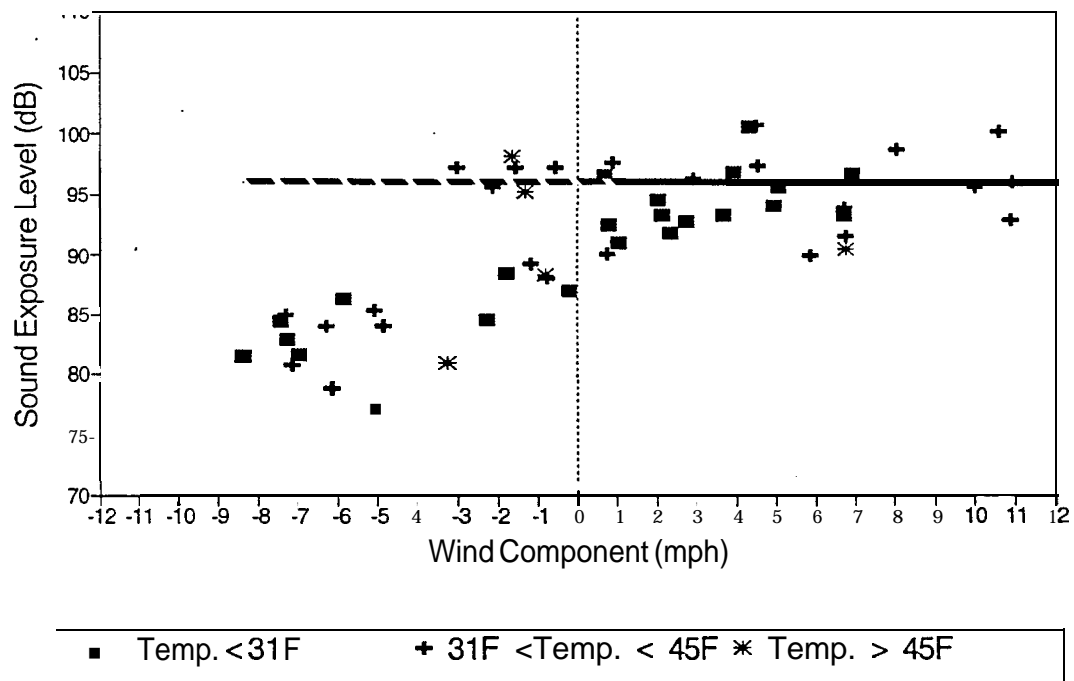


FIGURE 21. SEL VERSUS WIND SPEED FOR B-727:100/200 AT SITE 2

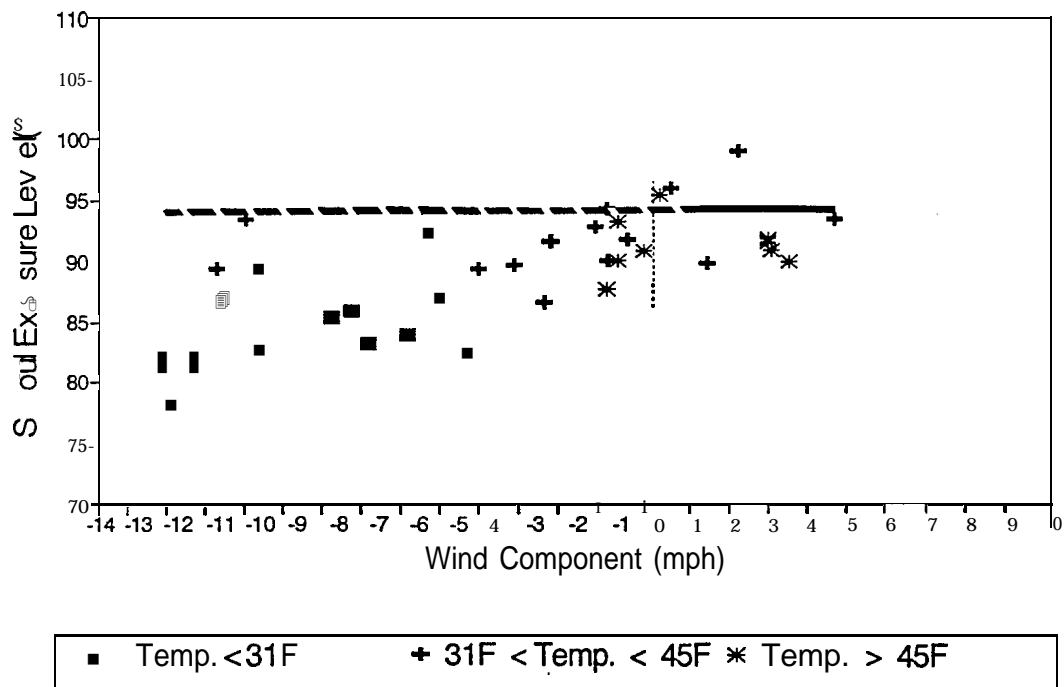


FIGURE 20. SEL VERSUS WIND SPEED FOR B-727:100/200 AT SITE 1

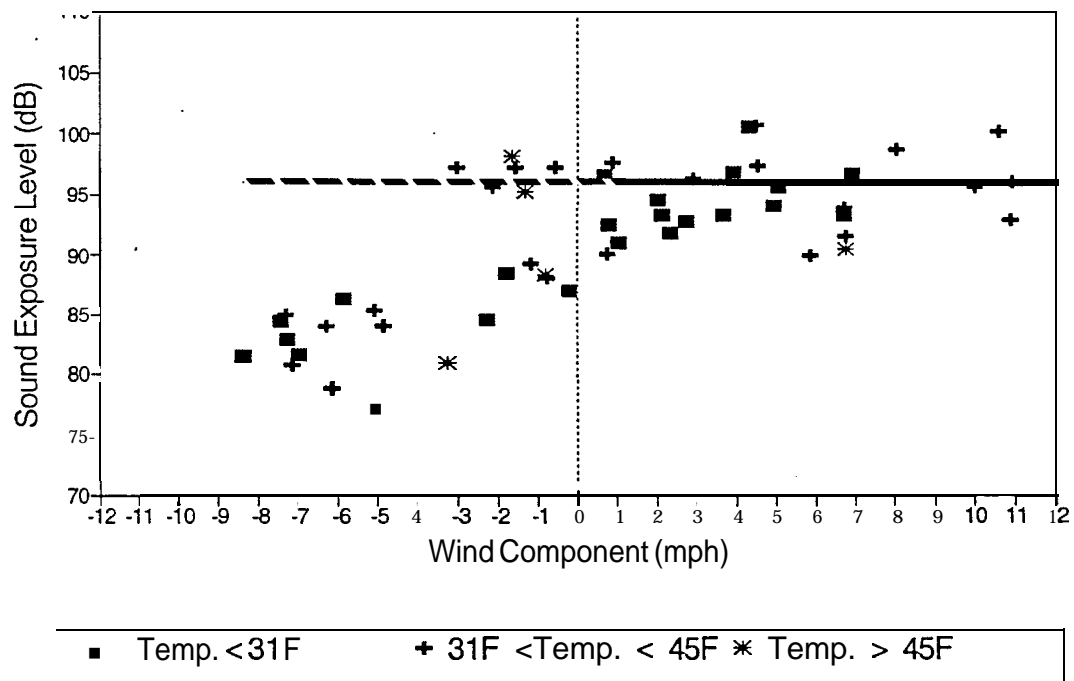


FIGURE 21. SEL VERSUS WIND SPEED FOR B-727:100/200 AT SITE 2

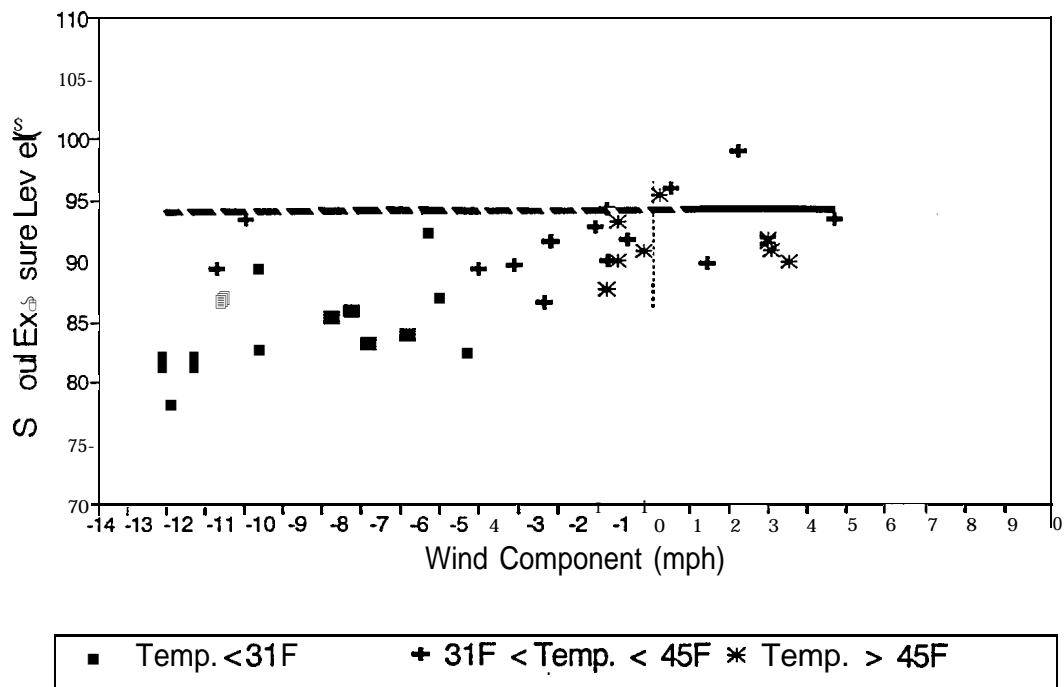


FIGURE 20. SEL VERSUS WIND SPEED FOR B-727:100/200 AT SITE 1

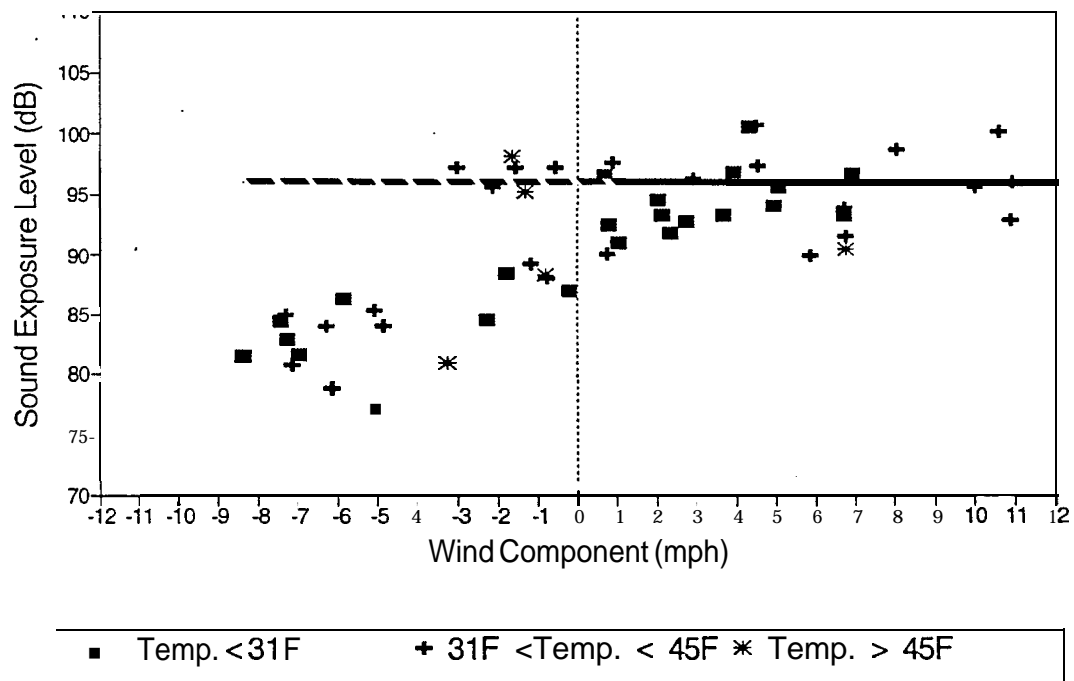


FIGURE 21. SEL VERSUS WIND SPEED FOR B-727:100/200 AT SITE 2

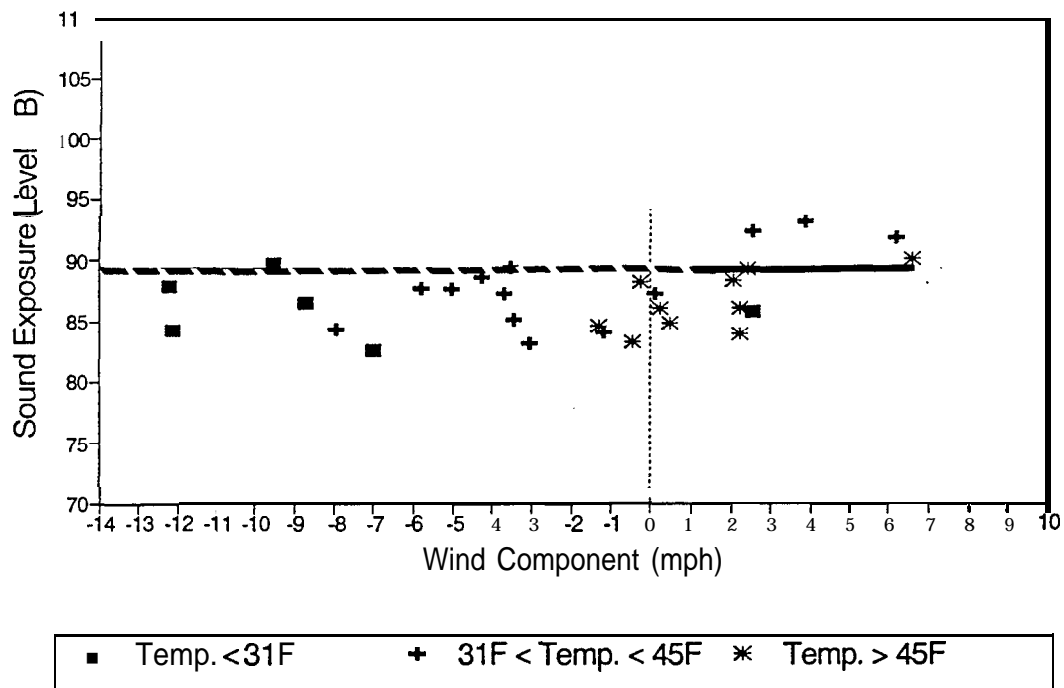


FIGURE 25. SEL VERSUS WIND SPEED FOR B-737:200 AT SITE 1

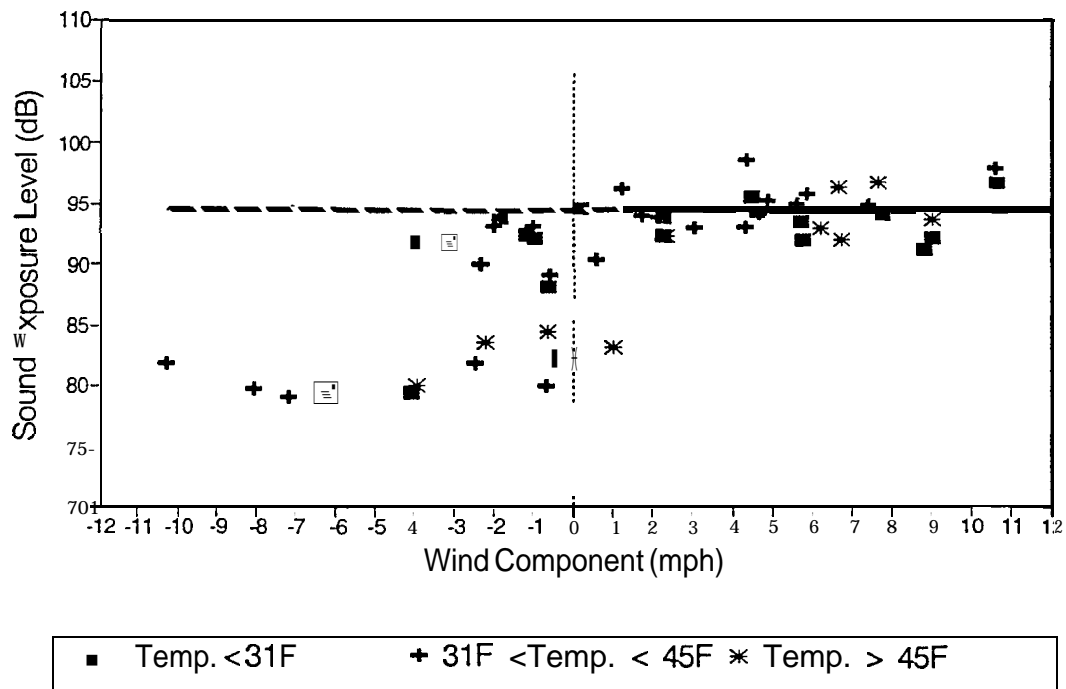


FIGURE 26. SEL VERSUS WIND SPEED FOR B-737:200 AT SITE 2

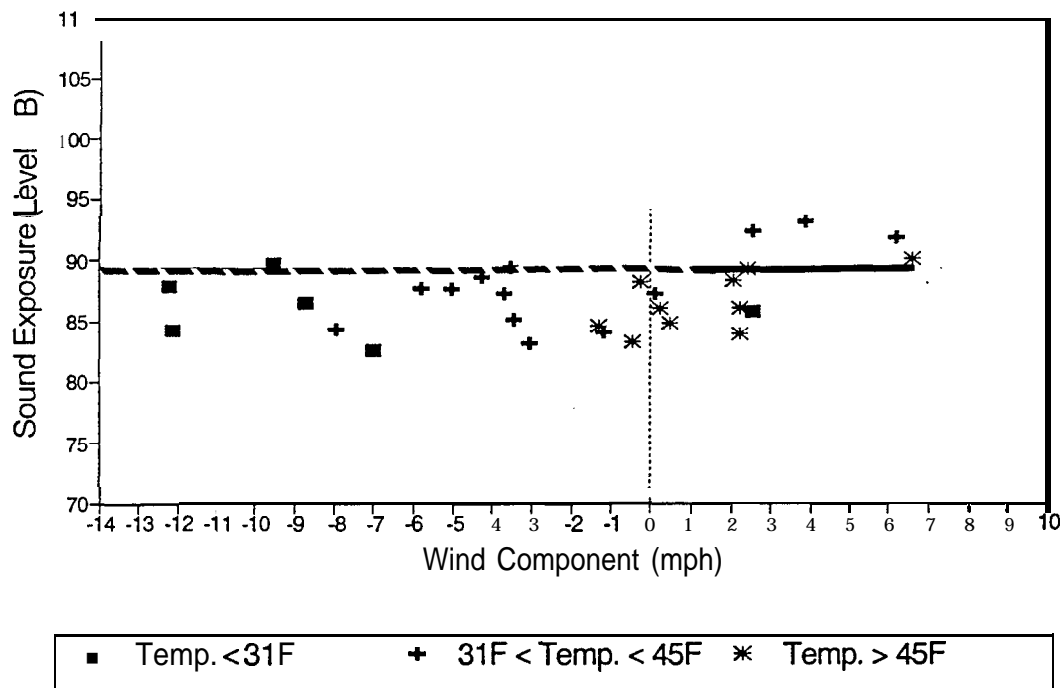


FIGURE 25. SEL VERSUS WIND SPEED FOR B-737:200 AT SITE 1

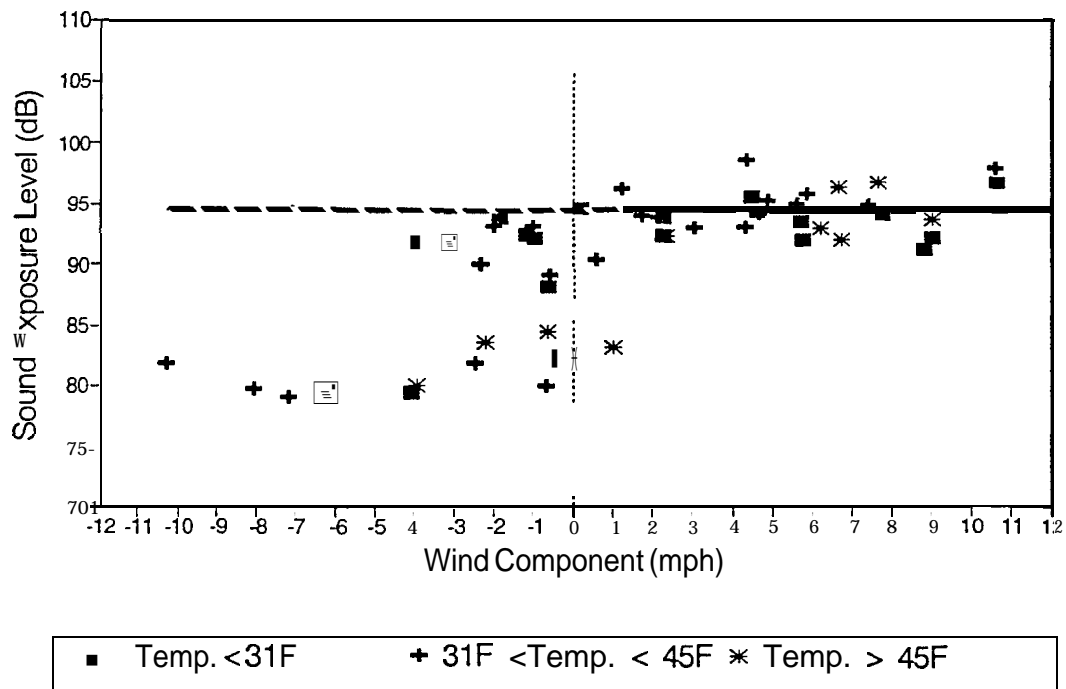


FIGURE 26. SEL VERSUS WIND SPEED FOR B-737:200 AT SITE 2

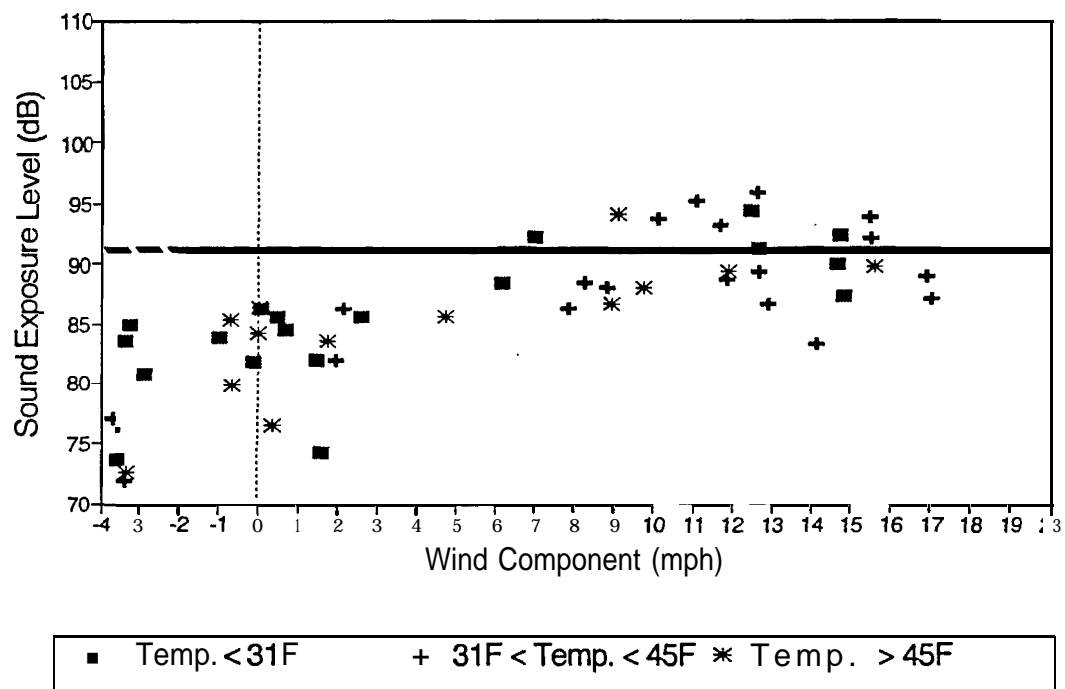


FIGURE 29. SEL VERSUS WIND SPEED FOR B-737:200 AT SITE 5

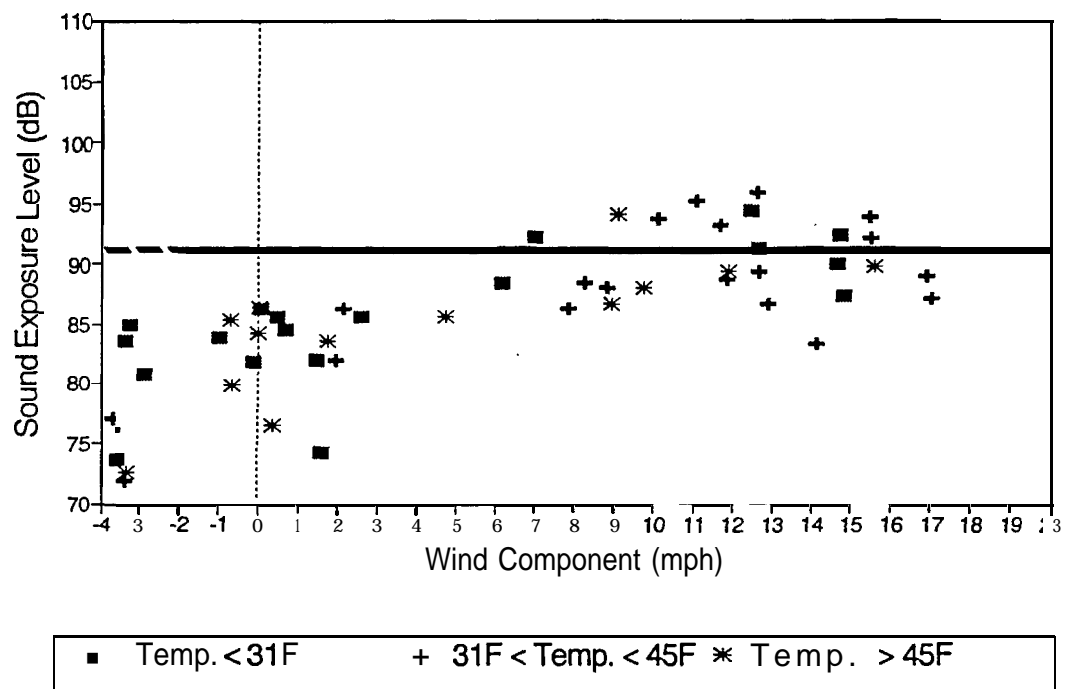


FIGURE 29. SEL VERSUS WIND SPEED FOR B-737:200 AT SITE 5

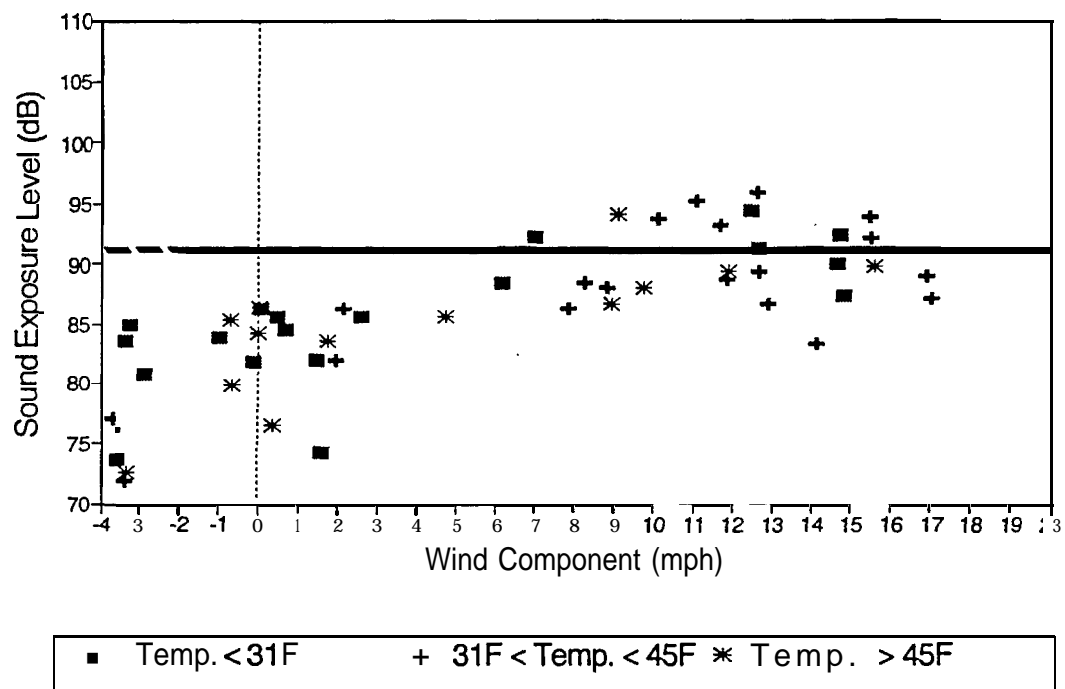


FIGURE 29. SEL VERSUS WIND SPEED FOR B-737:200 AT SITE 5

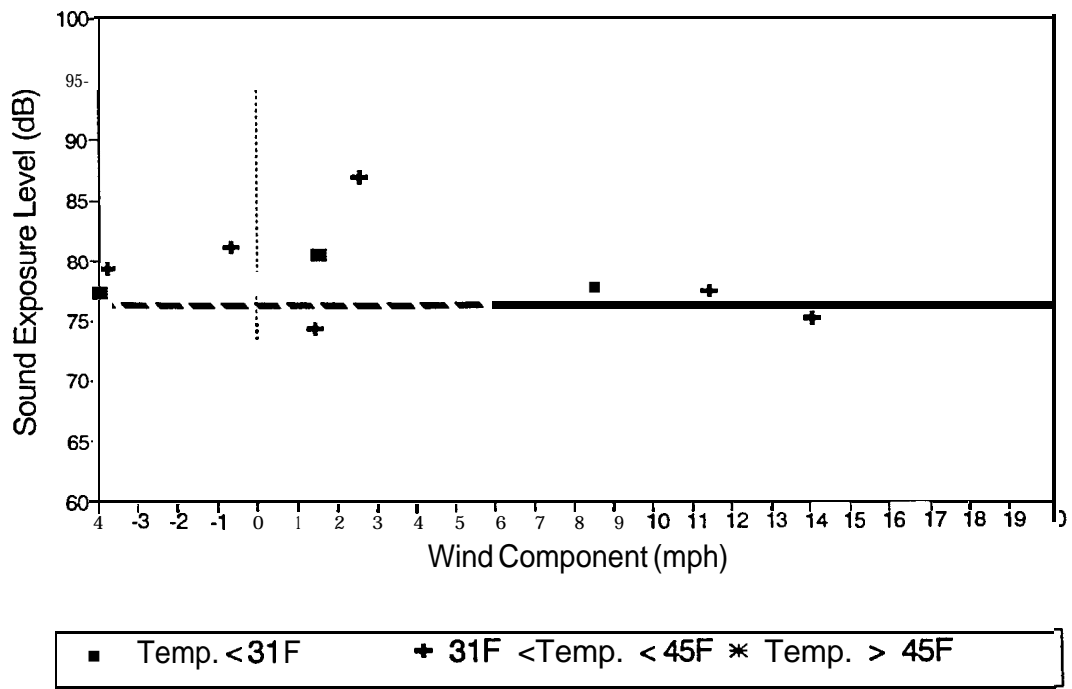


FIGURE 34. SEL VERSUS WIND SPEED FOR B-737:300/400 AT SITE 5

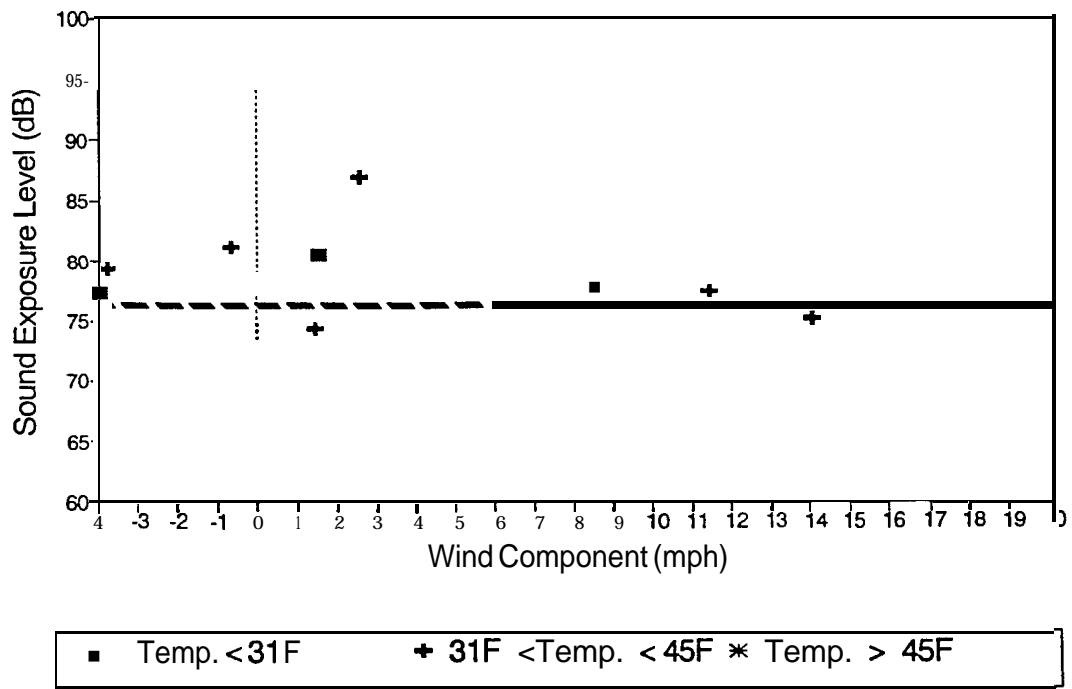


FIGURE 34. SEL VERSUS WIND SPEED FOR B-737:300/400 AT SITE 5

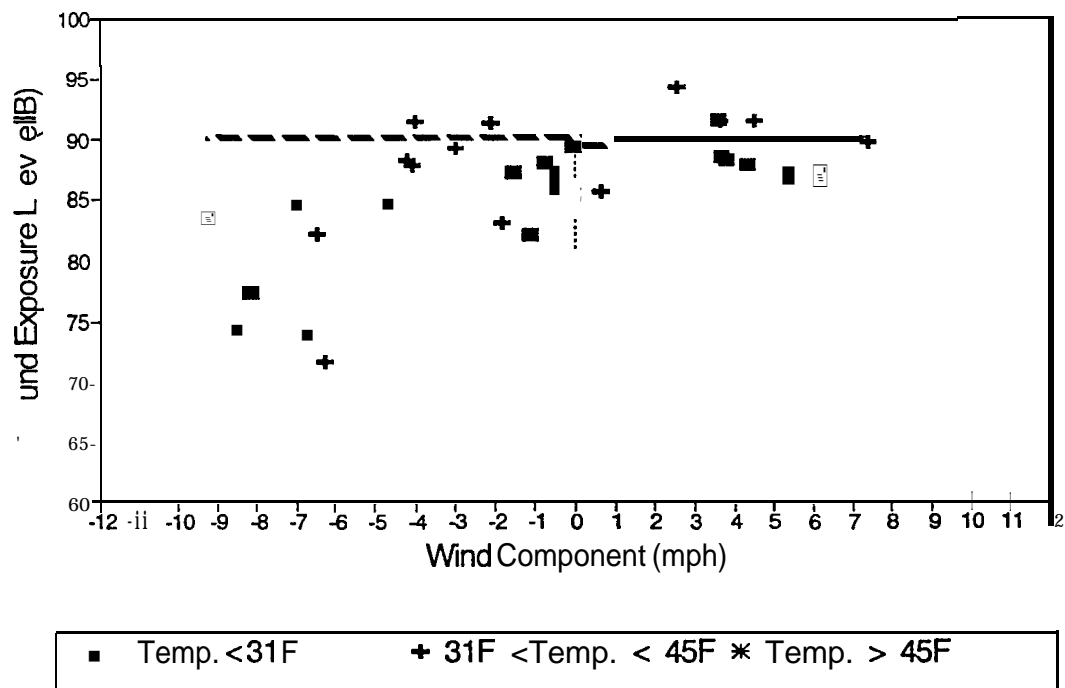


FIGURE 37. SEL VERSUS WIND SPEED FOR DC-9 (ALL MODELS) AT SITE 3

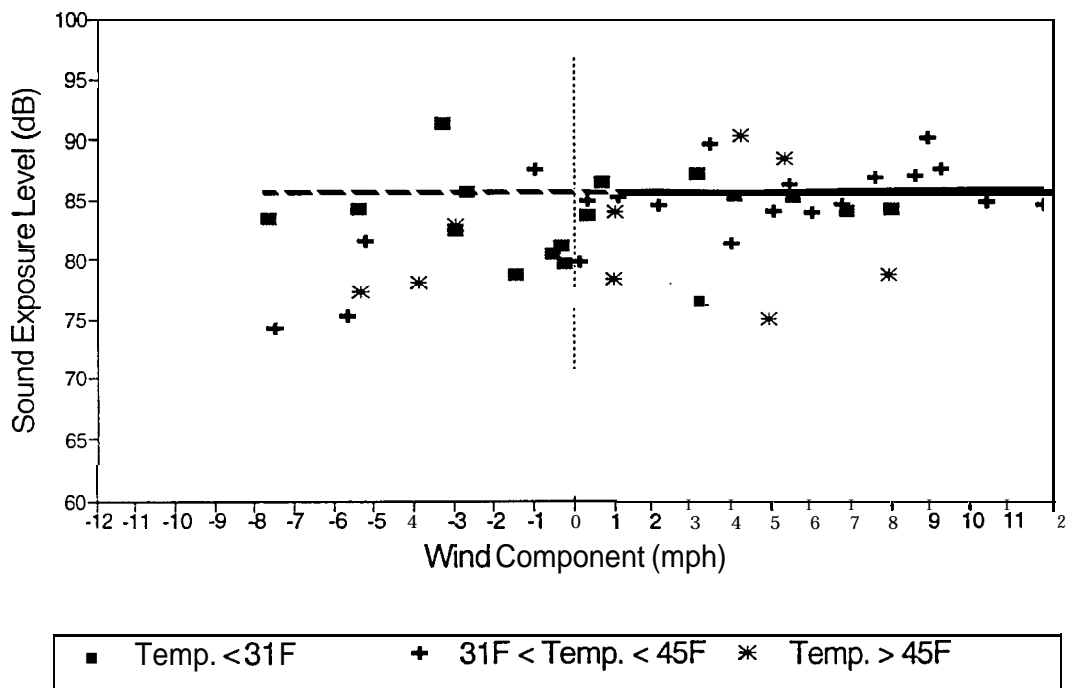


FIGURE 38. SEL VERSUS WIND SPEED FOR DC-9 (ALL MODELS) AT SITE 4

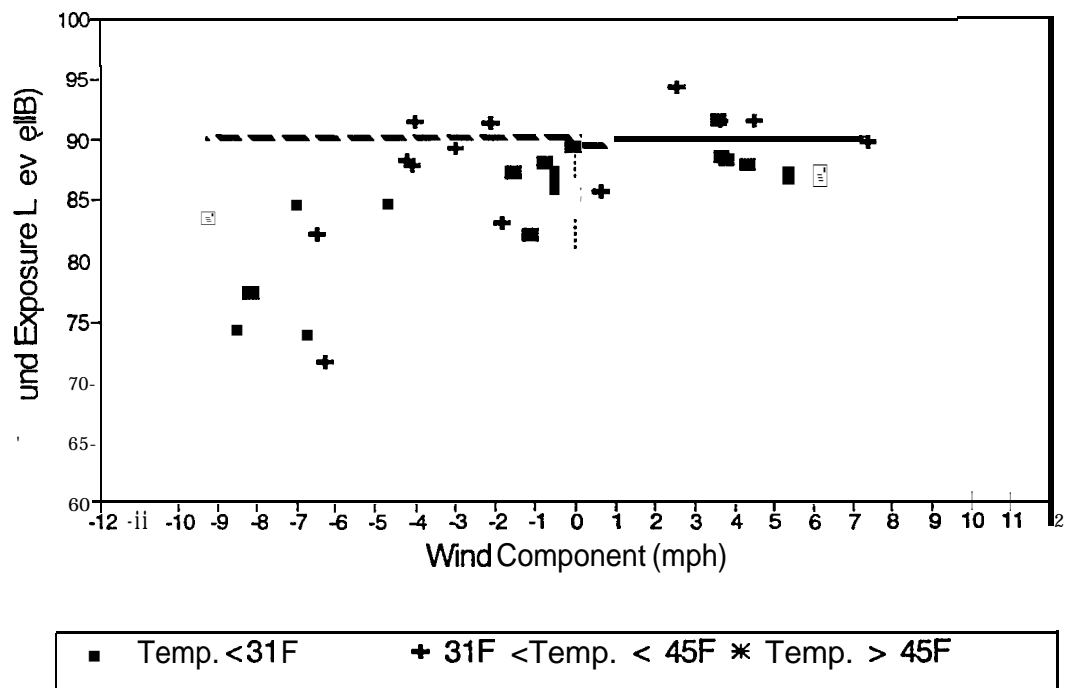


FIGURE 37. SEL VERSUS WIND SPEED FOR DC-9 (ALL MODELS) AT SITE 3

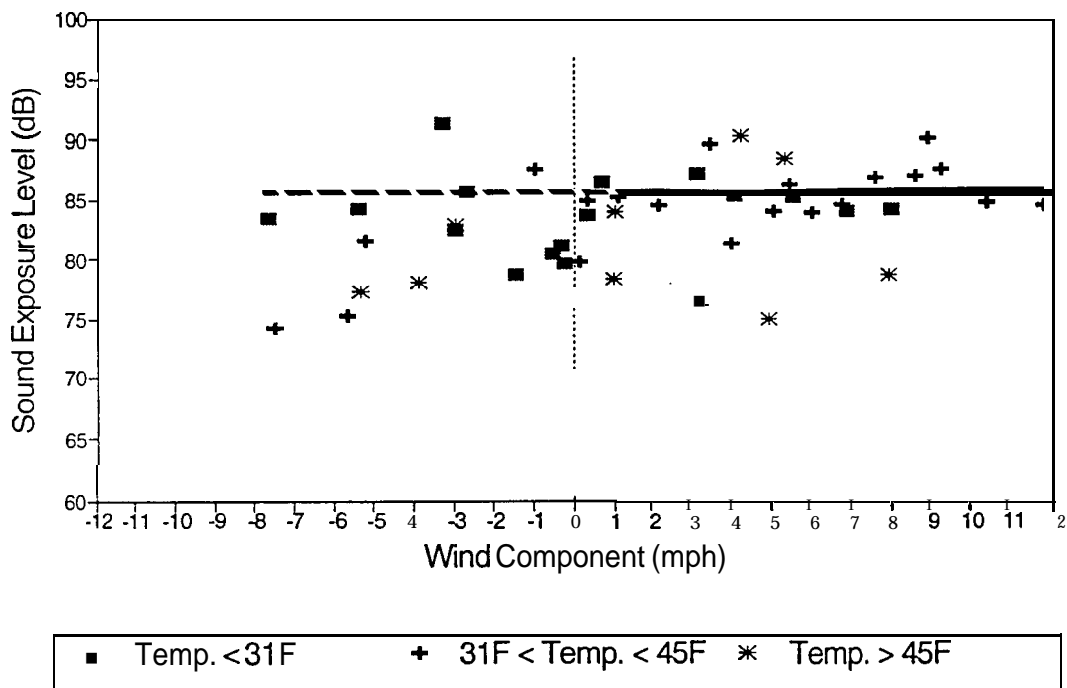


FIGURE 38. SEL VERSUS WIND SPEED FOR DC-9 (ALL MODELS) AT SITE 4

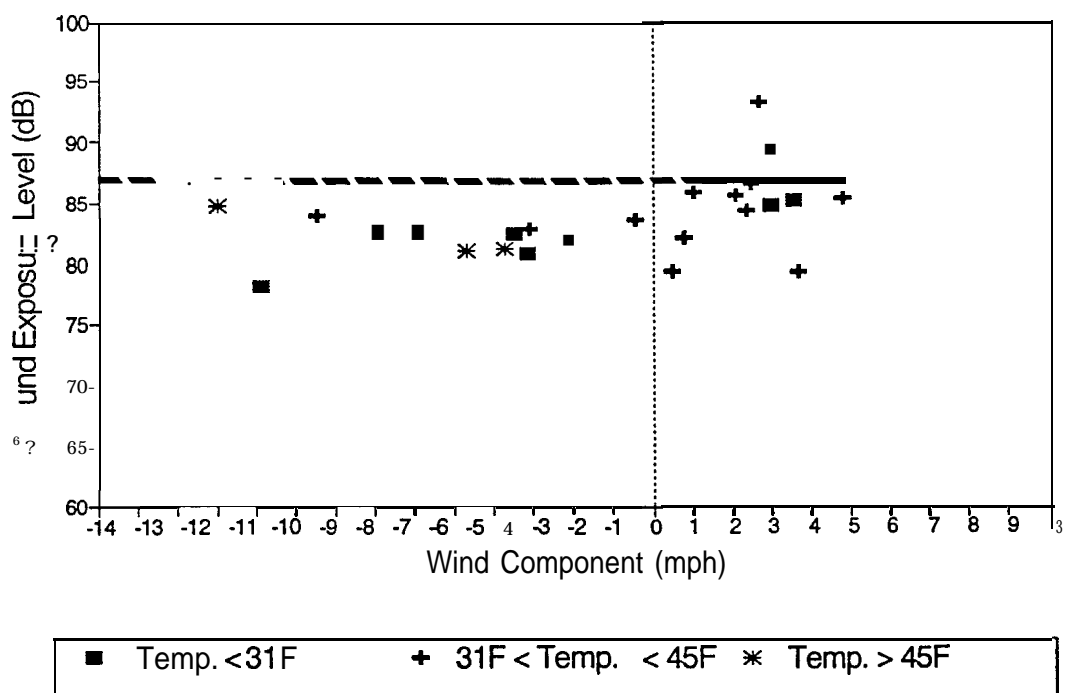


FIGURE 40. SEL VERSUS WIND SPEED FOR MD-SO (ALL MODELS) AT SITE 1

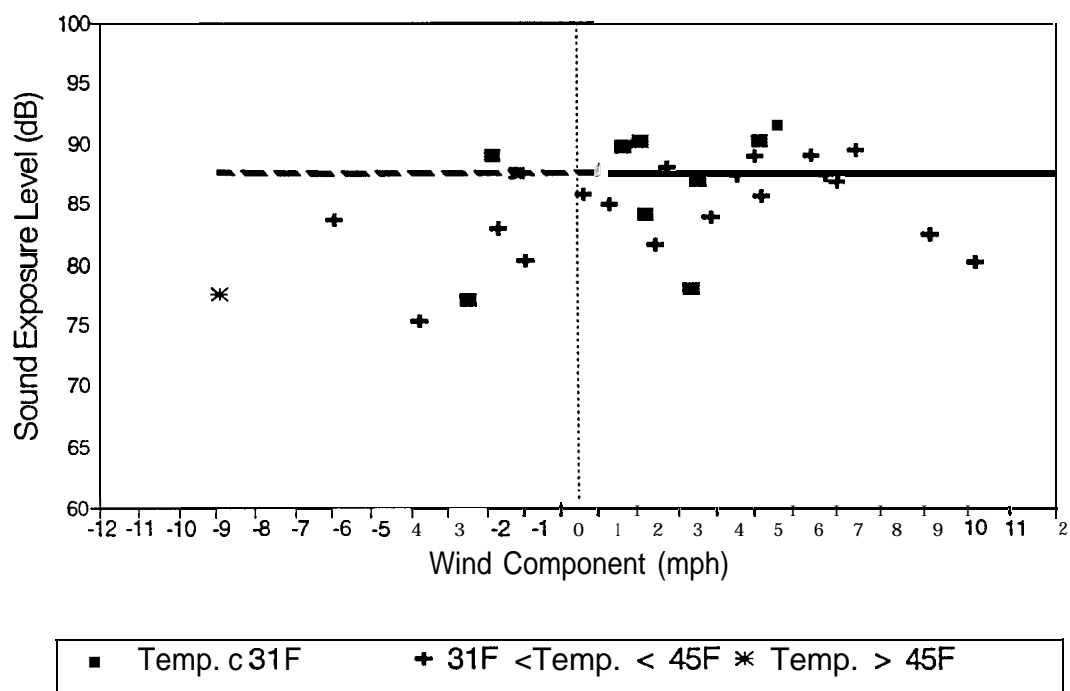


FIGURE 41. SEL VERSUS WIND SPEED FOR MD-SO (ALL MODELS) AT SITE 2

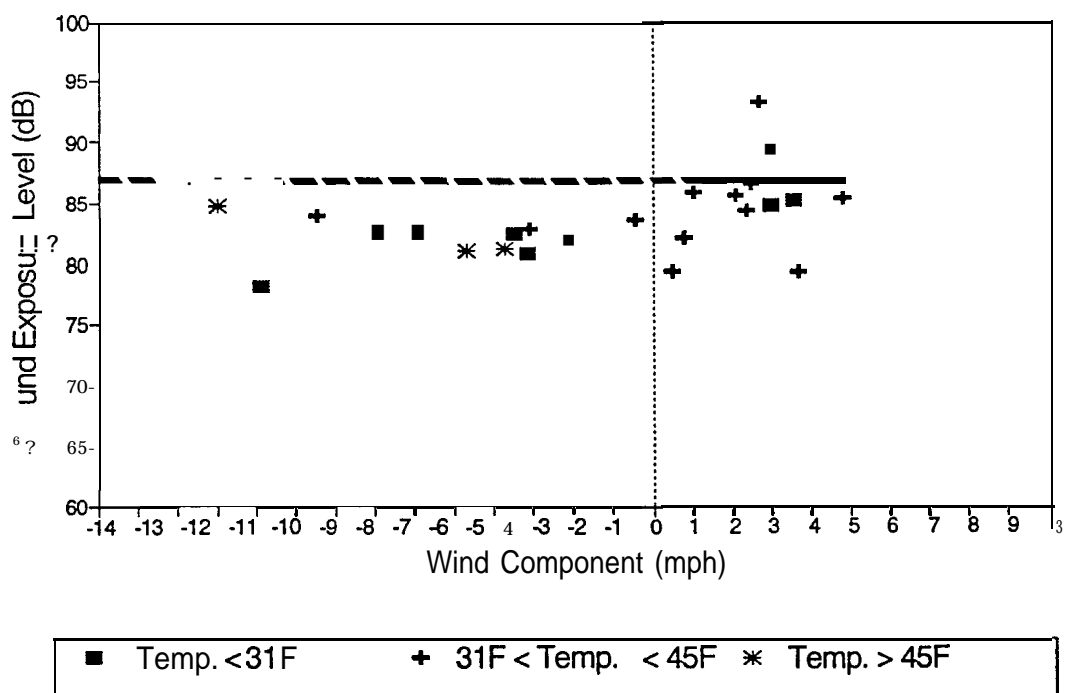


FIGURE 40. SEL VERSUS WIND SPEED FOR MD-SO (ALL MODELS) AT SITE 1

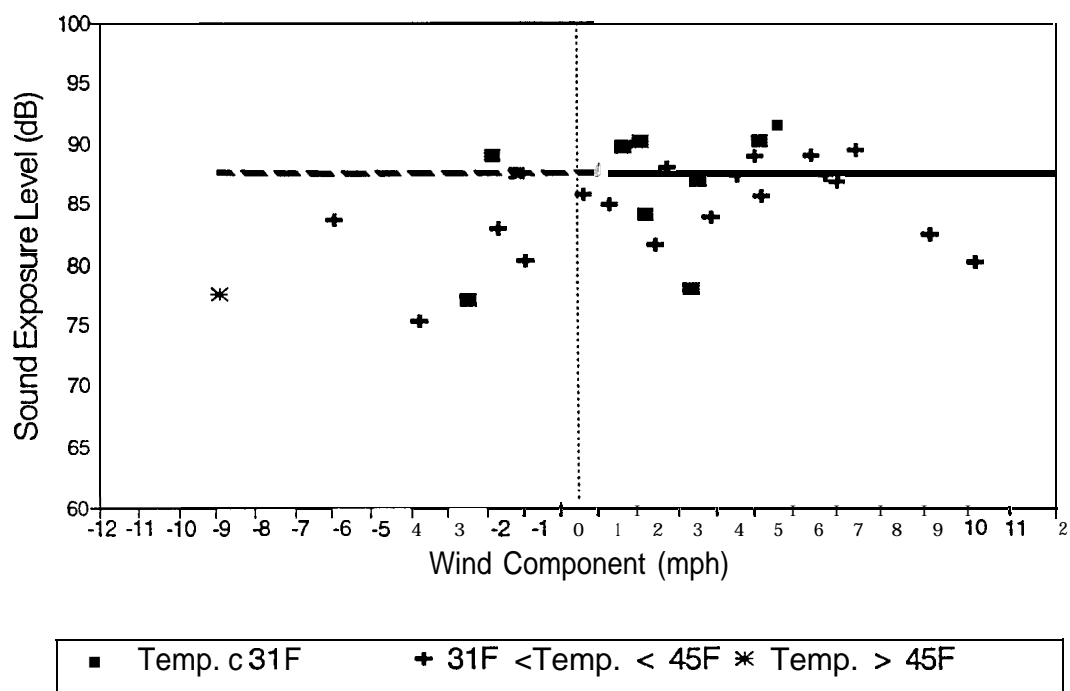


FIGURE 41. SEL VERSUS WIND SPEED FOR MD-SO (ALL MODELS) AT SITE 2

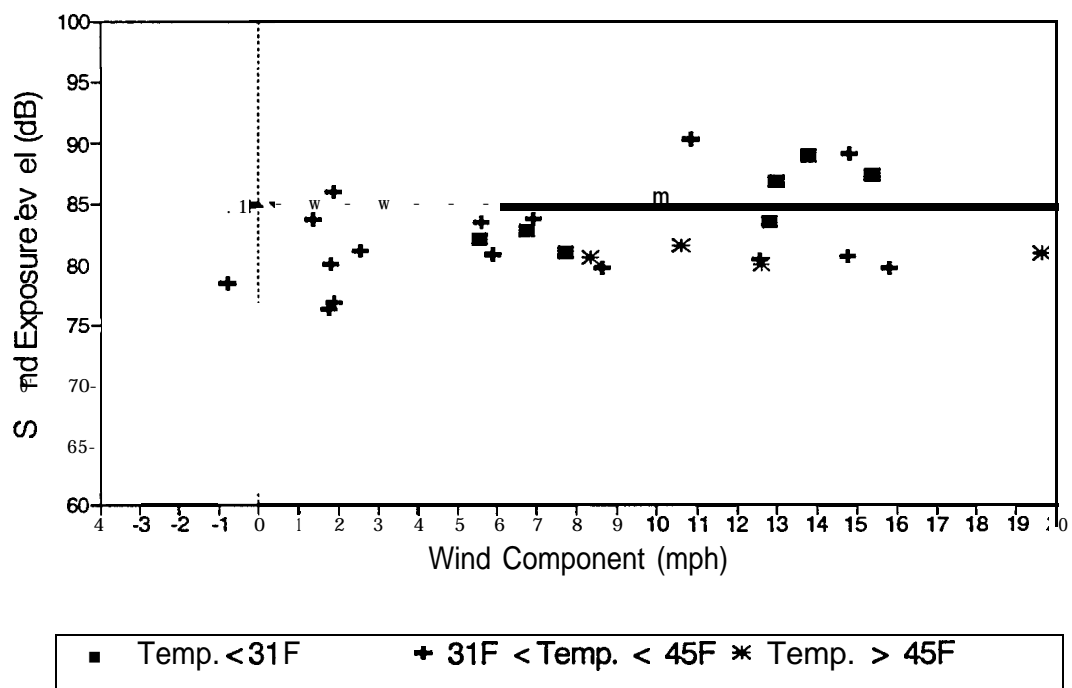


FIGURE 44. SEL VERSUS WIND SPEED FOR MD-SO (ALL MODELS) AT SITE 5

Several important observations may be made from these figures. First, a modest upwind condition can lower the measured **SEL** by as much as **10** decibels compared with the downwind conditions. This finding is in good agreement with the prior findings of a **U.S** Air Force sponsored **study**⁴.

Second, the upwind/downwind effect is not as pronounced at site 1 as the other sites. Figures **45** and **46** shed additional light on this observation. Figure **45** shows A-level time histories for a **B-727:200** aircraft under a moderate downwind propagation condition, while Figure **46** shows A-level time histories for the same aircraft type under upwind conditions. Two points of reference are important in interpreting the figures: the brake release time (nominally at **T=0**) and the liftoff time (nominally **T=+30**). Focusing first on the downwind case (Figure **45**), the clearly dominant portion of the noise energy at sites 2 through 5 occurs during the ground roll portion of the takeoff, with little energy contributed after liftoff. In contrast, at site 1 the maximum sound level occurs at or after the aircraft reaches the liftoff point. This situation most likely arises due to the noise **directivity** pattern of the engine exhaust as well as from reduced excess overground sound attenuation once the aircraft becomes airborne.

Upwind, the time histories at sites 2 through 5 in Figure **46** look very different **from** those shown in Figure **45**. At these sites the upwind sound shadow has greatly attenuated the ground roll portion of the signal, but after liftoff the measurement site is probably no longer in the shadow. Hence the large differences in **SEL** between the two conditions.

At site **1**, however, the dominant energy in the measured **SEL** occurs at or after liftoff in both the upwind *and* downwind cases. Thus wind effects on measured **SEL** at site 1 are less than at the *other* sites. The probable reason for this observation relates to the distance between site 1 and the runway: The distance is on the order of the aircraft ground roll distance to liftoff (and probably the maximum noise **directivity** angle). If site 1 had been located closer to the runway (*ie.* a multiple of the ground roll distance less than one) the upwind/downwind effect might likely have been **g r e a t e r**.

The third observation relates to the observed insensitivity of measured **SEL** to wind speed once the downwind speed exceeds a few miles per hour. Assuming a vertical wind gradient becomes established, sound rays from the source to the receiver are bent upwards into the atmosphere and then back down again to the receiver. The magnitude of the downwind speed simply determines the height to which the ray rises into the atmosphere before returning to the ground. Once the ray travels up and over any **local terrain** shielding effects, the effect of shielding is lost, and any further ray bending due to higher wind speeds has negligible effect (the total sound propagation path length only changes by a few percent due to increased bending, therefore there is little additional inverse square or atmospheric absorption loss). At site 1 a line of sight exists between the microphone and the aircraft during the entire flight trajectory. At sites **2, 3**, and 4 the only major acoustic shielding effects are one and two story residential structures (at some distance from the measurement sites). Thus, once wind speeds of only a few miles per hour are established, higher speeds have little effect on measured **SEL** at sites 1 through **4**.

In contrast, measured **SELs** at site 5 do not appear to reach a stable value until the downwind component reaches about 6 miles per hour. It is possible that this condition is due to the terrain shielding effect shown in Figure **6**. That is, higher wind velocities are needed to bend the sound rays up and over the terrain irregularities because the effective barrier height is greater at site 5 than at sites **2, 3**, and **4**.

⁴ Bishop, D.E., *Overground Excess Sound Attenuation (ESA): Volume 2. Analysis of Data for flat grassy Terrain Conditions*, AFAMRL-TR-84-017, Vol 2.

Several important observations may be made from these figures. First, a modest upwind condition can lower the measured **SEL** by as much as **10** decibels compared with the downwind conditions. This finding is in good agreement with the prior findings of a **U.S** Air Force sponsored **study**⁴.

Second, the upwind/downwind effect is not as pronounced at site 1 as the other sites. Figures **45** and **46** shed additional light on this observation. Figure **45** shows A-level time histories for a **B-727:200** aircraft under a moderate downwind propagation condition, while Figure **46** shows A-level time histories for the same aircraft type under upwind conditions. Two points of reference are important in interpreting the figures: the brake release time (nominally at **T=0**) and the liftoff time (nominally **T=+30**). Focusing first on the downwind case (Figure **45**), the clearly dominant portion of the noise energy at sites 2 through 5 occurs during the ground roll portion of the takeoff, with little energy contributed after liftoff. In contrast, at site 1 the maximum sound level occurs at or after the aircraft reaches the liftoff point. This situation most likely arises due to the noise **directivity** pattern of the engine exhaust as well as from reduced excess overground sound attenuation once the aircraft becomes airborne.

Upwind, the time histories at sites 2 through 5 in Figure **46** look very different **from** those shown in Figure **45**. At these sites the upwind sound shadow has greatly attenuated the ground roll portion of the signal, but after liftoff the measurement site is probably no longer in the shadow. Hence the large differences in **SEL** between the two conditions.

At site **1**, however, the dominant energy in the measured **SEL** occurs at or after liftoff in both the upwind *and* downwind cases. Thus wind effects on measured **SEL** at site 1 are less than at the *other* sites. The probable reason for this observation relates to the distance between site 1 and the runway: The distance is on the order of the aircraft ground roll distance to liftoff (and probably the maximum noise **directivity** angle). If site 1 had been located closer to the runway (*ie.* a multiple of the ground roll distance less than one) the upwind/downwind effect might likely have been **g r e a t e r**.

The third observation relates to the observed insensitivity of measured **SEL** to wind speed once the downwind speed exceeds a few miles per hour. Assuming a vertical wind gradient becomes established, sound rays from the source to the receiver are bent upwards into the atmosphere and then back down again to the receiver. The magnitude of the downwind speed simply determines the height to which the ray rises into the atmosphere before returning to the ground. Once the ray travels up and over any **local terrain** shielding effects, the effect of shielding is lost, and any further ray bending due to higher wind speeds has negligible effect (the total sound propagation path length only changes by a few percent due to increased bending, therefore there is little additional inverse square or atmospheric absorption loss). At site 1 a line of sight exists between the microphone and the aircraft during the entire flight trajectory. At sites **2, 3**, and 4 the only major acoustic shielding effects are one and two story residential structures (at some distance from the measurement sites). Thus, once wind speeds of only a few miles per hour are established, higher speeds have little effect on measured **SEL** at sites 1 through **4**.

In contrast, measured **SELs** at site 5 do not appear to reach a stable value until the downwind component reaches about 6 miles per hour. It is possible that this condition is due to the terrain shielding effect shown in Figure **6**. That is, higher wind velocities are needed to bend the sound rays up and over the terrain irregularities because the effective barrier height is greater at site 5 than at sites **2, 3**, and **4**.

⁴ Bishop, D.E., *Overground Excess Sound Attenuation (ESA): Volume 2. Analysis of Data for flat grassy Terrain Conditions*, AFAMRL-TR-84-017, Vol 2.

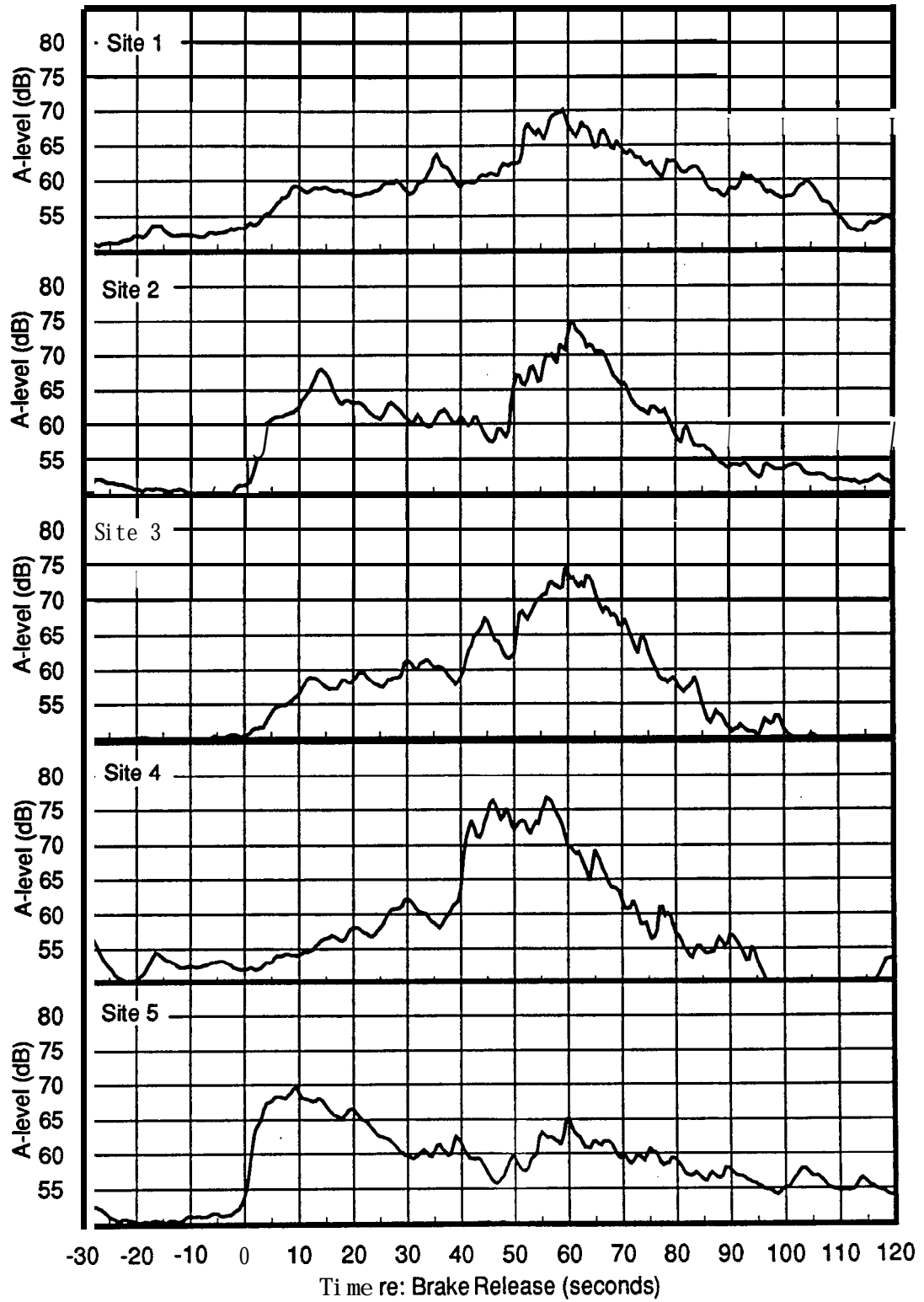


FIGURE 46. A-LEVEL TIME HISTORIES UNDER UPWIND CONDITIONS

4.3 Comparison of Measured Downwind Sound Levels With INM Predictions (Database 10)

Of particular interest in this study was the comparison of measured sound exposure levels (**SELs**) with the predictions of the Integrated Noise Model (**INM**). To present the completest possible picture, comparisons were made for each of the five aircraft types at each of the **five** measurement sites. For the purposes of this comparison, the measured **SEL** was defined as the energy average value measured under full downwind propagation. At sites 1 through 4 “full downwind” was defined as wind component speeds of 1 mile-per-hour or greater. At site 5 a criterion of 6 miles per hour was used in order to overcome the apparent shielding effect of the terrain (see Figure 6 for terrain profile and Figures **24, 29, 34, 39,** and **44** for **SEL** versus wind speed). The horizontal lines in Figures **20** through **44** show these energy average **SELs** which are tabulated in Table 6.

Also shown in Table 6 are the **SELs** calculated by **INM** Version **3.10** at each of the five measurement sites. These **SELs** were calculated by determining the proportions of various engine types observed in each aircraft’s downwind datapoints, and weighting the energy average of the **INM** calculated values by these proportions.

The differences reported in Table 6 are the measured values minus the **INM** prediction. In general, these differences are less than 3 decibels, but some notable exceptions exist. For example, the model consistently **underpredicts** at site 5 (an artifact of the **cardioid** shaped noise emission pattern built into the model at the start-of-roll. The differences obtained (measured minus predicted) for the **B737-300/400** appear to be somewhat larger than for other aircraft. This may be due in part to a potential data reduction bias where only those noise events with **sufficiently** high **signal-to-noise** ratios were used to compute the measured **SELs**.

4.3 Comparison of Measured Downwind Sound Levels With INM Predictions (Database 10)

Of particular interest in this study was the comparison of measured sound exposure levels (**SELs**) with the predictions of the Integrated Noise Model (**INM**). To present the completest possible picture, comparisons were made for each of the five aircraft types at each of the **five** measurement sites. For the purposes of this comparison, the measured **SEL** was defined as the energy average value measured under full downwind propagation. At sites 1 through 4 “full downwind” was defined as wind component speeds of 1 mile-per-hour or greater. At site 5 a criterion of 6 miles per hour was used in order to overcome the apparent shielding effect of the terrain (see Figure 6 for terrain profile and Figures **24, 29, 34, 39,** and **44** for **SEL** versus wind speed). The horizontal lines in Figures **20** through **44** show these energy average **SELs** which are tabulated in Table **6**.

Also shown in Table 6 are the **SELs** calculated by **INM** Version **3.10** at each of the five measurement sites. These **SELs** were calculated by determining the proportions of various engine types observed in each aircraft’s downwind datapoints, and weighting the energy average of the **INM** calculated values by these proportions.

The differences reported in Table 6 are the measured values minus the **INM** prediction. In general, these differences are less than 3 decibels, but some notable exceptions exist. For example, the model consistently **underpredicts** at site 5 (an artifact of the **cardioid** shaped noise emission pattern built into the model at the start-of-roll. The differences obtained (measured minus predicted) for the **B737-300/400** appear to be somewhat larger than for other aircraft. This may be due in part to a potential data reduction bias where only those noise events with **sufficiently** high **signal-to-noise** ratios were used to compute the measured **SELs**.

5. A METHOD FOR FINE TUNING THE INTEGRATED NOISE MODEL

A brief review of the predictive equation⁵ used by the **INM** to compute sound exposure levels in the vicinity of the start-of-takeoff roll suggests a relatively straightforward method for fine tuning the model without resorting to changes to the basic algorithms. Equation 1 shows this equation:

$$L_{AE}(S') = L_{AE}(P,d) + \delta V + \Delta(0,r) + \delta L \quad (1)$$

where: $L_{AE}(S')$ = **SEL** at location **S'** behind the start of takeoff roll,

$L_{AE}(P,d)$ = **SEL** extracted from the reference database at power setting **P** and distance **d**,

δV = speed adjustment between the normalized speed of **160** knots and the minimum speed at start of roll (**INM 3.9** uses **16** knots),

$\Delta(0,r)$ = lateral attenuation adjustment for elevation angle **0** and distance **r**,

δL = **directivity** pattern adjustment.

One convenient parameter, which is a part of the database and not the software per se, is the presumed starting speed of the aircraft, δV . The current starting speed used for all aircraft in **INM** Database 9 is **16** knots. This value was selected based on a measurement **program**⁶ conducted at Boston, Massachusetts' Logan International Airport. The results of that study indicated that predicted **SELs** using Equation 1 could be brought into better agreement with measured values by using the **16** knot value (a **32** knot value had been used previously).

All other things being equal, Equation 1 suggests that a halving of the starting speed to 8 knots, and a linear acceleration to the liftoff speed, should result in very close to a 3 decibel increase in the predicted **SEL**. In order to test this hypothesis, and also to determine the geographic area over which this modification would have influence, **SEL** contours were generated using the **INM** for two aircraft in the **INM** database (the "**727D17**" using Stage Length **4**, and the "**737300**" using Stage Length **4**). The speed profiles for these aircraft were then modified to halve the **16** knot starting speed to 8 knots, and the program was rerun to produce a second set of **SEL** contours for the same two aircraft.

Figures **47** and **48** show the results of the analysis. The solid contour lines in the figures represent the **16** knot starting speed and the dashed lines show the effect of the 8 knot speed. Both figures clearly indicate that by halving the starting speed (but making other changes to the speed profile) the **SEL** increases by approximately 3 decibels. Furthermore, the effect is localized to the immediate area around the start-of-roll, with little effect (**1** decibel or less) along most of the runway sideline.

⁵ Society of Automotive Engineers, *Procedure for the Calculation of Airplane Noise in the Vicinity of Airports*, Aerospace Information Report **1845**.

⁶ Eldred, K.M., and Miller, R.M., *Analysis of Selected Topics in the Methodology of the Integrated Noise Model*, Bolt Beranek and Newman Inc. Report **4413** (September 1980).

5. A METHOD FOR FINE TUNING THE INTEGRATED NOISE MODEL

A brief review of the predictive equation⁵ used by the **INM** to compute sound exposure levels in the vicinity of the start-of-takeoff roll suggests a relatively straightforward method for fine tuning the model without resorting to changes to the basic algorithms. Equation 1 shows this equation:

$$L_{AE}(S') = L_{AE}(P,d) + \delta V + \Delta(0,r) + \delta L \quad (1)$$

where: $L_{AE}(S')$ = **SEL** at location **S'** behind the start of takeoff roll,

$L_{AE}(P,d)$ = **SEL** extracted from the reference database at power setting **P** and distance **d**,

δV = speed adjustment between the normalized speed of **160** knots and the minimum speed at start of roll (**INM 3.9** uses **16** knots),

$\Delta(0,r)$ = lateral attenuation adjustment for elevation angle **0** and distance **r**,

δL = **directivity** pattern adjustment.

One convenient parameter, which is a part of the database and not the software per se, is the presumed starting speed of the aircraft, δV . The current starting speed used for all aircraft in **INM** Database 9 is **16** knots. This value was selected based on a measurement **program**⁶ conducted at Boston, Massachusetts' Logan International Airport. The results of that study indicated that predicted **SELs** using Equation 1 could be brought into better agreement with measured values by using the **16** knot value (a **32** knot value had been used previously).

All other things being equal, Equation 1 suggests that a halving of the starting speed to 8 knots, and a linear acceleration to the liftoff speed, should result in very close to a 3 decibel increase in the predicted **SEL**. In order to test this hypothesis, and also to determine the geographic area over which this modification would have influence, **SEL** contours were generated using the **INM** for two aircraft in the **INM** database (the "**727D17**" using Stage Length **4**, and the "**737300**" using Stage Length **4**). The speed profiles for these aircraft were then modified to halve the **16** knot starting speed to 8 knots, and the program was rerun to produce a second set of **SEL** contours for the same two aircraft.

Figures **47** and **48** show the results of the analysis. The solid contour lines in the figures represent the **16** knot starting speed and the dashed lines show the effect of the 8 knot speed. Both figures clearly indicate that by halving the starting speed (but making other changes to the speed profile) the **SEL** increases by approximately 3 decibels. Furthermore, the effect is localized to the immediate area around the start-of-roll, with little effect (**1** decibel or less) along most of the runway sideline.

⁵ Society of Automotive Engineers, *Procedure for the Calculation of Airplane Noise in the Vicinity of Airports*, Aerospace Information Report **1845**.

⁶ Eldred, K.M., and Miller, R.M., *Analysis of Selected Topics in the Methodology of the Integrated Noise Model*, Bolt Beranek and Newman Inc. Report **4413** (September 1980).

5. A METHOD FOR FINE TUNING THE INTEGRATED NOISE MODEL

A brief review of the predictive equation⁵ used by the **INM** to compute sound exposure levels in the vicinity of the start-of-takeoff roll suggests a relatively straightforward method for fine tuning the model without resorting to changes to the basic algorithms. Equation 1 shows this equation:

$$L_{AE}(S') = L_{AE}(P,d) + \delta V + \Delta(0,r) + \delta L \quad (1)$$

where: $L_{AE}(S')$ = **SEL** at location **S'** behind the start of takeoff roll,

$L_{AE}(P,d)$ = **SEL** extracted from the reference database at power setting **P** and distance **d**,

δV = speed adjustment between the normalized speed of **160** knots and the minimum speed at start of roll (**INM 3.9** uses **16** knots),

$\Delta(0,r)$ = lateral attenuation adjustment for elevation angle **0** and distance **r**,

δL = **directivity** pattern adjustment.

One convenient parameter, which is a part of the database and not the software per se, is the presumed starting speed of the aircraft, δV . The current starting speed used for all aircraft in **INM** Database 9 is **16** knots. This value was selected based on a measurement **program**⁶ conducted at Boston, Massachusetts' Logan International Airport. The results of that study indicated that predicted **SELs** using Equation 1 could be brought into better agreement with measured values by using the **16** knot value (a **32** knot value had been used previously).

All other things being equal, Equation 1 suggests that a halving of the starting speed to 8 knots, and a linear acceleration to the liftoff speed, should result in very close to a 3 decibel increase in the predicted **SEL**. In order to test this hypothesis, and also to determine the geographic area over which this modification would have influence, **SEL** contours were generated using the **INM** for two aircraft in the **INM** database (the "**727D17**" using Stage Length **4**, and the "**737300**" using Stage Length **4**). The speed profiles for these aircraft were then modified to halve the **16** knot starting speed to 8 knots, and the program was rerun to produce a second set of **SEL** contours for the same two aircraft.

Figures **47** and **48** show the results of the analysis. The solid contour lines in the figures represent the **16** knot starting speed and the dashed lines show the effect of the 8 knot speed. Both figures clearly indicate that by halving the starting speed (but making other changes to the speed profile) the **SEL** increases by approximately 3 decibels. Furthermore, the effect is localized to the immediate area around the start-of-roll, with little effect (**1** decibel or less) along most of the runway sideline.

⁵ Society of Automotive Engineers, *Procedure for the Calculation of Airplane Noise in the Vicinity of Airports*, Aerospace Information Report **1845**.

⁶ Eldred, K.M., and Miller, R.M., *Analysis of Selected Topics in the Methodology of the Integrated Noise Model*, Bolt Beranek and Newman Inc. Report **4413** (September 1980).

to determine the magnitude of this effect.

The excellent regression line fits to the aircraft tracking data suggest another body of data which could be explored to provide insight for appropriate acceleration models in the **INM** database. By **taking** the first derivative of a **3rd** order fit to the distance versus time data, distance/velocity relationships could be established for **modelling** purposes.

While gross weight alone might explain some of the currently unexplained scatter in the downwind **SEL** data, the available **dataset** provides the means for approximating gross engine thrust for each aircraft. By taking the **2nd** derivative of the **3rd** order fit to the distance versus time data, the acceleration at any point along the ground roll could be determined. If an early point in the ground roll were selected (**500 to 1000**) where the velocity (and associated drag) are low, it would be possible to compute an estimated thrust using the $F = ma$ relationship. Specifically,

$$\text{Approximate Engine Thrust} = (W_{\text{gate}} - W_{\text{fuel burn}}) / g * a + \text{Drag}_{\text{vel}} \quad (2)$$

where:

- W_{gate} = Aircraft gate weight,
- $W_{\text{fuel burn}}$ = An estimated weight of fuel burned from the gate to brake release,
- g = Acceleration due to gravity,
- a = Acceleration inferred from time/distance curve,
- Drag_{vel} = Estimated drag at small velocity.

This approximated engine thrust might prove a somewhat better explainer of the scatter than gross weight alone.

Engine thrust is also likely to be a factor of available runway length. That is, all other things being equal, pilots may select a greater thrust for short runways than for longer ones. Given **SEL** versus thrust relationships established from the above analysis, and aircraft flight manuals **as** a guide, the effects of runway length on **SEL** could be approximated to determine whether runway length is an important **modelling** parameter for start-of-takeoff roll noise.

After the gross weight and thrust issues are accounted for in the data, the effect of static versus rolling starts on measured **SEL** should be investigated. The effect is not expected to be large, and therefore should be investigated after larger effect variables have been accounted for.

In order to resolve the temperature issue, additional measurements are recommended. Using the same measurement protocol, but not necessarily at the same airport, the following list of considerations is offered:

- Protocol - The same aircraft tracking scheme and the same accounting for gross weight should be employed; similar measurement site locations should also be used,
- Runway Length - Data from long and short runways would be desirable if an analysis of the data suggest that a runway length effect could indeed be measured,
- Headways** - Preferably, aircraft **headways** should not be less than **90** seconds (this may preclude airports with heavy traffic volumes or significant **hubbing** operations,
- Ambient Noise - Ambient noise levels in the region of **40 dB(A)** or less at the measurement sites are required for successful capture of stage 3 aircraft noise levels,
- Aircraft Mix - A mix of stage 2 and stage 3 aircraft is highly desirable.

APPENDIX A. RUNWAY / MEASUREMENT SITE GEOMETRY

Appendix A provides detailed tables showing the geometric relationship between the measurement sites and the aircraft as a function of aircraft ground roll distance from brake release. The underlying runway and acoustic measurement site X/Y coordinates are shown in Table A-1. These coordinates were derived from Anne Arundel County, 1 inch to 200 foot scale topographic maps. The maps show the airport runways, the locations of all houses used as measurement sites, and state plane coordinate lines at 1000 foot intervals.

The tabulations presented in Tables A-2 through A-7 show aircraft / measurement site geometry for 200 foot increments of aircraft travel. For the purposes of compiling these tables, a nominal brake release point of 400 feet from the physical beginning of runway pavement was chosen. This nominal starting position was chosen based on observations made during the measurements.

The first column in the tables shows the distance from the nominal brake release point (in feet). The next two columns show the difference in state plane coordinates between the measurement site and the aircraft, **re: the aircraft**. The fourth column shows the line-of-sight distance from the aircraft to the measurement site (computed as square root of the sum of the squares of "Delta X" and "Delta Y". The last column shows the **directivity** angle relative to the aircraft heading down the runway. For example, a measurement site directly behind the aircraft (like site 5) would have a **directivity** angle very close to 180 degrees. A measurement site directly abeam the aircraft would have a **directivity** angle of 90 degrees.

Sites 2.1 and 2.2 were located within four houses of one another. Site 2.1 was used during the October measurements and site 2.2 was used during the December measurements.

**TABLE A-1. RUNWAY AND MEASUREMENT SITE COORDINATES
(MARYLAND STATE PLANE COORDINATE SYSTEM)**

Site ---	X (feet) --m-e-	Y (feet) - - - e -
1.0	897,520	492,035
2.1		
2.2	899,520	490,340
3.0	899,470	491,305
4.0		
5.0	900,885	488,475
R/W 28	897,736	487,952
R/W 10	888,706	488,576

Appendix A provides detailed tables showing the geometric relationship between the measurement sites and the aircraft as a function of aircraft ground roll distance from brake release. The underlying runway and acoustic measurement site X/Y coordinates are shown in Table A-1. These coordinates were derived from Anne Arundel County, 1 inch to 200 foot scale topographic maps. The maps show the airport runways, the locations of all houses used as measurement sites, and state plane coordinate lines at 1000 foot intervals.

The tabulations presented in Tables A-2 through A-7 show aircraft / measurement site geometry for 200 foot increments of aircraft travel. For the purposes of compiling these tables, a nominal brake release point of 400 feet from the physical beginning of runway pavement was chosen. This nominal starting position was chosen based on observations made during the measurements.

The first column in the tables shows the distance from the nominal brake release point (in feet). The next two columns show the difference in state plane coordinates between the measurement site and the aircraft, **re: the aircraft**. The fourth column shows the line-of-sight distance from the aircraft to the measurement site (computed as square root of the sum of the squares of "Delta X" and "Delta Y". The last column shows the **directivity** angle relative to the aircraft heading down the runway. For example, a measurement site directly behind the aircraft (like site 5) would have a **directivity** angle very close to 180 degrees. A measurement site directly abeam the aircraft would have a **directivity** angle of 90 degrees.

Sites 2.1 and 2.2 were located within four houses of one another. Site 2.1 was used during the October measurements and site 2.2 was used during the December measurements.

**TABLE A-1. RUNWAY AND MEASUREMENT SITE COORDINATES
(MARYLAND STATE PLANE COORDINATE SYSTEM)**

Site ---	X (feet) --m-e-	Y (feet) - - - e -
1.0	897,520	492,035
2.1		
2.2	899,520	490,340
3.0	899,470	491,305
4.0		
5.0	900,885	488,475
R/W 28	897,736	487,952
R/W 10	888,706	488,576

TABLE A-4. NOISE MONITOR SITE 2.2

Distance From Start of Runway (feet)	Distance From Aircraft to Measurement Site			Engine Directivity Angle (degrees)
	Delta X (feet)	Delta Y (feet)	Total (feet)	
0	1584	2402	2877	119.4
200	1784	2388	2981	122.8
400	1983	2374	3094	125.9
600	2183	2361	3215	128.8
800	2382	2347	3344	131.5
1000	2582	2333	3480	133.9
1200	2781	2319	3621	136.2
1400	2981	2305	3768	138.3
1600	3180	2292	3920	140.3
1800	3380	2278	4076	142.1
2000	3579	2264	4235	143.7
2200	3779	2250	4398	145.3
2400	3978	2236	4564	146.7
2600	4178	2223	4732	148.0
2800	4377	2209	4903	149.3
3000	4577	2195	5076	150.4
3200	4776	2181	5251	151.5
3400	4976	2167	5427	152.5
3600	5175	2154	5606	153.5
3800	5375	2140	5785	154.3
4000	5574	2126	5966	155.2
4200	5774	2112	6148	156.0
4400	5974	2098	6331	156.7
4600	6173	2085	6516	157.4
4800	6373	2071	6701	158.0
5000	6572	2057	6886	158.7
5200	6772	2043	7073	159.3
5400	6971	2029	7261	159.8
5600	7171	2016	7449	160.3
5800	7370	2002	7637	160.8
6000	7570	1988	7826	161.3
6200	7769	1974	8016	161.8
6400	7969	1960	8206	162.2
6600	8168	1947	8397	162.6
6800	8368	1933	8588	163.0
7000	8567	1919	8780	163.4
7200	8767	1905	8971	163.8
7400	8966	1891	9164	164.1
7600	9166	1878	9356	164.5
7800	9365	1864	9549	164.8
8000	9565	1850	9742	165.1

TABLE A-5. NOISE MONITOR SITE 3

Distance From Start of Runway (feet)	Distance From Aircraft to Measurement Site			Engine Directivity Angle (degrees)
	Delta X (feet)	Delta Y (feet)	Total (feet)	
0	1534	3367	3700	110.5
200	1734	3353	3775	113.4
400	1933	3339	3859	116.1
600	2133	3326	3951	118.7
800	2332	3312	4051	121.2
1000	2532	3298	4158	123.6
1200	2731	3284	4271	125.8
1400	2931	3270	4391	127.9
1600	3130	3257	4517	129.9
1800	3330	3243	4648	131.8
2000	3529	3229	4784	133.6
2200	3729	3215	4924	135.3
2400	3928	3201	5068	136.9
2600	4128	3188	5215	138.4
2800	4327	3174	5366	139.8
3000	4527	3160	5521	141.1
3200	4726	3146	5678	142.4
3400	4926	3132	5838	143.6
3600	5125	3119	6000	144.7
3800	5325	3105	6164	145.8
4000	5524	3091	6330	146.8
4200	5724	3077	6499	147.8
4400	5924	3063	6669	148.7
4600	6123	3050	6840	149.6
4800	6323	3036	7014	150.4
5000	6522	3022	7188	151.2
5200	6722	3008	7364	151.9
5400	6921	2994	7541	152.6
5600	7121	2981	7719	153.3
5800	7320	2967	7899	154.0
6000	7520	2953	8079	154.6
6200	7719	2939	8260	155.2
6400	7919	2925	8442	155.8
6600	8118	2912	8625	156.3
6800	8318	2898	8808	156.8
7000	8517	2884	8992	157.3
7200	8717	2870	9177	157.8
7400	8916	2856	9363	158.3
7600	9116	2843	9549	158.7
7800	9315	2829	9735	159.2
8000	9515	2815	9923	159.6

TABLE A-6. NOISE MONITOR SITE 4

Distance From Start of Runway (feet) mm- - - -	Distance From Aircraft to Measurement Site			Engine Directivity Angle (degrees)
	Delta X (feet)	Delta Y (feet)	Total (feet)	
0	2454	3962	4660	117.8
200	2654	3948	4757	119.9
400	2853	3934	4860	122.0
600	3053	3921	4969	123.9
800	3252	3907	5083	125.8
1000	3452	3893	5203	127.6
1200	3651	3879	5327	129.3
1400	3851	3865	5456	130.9
1600	4050	3852	5589	132.5
1800	4250	3838	5726	134.0
2000	4449	3824	5867	135.4
2200	4649	3810	6011	136.7
2400	4848	3796	6158	138.0
2600	5048	3783	6308	139.2
2800	5247	3769	6461	140.4
3000	5447	3755	6616	141.5
3200	5646	3741	6773	142.5
3400	5846	3727	6933	143.5
3600	6045	3714	7095	144.5
3800	6245	3700	7259	145.4
4000	6444	3686	7424	146.3
4200	6644	3672	7591	147.1
4400	6844	3658	7760	147.9
4600	7043	3645	7930	148.7
4800	7243	3631	8102	149.4
5000	7442	3617	8275	150.1
5200	7642	3603	8449	150.8
5400	7841	3589	8624	151.4
5600	8041	3576	8800	152.1
5800	8240	3562	8977	152.7
6000	8440	3548	9155	153.2
6200	8639	3534	9334	153.8
6400	8839	3520	9514	154.3
6600	9038	3507	9695	154.8
6800	9238	3493	9876	155.3
7000	9437	3479	10058	155.8
7200	9637	3465	10241	156.3
7400	9836	3451	10424	156.7
7600	10036	3438	10608	157.1
7800	10235	3424	10793	157.5
8000	10435	3410	10978	157.9

TABLE A-7. NOISE MONITOR SITE 5

Distance From Start of Runway (feet)	Distance From Aircraft to Measurement Site			Engine Directivity Angle (degrees)
	Delta X (feet)	Delta Y (feet)	Total (feet)	
0	2949	537	2997	165.7
200	3149	523	3192	166.6
400	3348	509	3387	167.4
600	3548	496	3582	168.1
800	3747	482	3778	168.7
1000	3947	468	3974	169.3
1200	4146	454	4171	169.8
1400	4346	440	4368	170.3
1600	4545	427	4565	170.7
1800	4745	413	4763	171.1
2000	4944	399	4960	171.4
2200	5144	385	5158	171.8
2400	5343	371	5356	172.1
2600	5543	358	5554	172.4
2800	5742	344	5753	172.6
3000	5942	330	5951	172.9
3200	6141	316	6150	173.1
3400	6341	302	6348	173.3
3600	6540	289	6547	173.5
3800	6740	275	6746	173.7
4000	6939	261	6944	173.9
4200	7139	247	7143	174.1
4400	7339	233	7342	174.2
4600	7538	220	7541	174.4
4800	7738	206	7740	174.5
5000	7937	192	7939	174.7
5200	8137	178	8139	174.8
5400	8336	164	8338	174.9
5600	8536	151	8537	175.0
5800	8735	137	8736	175.1
6000	8935	123	8936	175.3
6200	9134	109	9135	175.4
6400	9334	95	9334	175.5
6600	9533	82	9534	175.6
6800	9733	68	9733	175.6
7000	9932	54	9932	175.7
7200	10132	40	10132	175.8
7400	10331	26	10331	175.9
7600	10531	13	10531	176.0
7800	10730	-1	10730	176.0
8000	10930	-15	10930	176.1

TABLE A-6. NOISE MONITOR SITE 4

Distance From Start of Runway (feet)	Distance From Aircraft to Measurement Site			Engine Directivity Angle (degrees)
	Delta X (feet)	Delta Y (feet)	Total (feet)	
0	2454	3962	4660	117.8
200	2654	3948	4757	119.9
400	2853	3934	4860	122.0
600	3053	3921	4969	123.9
800	3252	3907	5083	125.8
1000	3452	3893	5203	127.6
1200	3651	3879	5327	129.3
1400	3851	3865	5456	130.9
1600	4050	3852	5589	132.5
1800	4250	3838	5726	134.0
2000	4449	3824	5867	135.4
2200	4649	3810	6011	136.7
2400	4848	3796	6158	138.0
2600	5048	3783	6308	139.2
2800	5247	3769	6461	140.4
3000	5447	3755	6616	141.5
3200	5646	3741	6773	142.5
3400	5846	3727	6933	143.5
3600	6045	3714	7095	144.5
3800	6245	3700	7259	145.4
4000	6444	3686	7424	146.3
4200	6644	3672	7591	147.1
4400	6844	3658	7760	147.9
4600	7043	3645	7930	148.7
4800	7243	3631	8102	149.4
5000	7442	3617	8275	150.1
5200	7642	3603	8449	150.8
5400	7841	3589	8624	151.4
5600	8041	3576	8800	152.1
5800	8240	3562	8977	152.7
6000	8440	3548	9155	153.2
6200	8639	3534	9334	153.8
6400	8839	3520	9514	154.3
6600	9038	3507	9695	154.8
6800	9238	3493	9876	155.3
7000	9437	3479	10058	155.8
7200	9637	3465	10241	156.3
7400	9836	3451	10424	156.7
7600	10036	3438	10608	157.1
7800	10235	3424	10793	157.5
8000	10435	3410	10978	157.9

TABLE A-7. NOISE MONITOR SITE 5

Distance From Start of Runway (feet)	Distance From Aircraft to Measurement Site			Engine Directivity Angle (degrees)
	Delta X (feet)	Delta Y (feet)	Total (feet)	
0	2949	537	2997	165.7
200	3149	523	3192	166.6
400	3348	509	3387	167.4
600	3548	496	3582	168.1
800	3747	482	3778	168.7
1000	3947	468	3974	169.3
1200	4146	454	4171	169.8
1400	4346	440	4368	170.3
1600	4545	427	4565	170.7
1800	4745	413	4763	171.1
2000	4944	399	4960	171.4
2200	5144	385	5158	171.8
2400	5343	371	5356	172.1
2600	5543	358	5554	172.4
2800	5742	344	5753	172.6
3000	5942	330	5951	172.9
3200	6141	316	6150	173.1
3400	6341	302	6348	173.3
3600	6540	289	6547	173.5
3800	6740	275	6746	173.7
4000	6939	261	6944	173.9
4200	7139	247	7143	174.1
4400	7339	233	7342	174.2
4600	7538	220	7541	174.4
4800	7738	206	7740	174.5
5000	7937	192	7939	174.7
5200	8137	178	8139	174.8
5400	8336	164	8338	174.9
5600	8536	151	8537	175.0
5800	8735	137	8736	175.1
6000	8935	123	8936	175.3
6200	9134	109	9135	175.4
6400	9334	95	9334	175.5
6600	9533	82	9534	175.6
6800	9733	68	9733	175.6
7000	9932	54	9932	175.7
7200	10132	40	10132	175.8
7400	10331	26	10331	175.9
7600	10531	13	10531	176.0
7800	10730	-1	10730	176.0
8000	10930	-15	10930	176.1

TABLE A-6. NOISE MONITOR SITE 4

Distance From Start of Runway (feet) mm-----	Distance From Aircraft to Measurement Site			Engine Directivity Angle (degrees)
	Delta X (feet) -----	Delta Y (feet) -----	Total (feet) -----	
0	2454	3962	4660	117.8
200	2654	3948	4757	119.9
400	2853	3934	4860	122.0
600	3053	3921	4969	123.9
800	3252	3907	5083	125.8
1000	3452	3893	5203	127.6
1200	3651	3879	5327	129.3
1400	3851	3865	5456	130.9
1600	4050	3852	5589	132.5
1800	4250	3838	5726	134.0
2000	4449	3824	5867	135.4
2200	4649	3810	6011	136.7
2400	4848	3796	6158	138.0
2600	5048	3783	6308	139.2
2800	5247	3769	6461	140.4
3000	5447	3755	6616	141.5
3200	5646	3741	6773	142.5
3400	5846	3727	6933	143.5
3600	6045	3714	7095	144.5
3800	6245	3700	7259	145.4
4000	6444	3686	7424	146.3
4200	6644	3672	7591	147.1
4400	6844	3658	7760	147.9
4600	7043	3645	7930	148.7
4800	7243	3631	8102	149.4
5000	7442	3617	8275	150.1
5200	7642	3603	8449	150.8
5400	7841	3589	8624	151.4
5600	8041	3576	8800	152.1
5800	8240	3562	8977	152.7
6000	8440	3548	9155	153.2
6200	8639	3534	9334	153.8
6400	8839	3520	9514	154.3
6600	9038	3507	9695	154.8
6800	9238	3493	9876	155.3
7000	9437	3479	10058	155.8
7200	9637	3465	10241	156.3
7400	9836	3451	10424	156.7
7600	10036	3438	10608	157.1
7800	10235	3424	10793	157.5
8000	10435	3410	10978	157.9

TABLE A-7. NOISE MONITOR SITE 5

Distance From Start of Runway (feet) -----	Distance From Aircraft to Measurement Site			Engine Directivity Angle (degrees)
	Delta X (feet) -----	Delta Y (feet) -----	Total (feet) -----	
0	2949	537	2997	165.7
200	3149	523	3192	166.6
400	3348	509	3387	167.4
600	3548	496	3582	168.1
800	3747	482	3778	168.7
1000	3947	468	3974	169.3
1200	4146	454	4171	169.8
1400	4346	440	4368	170.3
1600	4545	427	4565	170.7
1800	4745	413	4763	171.1
2000	4944	399	4960	171.4
2200	5144	385	5158	171.8
2400	5343	371	5356	172.1
2600	5543	358	5554	172.4
2800	5742	344	5753	172.6
3000	5942	330	5951	172.9
3200	6141	316	6150	173.1
3400	6341	302	6348	173.3
3600	6540	289	6547	173.5
3800	6740	275	6746	173.7
4000	6939	261	6944	173.9
4200	7139	247	7143	174.1
4400	7339	233	7342	174.2
4600	7538	220	7541	174.4
4800	7738	206	7740	174.5
5000	7937	192	7939	174.7
5200	8137	178	8139	174.8
5400	8336	164	8338	174.9
5600	8536	151	8537	175.0
5800	8735	137	8736	175.1
6000	8935	123	8936	175.3
6200	9134	109	9135	175.4
6400	9334	95	9334	175.5
6600	9533	82	9534	175.6
6800	9733	68	9733	175.6
7000	9932	54	9932	175.7
7200	10132	40	10132	175.8
7400	10331	26	10331	175.9
7600	10531	13	10531	176.0
7800	10730	-1	10730	176.0
8000	10930	-15	10930	176.1

This appendix provides a complete listing of the hourly atmospheric observations reported by the National Weather Service (**NWS**) for the nine measurement days of this study. It also provides plots of the continuous wind data acquired as a part of the study.

The first column of the hourly weather tables shows the local time (hours and minutes) when the observations were made. The second column shows the visibility (in miles). The third and fourth columns show the temperature (dry bulb) and dew point, respectively. The fifth column shows the relative humidity (which was calculated from the temperature, dew point and barometric pressure. The sixth and seventh columns show the wind direction in degrees and the wind speed in miles per hour. The wind direction is recorded only to the nearest **10** degrees by **NWS**. The last column shows the barometric pressure in inches of mercury.

The continuous wind monitoring plots show wind speed and direction as a function of time of day. The horizontal axis of the graphs show the time of day (local time) in hours. The three panels in the graph show different aspects of wind. Because of the second-to-second fluctuations in wind speed and direction the data has been time-averaged to improve the visualization of trends in the data. The averaging process used in these graphs is identical to the two-minute vector averaging process used to characterize the wind speed and direction for each aircraft takeoff. That is, sixty speed and direction data pairs each acquired every two seconds were converted to X and Y speed components. The X and Y components were averaged separately, and these average values were then converted back to a speed and direction.

The top panel in the graph shows the **2-minute** average wind speed in miles per hour. The middle panel is a gust indicator which plots the difference between the highest speed observed during the **2-minute** interval and the average value. The bottom panel shows the **2-minute** average wind direction. The indicated direction is the compass heading the wind is **coming from**. This plot can sometimes have a rather ragged appearance when the wind direction is drifting back and forth about **the** zero degree position. This condition is most evident on **19** December where the wind direction is actually very stable with total variability of **45** degrees or less. The plotting artifact however, gives the appearance of much greater fluctuations.

TABLE B-1. BWI AIRPORT WEATHER OBSERVATIONS FOR 22 OCTOBER 1991

Time (EDT)	Visibility (miles)	Temp (oF)	Dew Point (oF)	Rel Humidity (%)	----- Wind ----- Direction* Speed (degrees) (mph)	Barom. Pressure (in. Hg)
00:52	15	40	37	89	270 5	30.040
01:52	15	39	37	92	250 3	30.030
02:52	12	40	36	85	280 3	30.030
03:52			35	89	250 5	30.030
04:52	12		35	89	260 6	30.040
05:52	12	38	35	89	230 5	30.040
06:52	10	37	34	89	200 5	30.060
07:53	6		36	89	260 6	30.070
08:53	5	44	40	86	280 5	30.090
09:53	6	52	44	74	190 3	30.090
10:52	7	58	44	60	180 5	30.090
11:52	7	64	45	50	-- 0	30.090
12:52	7	67	47	49	180 3	30.070
13:52	7		46	44	-- 0	30.050
14:53	7	69	50	51	100 7	30.040
15:53	10		50	51	90 6	30.030
16:53	10	67	51	56	80 6	30.030
17:53	10	62	51	67	90 6	30.045
18:53	10	59	52	78	120 5	30.060
19:53	10	59	51	75	-- 0	30.070
20:53	10	57	50	77	-- 0	30.080
21:55	10	54	49	83	280 6	30.080
22:53	7	52	50	93	280 5	30.090
23:52	5	51	49	93	-- 0	30.100

TABLE B-2. BWI AIRPORT WEATHER OBSERVATIONS FOR 23 OCTOBER 1991

Time (EDT)	Visibility (miles)	Temp (oF)	Dew Point (oF)	Rel Humidity (%)	----- Wind ----- Direction* Speed (degrees) (mph)	Barom. Pressure (in. Hg)
00:52	5	50	47	89	-- 0	30.100
01:52	4	50	47	89	-- 0	30.100
02:52	4	50	47	89	-- 0	30.110
03:52	4	48	46	93	250 5	30.110
04:52	2.5	49	47	93	-- 0	30.120
05:52	2.5	52	50	93	20 3	30.130
06:52	2.5	52	51	96	30 3	30.140
07:52	0.375	53	52	96	40 5	30.160
08:52	0.375	54	53	96	20 5	30.175
09:52	0.375	56	55	96	80	30.185
10:52	1	60	56	87	80 8	30.190
11:52	2	64	57	78	90	30.190
12:52	3	69	59	70	130 3	30.175
13:52	4	70	60	71	130 9	30.160
14:52	4	72	59	64	130 3	30.155
15:53	6	72	60	66	100 9	30.150
16:53	6	71	59	66	120 10	30.145
17:53	6	68	59	73	110 8	30.145
18:53	7	64	58	81	140 6	30.160
19:53	7	62	58	87	170 6	30.175
20:53	7	60	58	93	40 6	30.190
21:53	7	60	58	93	60 3	30.200
22:53	4	58	57	96	90 7	30.210
23:52	4	58	57	96	60 5	30.220

* Note: Wind Direction re: True North

TABLE B-1. BWI AIRPORT WEATHER OBSERVATIONS FOR 22 OCTOBER 1991

Time (EDT)	Visibility (miles)	Temp (oF)	Dew Point (oF)	Rel Humidity (%)	----- Wind ----- Direction* Speed (degrees) (mph)	Barom. Pressure (in. Hg)
00:52	15	40	37	89	270 5	30.040
01:52	15	39	37	92	250 3	30.030
02:52	12	40	36	85	280 3	30.030
03:52			35	89	250 5	30.030
04:52	12		35	89	260 6	30.040
05:52	12	38	35	89	230 5	30.040
06:52	10	37	34	89	200 5	30.060
07:53	6		36	89	260 6	30.070
08:53	5	44	40	86	280 5	30.090
09:53	6	52	44	74	190 3	30.090
10:52	7	58	44	60	180 5	30.090
11:52	7	64	45	50	-- 0	30.090
12:52	7	67	47	49	180 3	30.070
13:52	7		46	44	-- 0	30.050
14:53	7	69	50	51	100 7	30.040
15:53	10		50	51	90 6	30.030
16:53	10	67	51	56	80 6	30.030
17:53	10	62	51	67	90 6	30.045
18:53	10	59	52	78	120 5	30.060
19:53	10	59	51	75	-- 0	30.070
20:53	10	57	50	77	-- 0	30.080
21:55	10	54	49	83	280 6	30.080
22:53	7	52	50	93	280 5	30.090
23:52	5	51	49	93	-- 0	30.100

TABLE B-2. BWI AIRPORT WEATHER OBSERVATIONS FOR 23 OCTOBER 1991

Time (EDT)	Visibility (miles)	Temp (oF)	Dew Point (oF)	Rel Humidity (%)	----- Wind ----- Direction* Speed (degrees) (mph)	Barom. Pressure (in. Hg)
00:52	5	50	47	89	-- 0	30.100
01:52	4	50	47	89	-- 0	30.100
02:52	4	50	47	89	-- 0	30.110
03:52	4	48	46	93	250 5	30.110
04:52	2.5	49	47	93	-- 0	30.120
05:52	2.5	52	50	93	20 3	30.130
06:52	2.5	52	51	96	30 3	30.140
07:52	0.375	53	52	96	40 5	30.160
08:52	0.375	54	53	96	20 5	30.175
09:52	0.375	56	55	96	80	30.185
10:52	1	60	56	87	80 8	30.190
11:52	2	64	57	78	90	30.190
12:52	3	69	59	70	130 3	30.175
13:52	4	70	60	71	130 9	30.160
14:52	4	72	59	64	130 3	30.155
15:53	6	72	60	66	100 9	30.150
16:53	6	71	59	66	120 10	30.145
17:53	6	68	59	73	110 8	30.145
18:53	7	64	58	81	140 6	30.160
19:53	7	62	58	87	170 6	30.175
20:53	7	60	58	93	40 6	30.190
21:53	7	60	58	93	60 3	30.200
22:53	4	58	57	96	90 7	30.210
23:52	4	58	57	96	60 5	30.220

* Note: Wind Direction re: True North

TABLE B-5. BWI AIRPORT WEATHER OBSERVATIONS FOR 15 DECEMBER 1991

Time (EST)	Visibility (miles)	Temp (oF)	Dew Point (oF)	Rel Humidity (%)	----- Wind Direction* (degrees)	----- Speed (mph)	Barom. Pressure (in. Hg)
00:52	20	36	12	33	300	20	29.870
01:52	20	35	12	34	290	21	29.880
02:52	20	35	13	36	260	17	29.910
03:52	20	34	13	37	260	18	29.920
04:52	20	33	12	37	250	17	29.920
05:52	20	32	13	41	240	12	29.930
06:52	20	31	13	42	250	15	29.950
07:52	20	32	13	41	250	16	29.975
08:52	20	34	12	36	270	17	30.000
09:52	20	35	11	33	270	18	30.020
10:52	20	36	10	30	280	18	30.020
11:52	20	38	9	26	260	20	30.000
12:52	20	38	8	25	280	22	29.975
	20	39	4	19	260	23	29.965
14:52	20	40	4	19	280	20	29.940
15:53	20	38	4	20	280	12	29.935
16:53	20	34	6	26	250	7	29.930
17:53	20	35	5	24	260	5	29.940
18:53	20	34	7	28	200	5	29.945
19:53	20	32	11	37	200	8	29.935
20:53	20	34	10	32	310	8	29.940
21:53	20	36	10	30	290	10	29.940
22:53	20	32	10	35	250	7	29.930
23:53	15	30	11	40	280	10	29.920

TABLE B-6. BWI AIRPORT WEATHER OBSERVATIONS FOR 16 DECEMBER 1991

Time (EST)	Visibility (miles)	Temp (oF)	Dew Point (oF)	Rel Humidity (%)	----- Wind Direction* (degrees)	----- Speed (mph)	Barom. Pressure (in. Hg)
00:52	15	33	14	41	260	18	29.920
01:52	15	33	16	41	260	22	29.940
02:52	15	30	13	51	290	16	29.980
03:52	15	29		46	300	16	29.980
04:52	15	27	10	44	300	18	30.010
05:52	15	26	7	40	290	17	30.050
06:52	20	24	6	41	280	15	30.090
07:52	20	24	4	37	290	15	30.125
08:52	20			34	290	17	30.150
09:52	20	25	5	36	290	20	30.170
10:52	20	27	5	34	290	17	30.160
11:52	20	28		31	280	15	30.140
12:52			4		300		30.130
13:52	20	28	0	25	290	16	30.125
14:52	20	28	2	28	290	13	30.125
15:53	20	27	2	29	270	14	30.140
16:53	20	25	2	32	300	6	30.140
17:53	20	24	3	35	270	5	30.140
18:53	20	24	7	43	200	3	30.155
19:53	20	24	10	51	200	5	30.160
20:53	20	25	11	51	200	3	30.150
21:53	15	26	11	48	200	3	30.150
22:53	15	25	9	46	180	3	30.150
23:53	15	25	12	53	210	3	30.145

* Note: Wind Direction re: True North

TABLE B-7. BWIAI RPORT WEATHER OBSERVATIONS FOR 17 DECEMBER 1991

Time (EST)	Visibility (miles)	Temp (oF)	Dew Point (oF)	Rel Humidity (%)	----- Wind ----- Direction* (degrees)	Speed (mph)	Barom. Pressure (in. Hg)
00:53	15	25	13	56	110	3	30.130
01:53	15	26	11	48	90	3	30.125
02:53	15	25	9	46	90	5	30.125
03:53	15	26	14	56	100	3	30.100
04:53	15	28	15	54	130	6	30.080
05:53	15	28	17	59	80	6	30.080
06:53	15	29	18	59	130	7	30.070
07:52	15	29	18	59	90	7	30.055
08:52	15	30	18	57	120	7	30.035
09:52	20	32	21	60	100	7	30.000
10:52	20	36	27	68	140	9	29.955
11:52	20	39	21	45	180	10	29.900
12:52	20	40	18	38	160	12	29.830
13:52	20	41	18	36	170	8	29.785
14:52	20	45	19	33	190	9	29.765
15:52	20	44	20	36	170	6	29.755
16:52	20	41	21	42	140	6	29.745
17:52	20	39	25	55	150	5	29.745
18:52	20	37	25	59	—	0	29.745
19:52	20	33	23	63	220	5	29.755
20:52	20	32	23	66	230	6	29.765
21:52	20	35	23	58	300	8	29.785
22:52	20	41	24	48	310	14	29.820
23:53	20	39	23	50	310	10	29.850

TABLE B-8. BWI AI RPORT WEATHER OBSERVATIONS FOR 18 DECEMBER 1991

Time (EST)	Visibility (miles)	Temp (oF)	Dew Point (oF)	Rel Humidity (%)	----- Wind ----- Direction* (degrees)	Speed (mph)	Barom. Pressure (in. Hg)
00:53	20	37	18	42	290	12	29.865
01:53	20	38	16	37	310	18	29.890
02:53	20	33	17	47	220	9	29.915
03:53	20	36	16	40	240	15	29.920
04:53	20	34	17	45	260	14	29.935
05:53	20	34	15	41	270	12	29.950
06:53	20	34	16	43	270	9	29.960
07:52	20	34	17	45	280	7	30.000
08:52	20	35	21	53	280	8	30.015
09:52	20	35	19	48	280	16	30.040
10:52	20	37	12	32	300	15	30.040
11:52	20	38	14	33	280	18	30.025
12:52	20	37	11	30	280	18	30.025
13:52	20	36	10	30	300	16	30.030
14:52	20	35	10	31	290	14	30.060
15:52	20	34	13	37	290	16	30.080
16:52	20	32	10	35	310	16	30.120
17:52	20	31	8	33	280	17	30.160
18:52	20	30	8	35	290	15	30.190
19:52	20	28	11	44	280	12	30.220
20:52	20	28	10	42	290	13	30.240
21:52	20	27	10	44	290	14	30.260
22:52	20	27	7	38	310	17	30.280
23:53	20	24	0	30	330	17	30.330

* Note: Wind Direction re: True North

TABLE B-7. BWIAI RPORT WEATHER OBSERVATIONS FOR 17 DECEMBER 1991

Time (EST)	Visibility (miles)	Temp (oF)	Dew Point (oF)	Rel Humidity (%)	Wind Direction* (degrees)	Speed (mph)	Barom. Pressure (in. Hg)
00:53	15	25	13	56	110	3	30.130
01:53	15	26	11	48	90	3	30.125
02:53	15	25	9	46	90	5	30.125
03:53	15	26	14	56	100	3	30.100
04:53	15	28	15	54	130	6	30.080
05:53	15	28	17	59	80	6	30.080
06:53	15	29	18	59	130	7	30.070
07:52	15	29	18	59	90	7	30.055
08:52	15	30	18	57	120	7	30.035
09:52	20	32	21	60	100	7	30.000
10:52	20	36	27	68	140	9	29.955
11:52	20	39	21	45	180	10	29.900
12:52	20	40	18	38	160	12	29.830
13:52	20	41	18	36	170	8	29.785
14:52	20	45	19	33	190	9	29.765
15:52	20	44	20	36	170	6	29.755
16:52	20	41	21	42	140	6	29.745
17:52	20	39	25	55	150	5	29.745
18:52	20	37	25	59	—	0	29.745
19:52	20	33	23	63	220	5	29.755
20:52	20	32	23	66	230	6	29.765
21:52	20	35	23	58	300	8	29.785
22:52	20	41	24	48	310	14	29.820
23:53	20	39	23	50	310	10	29.850

TABLE B-8. BWI AI RPORT WEATHER OBSERVATIONS FOR 18 DECEMBER 1991

Time (EST)	Visibility (miles)	Temp (oF)	Dew Point (oF)	Rel Humidity (%)	Wind Direction* (degrees)	Speed (mph)	Barom. Pressure (in. Hg)
00:53	20	37	18	42	290	12	29.865
01:53	20	38	16	37	310	18	29.890
02:53	20	33	17	47	220	9	29.915
03:53	20	36	16	40	240	15	29.920
04:53	20	34	17	45	260	14	29.935
05:53	20	34	15	41	270	12	29.950
06:53	20	34	16	43	270	9	29.960
07:52	20	34	17	45	280	7	30.000
08:52	20	35	21	53	280	8	30.015
09:52	20	35	19	48	280	16	30.040
10:52	20	37	12	32	300	15	30.040
11:52	20	38	14	33	280	18	30.025
12:52	20	37	11	30	280	18	30.025
13:52	20	36	10	30	300	16	30.030
14:52	20	35	10	31	290	14	30.060
15:52	20	34	13	37	290	16	30.080
16:52	20	32	10	35	310	16	30.120
17:52	20	31	8	33	280	17	30.160
18:52	20	30	8	35	290	15	30.190
19:52	20	28	11	44	280	12	30.220
20:52	20	28	10	42	290	13	30.240
21:52	20	27	10	44	290	14	30.260
22:52	20	27	7	38	310	17	30.280
23:53	20	24	0	30	330	17	30.330

* Note: Wind Direction re: True North

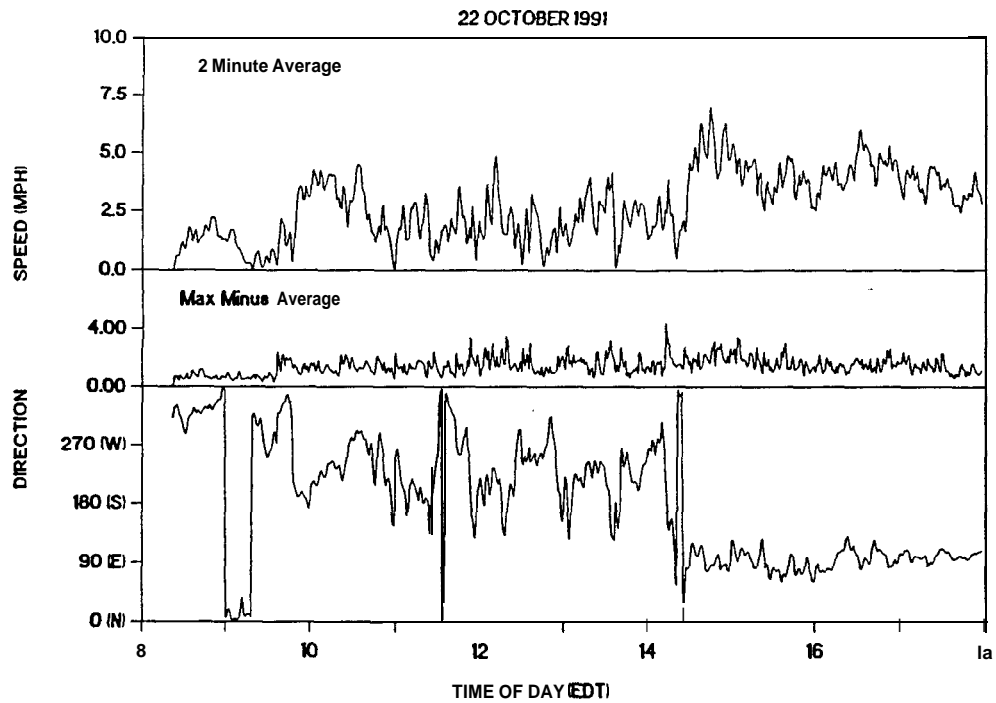


FIGURE E1. WIND SPEED AND DIRECTION – 22 OCTOBER 1992

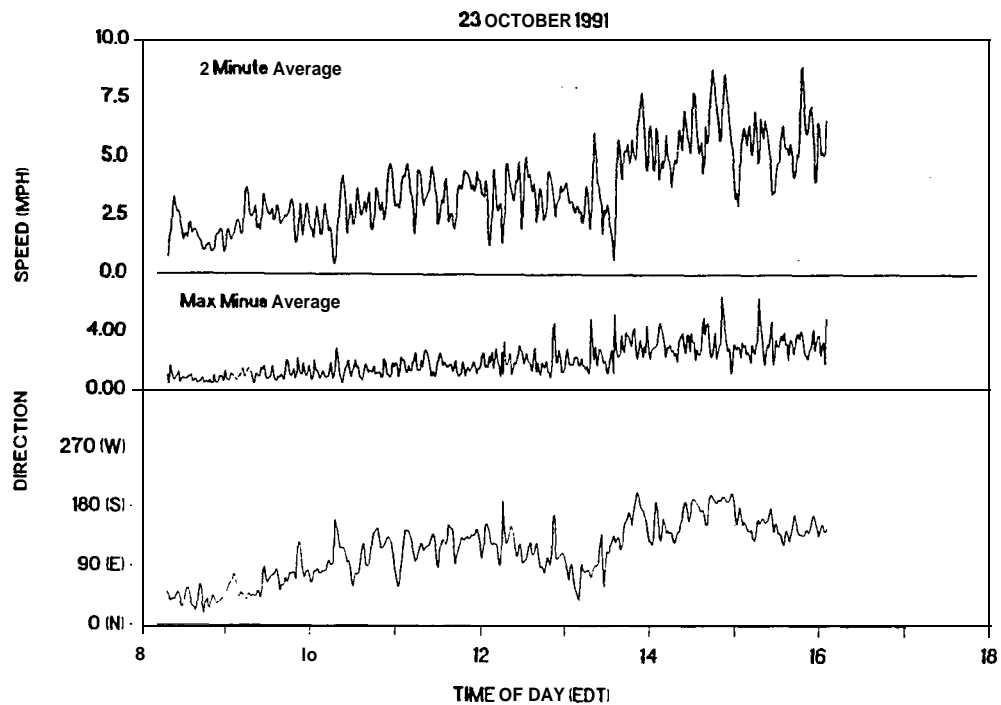


FIGURE B-2. WIND SPEED AND DIRECTION – 23 OCTOBER 1992

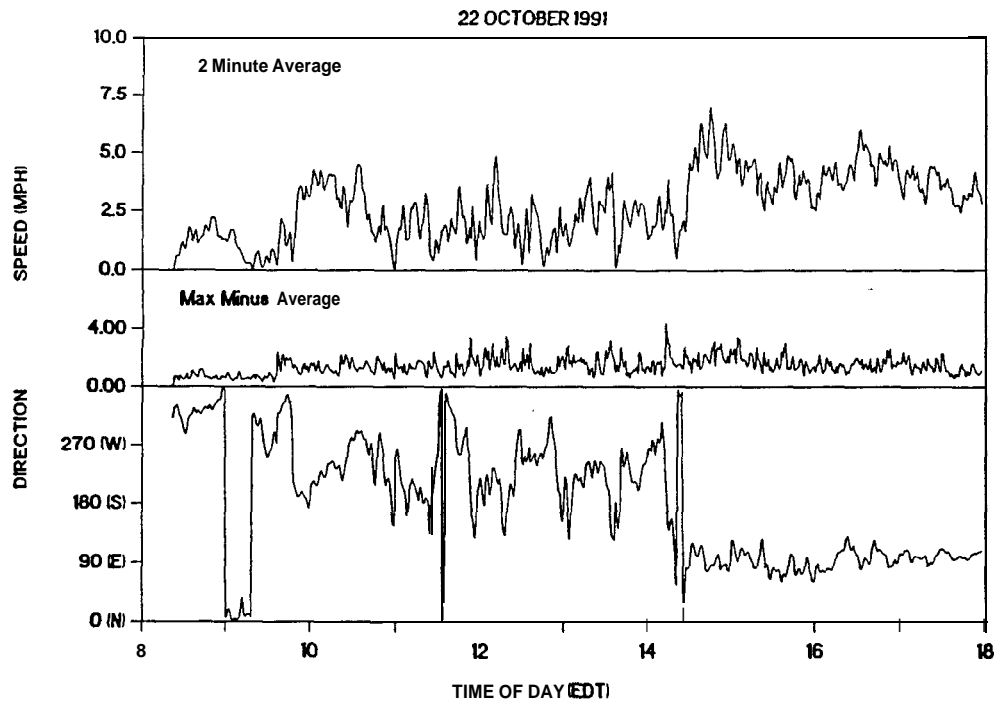


FIGURE E1. WIND SPEED AND DIRECTION – 22 OCTOBER 1992

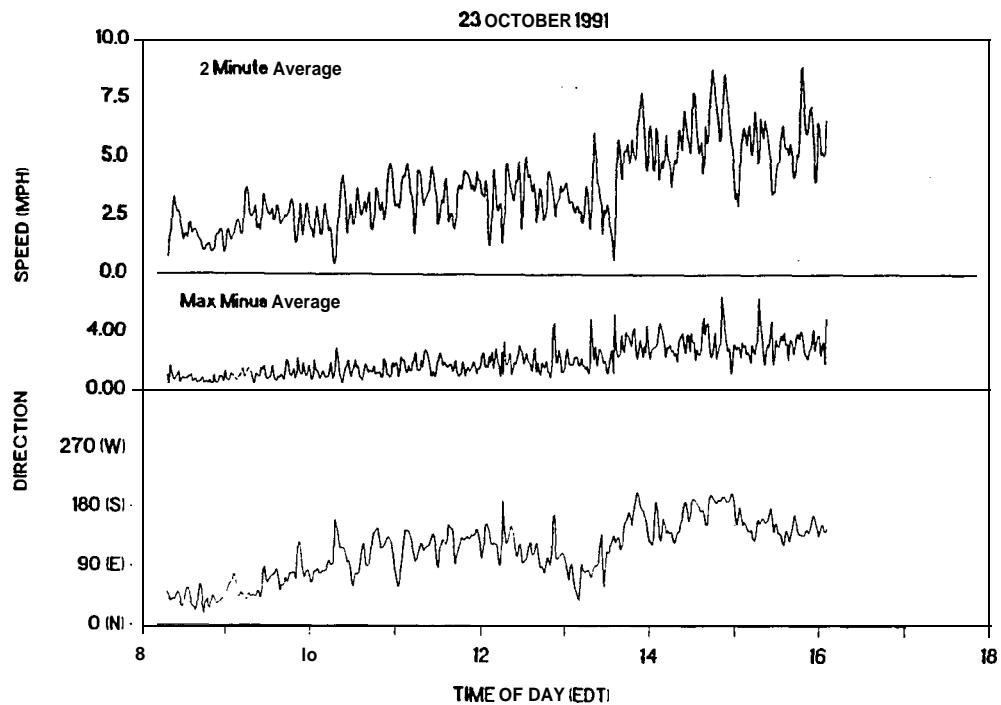


FIGURE B-2. WIND SPEED AND DIRECTION – 23 OCTOBER 1992

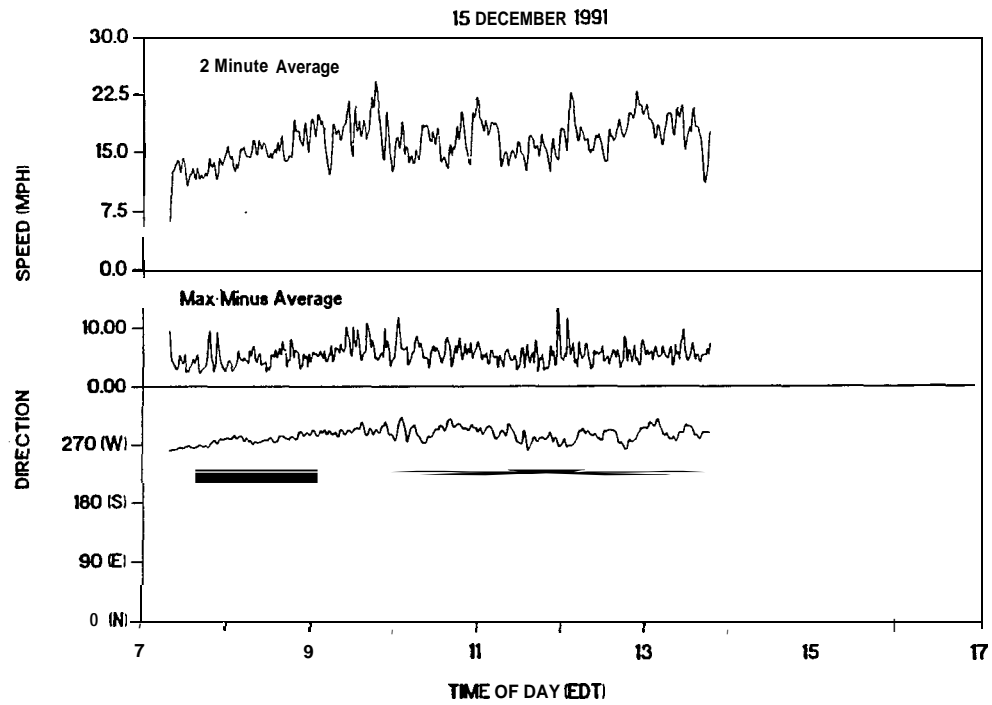


FIGURE B-5. WIND SPEED AND DIRECTION – 15 DECEMBER 1992

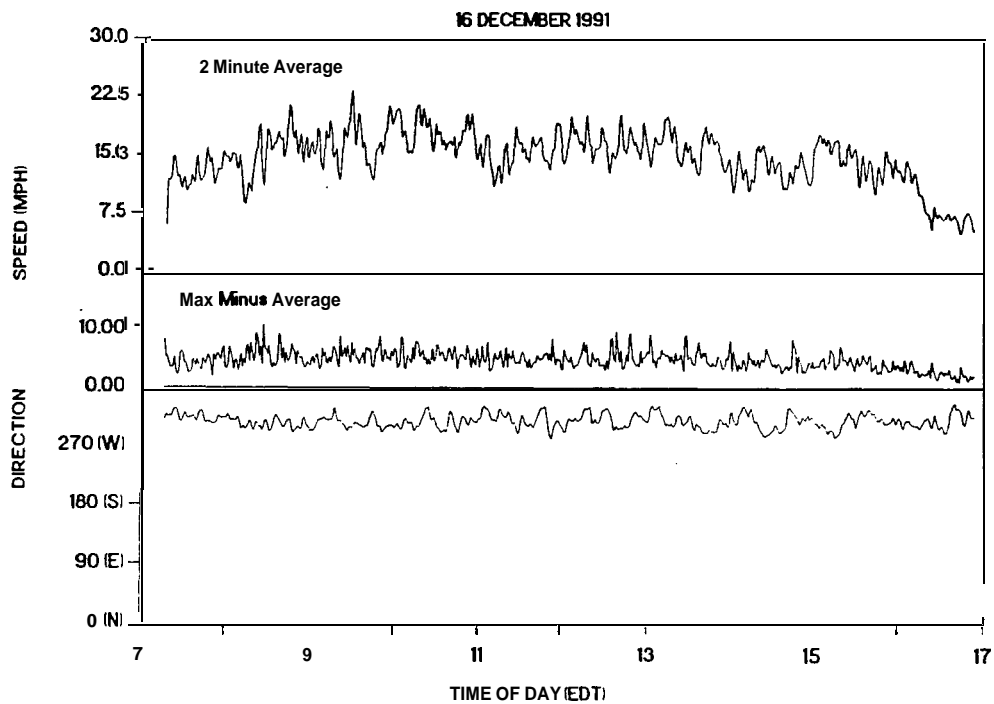


FIGURE B-6. WIND SPEED AND DIRECTION – 16 DECEMBER 1992

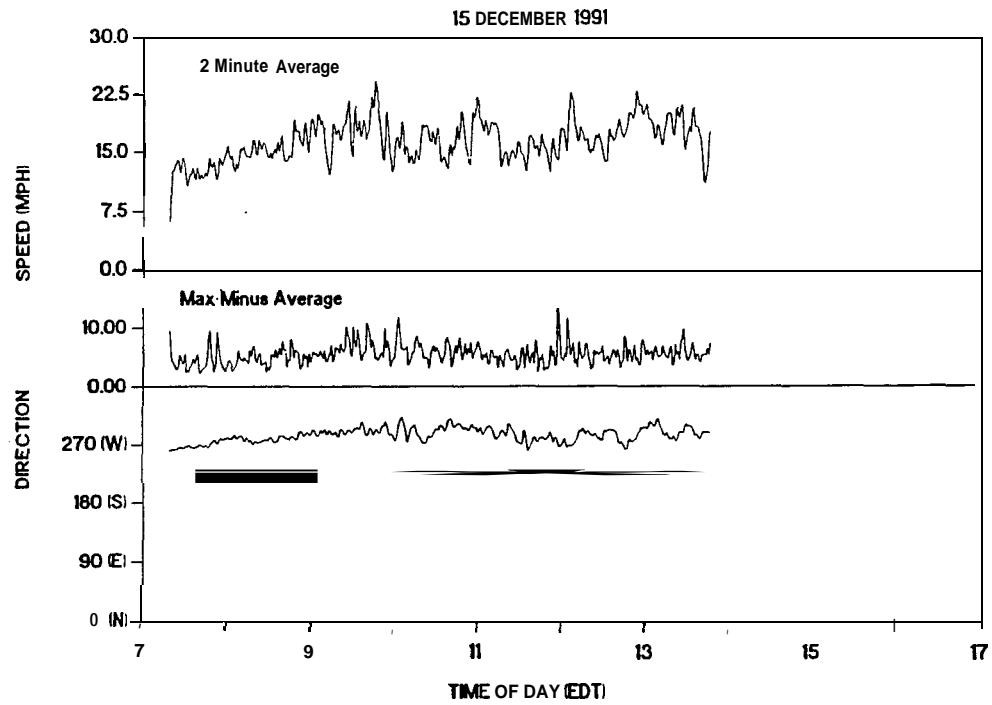


FIGURE B-5. WIND SPEED AND DIRECTION – 15 DECEMBER 1992

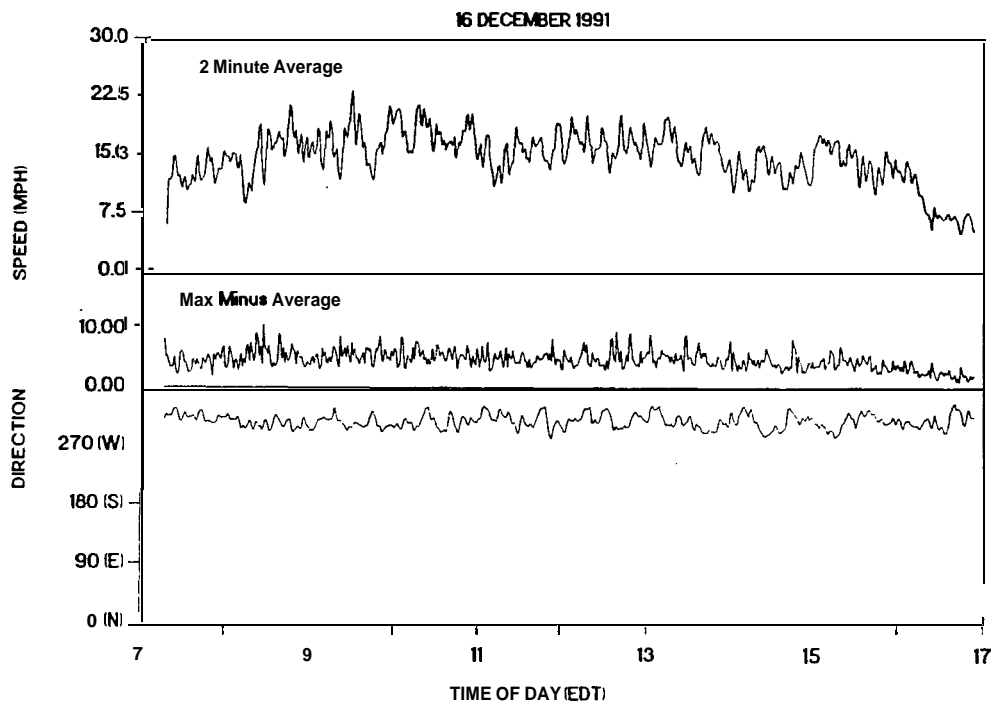


FIGURE B-6. WIND SPEED AND DIRECTION – 16 DECEMBER 1992

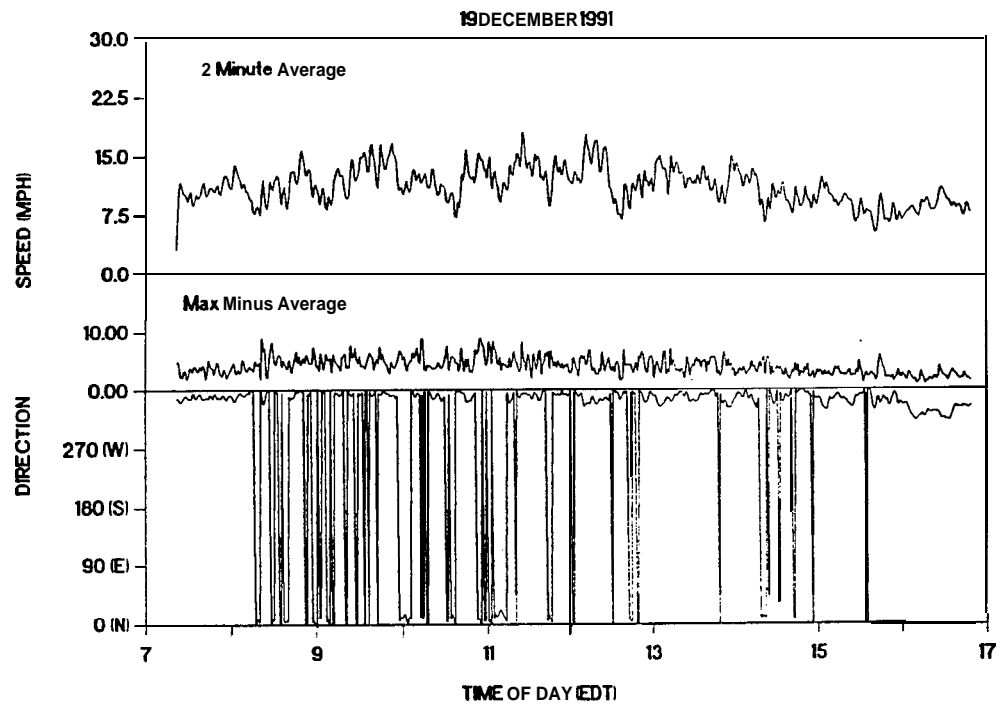


FIGURE B-9. WIND SPEED AND DIRECTION – 19 DECEMBER 1992

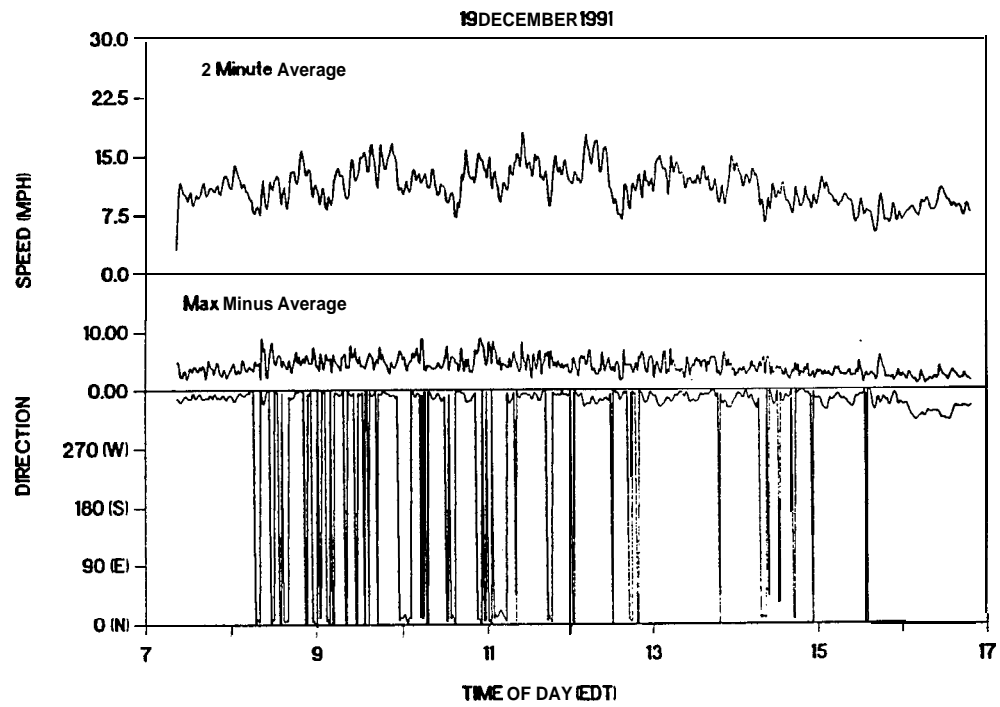


FIGURE B-9. WIND SPEED AND DIRECTION – 19 DECEMBER 1992

This appendix provides a list of the database files assembled from the measured data (and discussed in Sections 3.2 and 3.3 of the report. Table C-1 identifies the names of the database files by measurement date. Table C-2 provides a complete list of **all** the data fields in the master databases, the spreadsheet column in which they appear if brought into a commercially available spreadsheet, and a description of the variable contained in the field.

For the most part the variables are self explanatory. One exception is the cursor position used to bracket the portion of the A-level time history used in the **SEL** calculations. The cursor position is reported in units of screen pixels (**40** corresponds to **-60** seconds **re:** brake release, and **410** corresponds to + **150** seconds. The equation below may be used to translate the cursor position in pixels to time **re:** brake release in seconds.

$$\text{Time (sec)} = 0.5676 * \text{Pixels} - 82.7 \quad (\text{C-1})$$

TABLE C-1. DATABASE (*.DBF) FILES

Date	Master Database	Site #1	Site #2	Site #3	Site #4	Site #5
10-22-91	MSTR1022	01HST295	02HST295	- - -	04HST295	05HST295
10-23-91	MSTR1023	01HST296	02HST296	- - -	04HST296	05HST296
10-24-91	MSTR1024	01HST297	02HST297	- - -	04HST297	05HST297
10-25-91	MSTR1025	01HST298	02HST298	- - -	04HST298	05HST298
12-15-91	MSTR1215	01HST348	02HST348	- - -	04HST348	05HST348
12-16-91	MSTR1216	01HST349	02HST349	03HST349	04HST349	05HST349
12-17-91	MSTR1217	01HST350	02HST350	03HST350	04HST350	05HST350
12-18-91	MSTR1218	01HST351	02HST351	03HST351	04HST351	05HST351
12-19-91	MSTR1219	01HST352	02HST352	03HST352	04HST352	05HST352

This appendix provides a list of the database files assembled from the measured data (and discussed in Sections 3.2 and 3.3 of the report. Table C-1 identifies the names of the database files by measurement date. Table C-2 provides a complete list of **all** the data fields in the master databases, the spreadsheet column in which they appear if brought into a commercially available spreadsheet, and a description of the variable contained in the field.

For the most part the variables are self explanatory. One exception is the cursor position used to bracket the portion of the A-level time history used in the **SEL** calculations. The cursor position is reported in units of screen pixels (**40** corresponds to **-60** seconds **re:** brake release, and **410** corresponds to + **150** seconds. The equation below may be used to translate the cursor position in pixels to time **re:** brake release in seconds.

$$\text{Time (sec)} = 0.5676 * \text{Pixels} - 82.7 \quad (\text{C-1})$$

TABLE C-1. DATABASE (*.DBF) FILES

Date	Master Database	Site #1	Site #2	Site #3	Site #4	Site #5
10-22-91	MSTR1022	01HST295	02HST295	- - -	04HST295	05HST295
10-23-91	MSTR1023	01HST296	02HST296	- - -	04HST296	05HST296
10-24-91	MSTR1024	01HST297	02HST297	- - -	04HST297	05HST297
10-25-91	MSTR1025	01HST298	02HST298	- - -	04HST298	05HST298
12-15-91	MSTR1215	01HST348	02HST348	- - -	04HST348	05HST348
12-16-91	MSTR1216	01HST349	02HST349	03HST349	04HST349	05HST349
12-17-91	MSTR1217	01HST350	02HST350	03HST350	04HST350	05HST350
12-18-91	MSTR1218	01HST351	02HST351	03HST351	04HST351	05HST351
12-19-91	MSTR1219	01HST352	02HST352	03HST352	04HST352	05HST352

TABLE C-2 (CON'T). DESCRIPTION OF DATABASE FIELDS

Field Name	Spreadsheet Column	Description
SEL210	AR	SEL over top 10 dB at site #2 (dB)
GOOD210	AS	SEL over top 10 dB at site #2 OK? (0=N, 1=Y)
SEL215	AT	SEL over top 15 dB at site #2 (dB)
GOOD215	AU	SEL over top 15 dB at site #2 OK? (0=N, 1=Y)
SEL220	AV	SEL over top 20 dB at site #2 (dB)
GOOD220	AW	SEL over top 20 dB at site #2 OK? (0=N, 1=Y)
BKGND2	AX	Background A-weighted sound level at site #2 (dB)
START2	AY	Left cursor position for site #2
STOP2	AZ	Right cursor position for site #2
SEL310	BA	SEL over top 10 dB at site #3 (dB)
GOOD310	BB	SEL over top 10 dB at site #3 OK? (0=N, 1=Y)
SEL315	BC	SEL over top 15 dB at site #3 (dB)
GOOD315	BD	SEL over top 15 dB at site #3 OK? (0=N, 1=Y)
SEL320	BE	SEL over top 20 dB at site #3 (dB)
GOOD320	BF	SEL over top 20 dB at site #3 OK? (0=N, 1=Y)
BKGND3	BG	Background A-weighted sound level at site #3 (dB)
START3	BH	Left cursor position for site #3
STOP3	BI	Right cursor position for site #3
SEL410	BJ	SEL over top 10 dB at site #4 (dB)
GOOD410	BK	SEL over top 10 dB at site #4 OK? (0=N, 1=Y)
SEL415	BL	SEL over top 15 dB at site #4 (dB)
GOOD415	BM	SEL over top 15 dB at site #4 OK? (0=N, 1=Y)
SEL420	BN	SEL over top 20 dB at site #4 (dB)
GOOD420	BO	SEL over top 20 dB at site #4 OK? (0=N, 1=Y)
BKGND4	BP	Background A-weighted sound level at site #4 (dB)
START4	BQ	Left cursor position for site #4
STOP4	BR	Right cursor position for site #4
SEL510	BS	SEL over top 10 dB at site #5 (dB)
GOOD510	BT	SEL over top 10 dB at site #5 OK? (0=N, 1=Y)
SEL515	BU	SEL over top 15 dB at site #5 (dB)
GOOD515	BV	SEL over top 15 dB at site #5 OK? (0=N, 1=Y)
SEL520	BW	SEL over top 20 dB at site #5 (dB)
GOOD520	BX	SEL over top 20 dB at site #5 OK? (0=N, 1=Y)
BKGND5	BY	Background A-weighted sound level at site #5 (dB)
START5	BZ	Left cursor position for site #5
STOP5	CA	Right cursor position for site #5
INTRO	CB	Time of potential interference event (hours).
ITYP0	CC	Type and status of interference event.
INTR1	CD	Time of potential interference event (hours).
ITYP1	CE	Type and status of interference event.
INTR2	CF	Time of potential interference event (hours).
ITYP2	CG	Type and status of interference event.
INTR3	CH	Time of potential interference event (hours).
ITYP3	CI	Type and status of interference event.

TABLE C-2 (CON'T). DESCRIPTION OF DATABASE FIELDS

Field Name	Spreadsheet Column	Description
INTR4	CJ	Time of potential interference event (hours).
ITYP4	CK	Type and status of interference event.
INTR5	CL	Time of potential interference event (hours).
ITYP5	CM	Type and status of interference event.
INTR6	CN	Time of potential interference event (hours).
ITYP6	CO	Type and status of interference event.
INTR7	CP	Time of potential interference event (hours).
ITYP7	CQ	Type and status of interference event.
INTR8	CR	Time of potential interference event (hours).
ITYP8	CS	Type and status of interference event.
INTR9	CT	Time of potential interference event (hours).
ITYP9	CU	Type and status of interference event.
MAX1	CV	Maximum A-weighted sound level at site #1
MAX2	CW	Maximum A-weighted sound level at site #2
MAX3	CX	Maximum A-weighted sound level at site #3
MAX4	CY	Maximum A-weighted sound level at site #4
MAX5	CZ	Maximum A-weighted sound level at site #5

TABLE C-2 (CON'T). DESCRIPTION OF DATABASE FIELDS

Field Name	Spreadsheet Column	Description
INTR4	CJ	Time of potential interference event (hours).
ITYP4	CK	Type and status of interference event.
INTR5	CL	Time of potential interference event (hours).
ITYP5	CM	Type and status of interference event.
INTR6	CN	Time of potential interference event (hours).
ITYP6	CO	Type and status of interference event.
INTR7	CP	Time of potential interference event (hours).
ITYP7	CQ	Type and status of interference event.
INTR8	CR	Time of potential interference event (hours).
ITYP8	CS	Type and status of interference event.
INTR9	CT	Time of potential interference event (hours).
ITYP9	CU	Type and status of interference event.
MAX1	CV	Maximum A-weighted sound level at site #1
MAX2	CW	Maximum A-weighted sound level at site #2
MAX3	CX	Maximum A-weighted sound level at site #3
MAX4	CY	Maximum A-weighted sound level at site #4
MAX5	CZ	Maximum A-weighted sound level at site #5

TABLE C-2 (CON'T). DESCRIPTION OF DATABASE FIELDS

Field Name	Spreadsheet Column	Description
INTR4	CJ	Time of potential interference event (hours).
ITYP4	CK	Type and status of interference event.
INTR5	CL	Time of potential interference event (hours).
ITYP5	CM	Type and status of interference event.
INTR6	CN	Time of potential interference event (hours).
ITYP6	CO	Type and status of interference event.
INTR7	CP	Time of potential interference event (hours).
ITYP7	CQ	Type and status of interference event.
INTR8	CR	Time of potential interference event (hours).
ITYP8	CS	Type and status of interference event.
INTR9	CT	Time of potential interference event (hours).
ITYP9	CU	Type and status of interference event.
MAX1	CV	Maximum A-weighted sound level at site #1
MAX2	CW	Maximum A-weighted sound level at site #2
MAX3	CX	Maximum A-weighted sound level at site #3
MAX4	CY	Maximum A-weighted sound level at site #4
MAX5	CZ	Maximum A-weighted sound level at site #5

This appendix describes the operation of the Sound Exposure Level computation software package, **JTOPLOT**.

D.1 Getting Started

The required hardware is an IBM-PC or compatible computer running MS-DOS **3.0** or higher and a VGA color monitor. A hard disk is highly recommended, but not required. The hard disk should have at least **1,500,000** bytes free in order to store the program and the database files for one measurement day. The following steps should be performed prior to starting the program:

Create a subdirectory on the hard disk and make this the current directory.

Copy the program **JTOPLOT.EXE** to the hard disk.

Copy the master database (eg. **MSTR1022.dbf**) for the measurement day to be processed to the hard disk.

Copy the A-level time history databases (eg. **01HST249.DBF**) for the same measurement day to the hard disk.

D.2 Starting the Program

At the DOS prompt type:

> **JTOPLOT** <enter>

The startup screen will prompt for two file names:

JTOLdBase: The site 1 acoustic database file name:
The naming convention is a **2-digit** site number, the letters "**HST**", the Julian date, and a **.DBF** extension. The program default is "**01HST349.DBF**". The program will look for the site 1 file as well as files for sites 2 through 5 (ie. it will look for **01HSTxxx.DBF**, **02HSTxxx.DBF**, **03HSTxxx.DBF**, **04HSTxxx.DBF**, a n d **05HSTxxx.DBF**. If any of these files are missing the measurement site will be ignored.

TIME dBases: The master database file name:
The naming convention is the letters "**MSTR**" followed by two month digits and two day digits, with a **.DBF** extension. The program default is "**JTOL1215.DBF**".

The arrow keys can be used to move back and forth between the two file names. After modifying a file name type <enter> to save the new entry.

After the file names are entered, press the **F2** key to start the program. Pressing the <**ESC**> key will terminate the program and return to the DOS prompt.

D.3 Data Viewing and Manipulation

After pressing the **F2** key the data viewing screen will appear along with the data from the first record in the database (the first recorded flight of the day).

D.3.1 The Viewing Screen

Please see Figure 17 in the main text for an illustration of the noise event viewing screen.

Annotation Box (Lower Right Corner):

Aircraft: FAA confirmed aircraft type (from master database parameter "**AACTYPE**").
Obs Time: Time reported in Jet Transport Observer Log (master database parameter "TIME") in **Hour:Minute:Second** format.
Twr Time: Brake release time recorded by aircraft tracking observer (master database parameter "**TARG_0**") in **Hour:Minute:Second** format.
Rec: Database record number (each measurement day begins with **1**).
Date: Measurement date.

A-Weighted Sound Level Time Histories:

Sites: 1 through **5**, top to bottom.
Time: **-60** seconds to **+150** seconds **re:** brake release time ("**Twr Time**" if available, ie. non-zero, otherwise "**Obs Time**").
SPL: Top **30 dB** of signal; maximum **SPL** shown to left of time-history panel.
Graticule: **30** seconds/division horizontal, **10 dB/division** vertical.

InterferenceParameters:

"LND":	Yellow Circle	- Jet landing on runway 33L (the norm).
	Red Circle	- Jet landing on runway 28 (occasional) . . . note aircraft flies right by site 5 .
	White Circle	- Propeller aircraft landing on runway 33R .
"JTO":	Yellow Circle	- Brake release, jet takeoff on runway 28 .
"PTO":	Yellow Circle	- Brake release, propeller aircraft takeoff from runway 33R . . . note aircraft flies right by site 1 .
"OPR":	Blue Line	- One or more propeller aircraft currently on taxiway or at hold short line to runway 33R .
	Yellow Circle	- Status Update, 1 aircraft on taxiway .
	White Circle	- Status Update, 2 aircraft on taxiway .
	Red Circle	- Status Update, 3 aircraft on taxiway .
	Magenta Circle	- Status Update, 4 aircraft on taxiway .
	Cyan Circle	- Status Update, 5 aircraft on taxiway .
	Green Circle	- Status Update, 6 aircraft on taxiway .

D.3.2 Data Manipulation and SEL Computation

The table below shows the keystroke commands recognized by the program and the function they perform. Please note that any command, even moving cursors back and forth, which result in a change to the screen changes the master database file accordingly. Cursors in each sound level time-history panel window the area over which the program will search for the maximum A-level and calculate the **SELs** over the top **10,15** and **20** decibels of the signal.

D.3.1 The Viewing Screen

Please see Figure 17 in the main text for an illustration of the noise event viewing screen.

Annotation Box (Lower Right Corner):

Aircraft: FAA confirmed aircraft type (from master database parameter "**AACTYPE**").
Obs Time: Time reported in Jet Transport Observer Log (master database parameter "TIME") in **Hour:Minute:Second** format.
Twr Time: Brake release time recorded by aircraft tracking observer (master database parameter "**TARG_0**") in **Hour:Minute:Second** format.
Rec: Database record number (each measurement day begins with **1**).
Date: Measurement date.

A-Weighted Sound Level Time Histories:

Sites: 1 through **5**, top to bottom.
Time: **-60** seconds to **+150** seconds **re:** brake release time ("**Twr Time**" if available, ie. non-zero, otherwise "**Obs Time**").
SPL: Top **30 dB** of signal; maximum **SPL** shown to left of time-history panel.
Graticule: **30** seconds/division horizontal, **10 dB/division** vertical.

InterferenceParameters:

"LND":	Yellow Circle	- Jet landing on runway 33L (the norm).
	Red Circle	- Jet landing on runway 28 (occasional) . . . note aircraft flies right by site 5 .
	White Circle	- Propeller aircraft landing on runway 33R .
"JTO":	Yellow Circle	- Brake release, jet takeoff on runway 28 .
"PTO":	Yellow Circle	- Brake release, propeller aircraft takeoff from runway 33R . . . note aircraft flies right by site 1 .
"OPR":	Blue Line	- One or more propeller aircraft currently on taxiway or at hold short line to runway 33R .
	Yellow Circle	- Status Update, 1 aircraft on taxiway .
	White Circle	- Status Update, 2 aircraft on taxiway .
	Red Circle	- Status Update, 3 aircraft on taxiway .
	Magenta Circle	- Status Update, 4 aircraft on taxiway .
	Cyan Circle	- Status Update, 5 aircraft on taxiway .
	Green Circle	- Status Update, 6 aircraft on taxiway .

D.3.2 Data Manipulation and SEL Computation

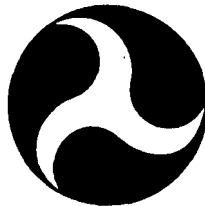
The table below shows the keystroke commands recognized by the program and the function they perform. Please note that any command, even moving cursors back and forth, which result in a change to the screen changes the master database file accordingly. Cursors in each sound level time-history panel window the area over which the program will search for the maximum A-level and calculate the **SELs** over the top **10,15** and **20** decibels of the signal.

Report No. FAA-EE-92-01
DOT-VNTSC-FAA-92-5

**ANALYSIS OF AIRCRAFT NOISE LEVELS IN THE
VICINITY OF START-OF-TAKEOFF ROLL
AT BALTIMORE-WASHINGTON
INTERNATIONAL AIRPORT**

Richard D. Horonjeff

Harris, Miller, Miller & Hanson, Inc.
429 Marrett Road
Lexington, MA 02173



MAY 1992

FINAL REPORT

Document is available to the U.S. Public through the
National Technical Information Service,
Springfield, Virginia 22161

Prepared for

U.S. DEPARTMENT OF TRANSPORTATION
RESEARCH AND SPECIAL PROGRAMS ADMINISTRATION
VOLPE NATIONAL TRANSPORTATION SYSTEMS CENTER
CAMBRIDGE, MA 02142-1 093